THE UNIVERSITY OF QUEENSLAND

SCHOOL OF CIVIL ENGINEERING

REPORT CH76/10

UNSTEADY TURBULENCE IN BREAKING TIDAL BORES: THE EFFECTS OF BED ROUGHNESS

AUTHOR: Nicholas J. DOCHERTY and Hubert CHANSON

HYDRAULIC MODEL REPORTS

This report is published by the School of Civil Engineering at the University of Queensland. Lists of recently-published titles of this series and of other publications are provided at the end of this report. Requests for copies of any of these documents should be addressed to the Civil Engineering Secretary.

School of Civil Engineering
The University of Queensland
Brisbane QLD 4072
AUSTRALIA

Telephone: (61 7) 3365 3619
Fax: (61 7) 3365 4599

URL: http://www.eng.uq.edu.au/civil/

First published in 2010 by
School of Civil Engineering
The University of Queensland, Brisbane QLD 4072, Australia

ISBN No. 9781864999884

The University of Queensland, St Lucia QLD

CHARACTERISATION OF UNSTEADY TURBULENCE IN BREAKING TIDAL BORES INCLUDING THE EFFECTS OF BED ROUGHNESS

by

Nicholas J. DOCHERTY

and

Hubert CHANSON

The University of Queensland, School of Civil Engineering,

Brisbane QLD 4072, Australia

Ph.: (61 7) 3365 3619, Fax: (61 7) 3365 4599, Email: h.chanson@uq.edu.au

Url: http://www.uq.edu.au/~e2hchans/

REPORT No. CH76/10

ISBN 9781864999884

School of Civil Engineering, The University of Queensland

March 2010

Breaking tidal bore of the Garonne River at Cadillac (France) on 28 September 2008

Abstract

A tidal bore is an unsteady flow motion generated by the rapid water level rise at the river mouth during the early flood tide. With time, the leading edge of the tidal wave becomes steeper and steeper until it forms a wall of water that is the tidal bore. Herein the turbulence in breaking tidal bores was investigated experimentally under controlled conditions with two types of bed roughness: smooth PVC and fixed gravel bed (k_s = 3.4 mm). Some qualitative observations were conducted with both undular and breaking bores. The tidal bore flow patterns were independent of the bed roughness, as well as of the initial steady flow conditions, while the free-surface properties were close to earlier findings. Using an ensemble-averaging technique, the free-surface fluctuations of breaking bores were characterised. Immediately prior to the roller, the free-surface curved gradually upwards and the gentle surface elevation rise was about $0.1 \times d_o$ where d_o is the initial water depth. The passage of the bore roller was associated with some large water depth fluctuations. Some detailed turbulent velocity measurements were performed at several vertical elevations during and shortly after the breaking bore passage. Both the instantaneous and ensemble-averaged velocity data highlighted some seminal features of breaking bores. Namely a strong flow deceleration was observed at all elevations during the tidal bore passage. Close to the bed, the longitudinal velocity component became negative immediately after the roller passage implying the existence of a transient recirculation "bubble". The vertical velocity data presented some positive, upward motion during the bore front passage with increasing maximum vertical velocity with increasing distance from the bed. The vertical motion was believed to be linked with some streamline curvature. The transverse velocity data presented some large fluctuations with a non-zero ensemble-average after the roller passage that highlighted some intense secondary motion advected behind the bore front. A comparison between ensemble-average (EA) and variable interval time average (VITA) velocity data was performed. The EA and VITA results showed some comparable velocity pattern with some relatively-long-term data trend superposed to some high-frequency turbulent fluctuations. The data showed however that the VITA calculations for a single experiment presented some non-negligible difference with the EA median value for all velocity components. Overall the study demonstrated the intensive turbulence and turbulent mixing under a breaking tidal bore.

Keywords: Breaking tidal bores, Unsteady turbulence, Turbulent Mixing, Acoustic Doppler velocimetry, Signal processing, Ensemble average (EA), Variable interval time average (VITA), Fixed gravel bed roughness, Turbulent shear stresses.

TABLE OF CONTENTS

APPENDICES

List of symbols

The following symbols are used in this report:

A	flow cross-section area (m^2);
a_w	wave amplitude (m);
a_o	Minnaert factor (m/s);
B	channel width (m);
D_{ab}	air bubble diameter (m);
D_H	hydraulic diameter: $D_H = 4 \times A/P_w$;
d	(a) flow depth (m) measured normal to the invert;
	(b) flow depth (m) measured above the fixed gravel bed;
d_c	critical flow depth (m): $d_c = \sqrt{q^2 / g}$ in a rectangular channel;
d_{conj}	conjugate flow depth (m) measured immediately behind the tidal bore front;
d_{max}	flow depth (m) at the first wave crest;
d_s	median sediment size (m);
d_o	initial flow depth (m) measured normal to the chute invert;
F	frequency (Hz);
F_{cutoff}	cutoff frequency (Hz) for low/high pass filtering;
Fr	tidal bore Froude number defined as: $Fr = (V_o + U) / \sqrt{g \times d_o}$;
f	Darcy-Weisbach friction factor;
g	gravity constant (m/s^2): $g = 9.80$ m/s^2 in Brisbane, Australia;
h	gate opening (m) after gate closure;
h_s	rise in free-surface elevation (m) in front of the breaking bore front (Fig. 3-8);
k_s	equivalent sand roughness height (m);
L	length (m);
L_w	wave length (m) measured from crest to crest;
P	pressure (Pa);
P_w	wetted perimeter (m);
p	pressure fluctuation (Pa);
Q	volume flow rate (m^3/s);
q	volume flow rate per unit width (m^2/s): $q = Q/B$;
Re	Reynolds number;
S_o	bed slope : $S_o = \sin\theta$;
T	averaging period (s);
t	time (s);
t'	time (s);
t_{peak}	characteristic time (s) for which the free-surface fluctuations are maximum;
t_1, t_2, t_3	characteristic times (s) of the breaking bore front (Fig. 3-8);

U	tidal bore front celerity (m/s) for an observer standing on the bank, positive upstream;
V	(a) flow velocity (m/s) positive downstream; (b) instantaneous velocity component (m/s);
V_{conj}	conjugate flow velocity (m/s) immediately behind the tidal bore front;
V_o	initial flow velocity (m/s) positive downstream: $V_o = q/d_o$;
V_x	longitudinal velocity (m/s) positive downstream;
V_y	transverse velocity (m/s) positive towards the left sidewall;
V_z	vertical velocity (m/s) positive upwards;
$\overline{V}$	(a) time-averaged velocity (m/s); (b) ensemble-averaged (EA) velocity (m/s); (c) variable interval time averaged (VITA) velocity (m/s);
v	turbulent velocity fluctuation (m/s): $v = V - \overline{V}$;
v'	root mean square of turbulent velocity component (m/s);
x	longitudinal distance (m) measured from the channel upstream end, positive downstream;
x_{gate}	downstream gate position (m);
x_s	tidal bore front location (m);
y	transverse distance (m) measured from the channel centreline, positive towards the left sidewall;
z	distance (m) normal to the bed; it is the vertical distance (m) for a horizontal channel; for the fixed ravel bed, z is measured above the top of the gravel bed;

Greek symbols

δ	boundary layer thickness (m) defined in terms of 99% of the free-stream velocity;
δt	time increment (s);
γ	specific heat ratio;
μ	dynamic viscosity (Pa.s);
π	$\pi = 3.14159265358979323846264 3$;
θ	bed slope angle with the horizontal, positive downwards;
ρ	water density (kg/m^3);

Subscript

conj	conjugate flow conditions: i.e., immediately behind the tidal bore front;
low	low-pass filtered component;
max	maximum value;
median	median value (i.e. 50% percentile);
min	minimum value;
x	longitudinal component positive downstream;
y	component transverse to the channel centreline;

z	component normal to the invert;
o	initial flow conditions : i.e., upstream of the positive surge front;
10	10% percentile;
25	25% percentile;
75	75% percentile;
90	90% percentile;

Abbreviations

ADM	acoustic displacement meter;
ADV	acoustic Doppler velocimeter;
DPIV	digital particle image velocimetry;
EA	ensemble average;
Std	standard deviation
VITA	variable interval time average;

Notation

Ø	diameter;
$\overline{V}$	time-average of V;
$\frac{\partial}{\partial y}$	partial differentiation with respect to y.

1. Introduction

A tidal bore is an unsteady flow motion generated by the rapid water level rise at the river mouth during the early flood tide. With time, the leading edge of the tidal wave becomes steeper and steeper until it forms a wall of water: i.e., the tidal bore (BARRÉ de SAINT VENANT 1871, CHANSON 2005,2010a). After the formation of the bore, there is an abrupt rise in water depth at the bore front that is discontinuity in water depth and velocity field. Figure 1-1 shows some photographs of tidal bores. Once formed, the flow properties immediately before and after the tidal bore must satisfy the continuity and momentum principles (RAYLEIGH 1908, HENDERSON 1966, LIGGETT 1994). The integral form of the equations of conservation of mass and momentum gives a series of relationships between the flow properties in front of and behind the bore front. For a rectangular horizontal channel and neglecting bed friction, it yields (CHANSON 2004):

$$\frac{d_{conj}}{d_o} = \frac{1}{2}\left(\sqrt{1+8\times Fr^2}-1\right) \quad (1\text{-}1)$$

where d_o is the initial water depth, d_{conj} is the conjugate flow depth immediately after the bore passage, V_o is the initial river flow velocity positive downstream, U is the tidal bore celerity for an observer standing on the bank positive upstream, and Fr is the tidal bore Froude number defined as:

$$Fr = \frac{V_o + U}{\sqrt{g\times d_o}} \quad (1\text{-}2)$$

The Froude number of the tidal bore is always greater than unity. For Fr < 1, the tidal wave cannot become a tidal bore. For a tidal bore Froude number between unity and 1.5 to 1.8, the bore front is followed by a train of secondary waves that are well-formed, quasi-periodic undulations, called whelps. This is the undular (non-breaking) bore (Fig. 1-1A). For larger bore Froude numbers Fr, the bore is characterised by a breaking front (Fig. 1-1B). Both types of tidal bores are illustrated in Figure 1-1.

Historically, some major contributions on tidal bores included the works of BAZIN (1865), BARRÉ de SAINT VENANT (1871), BOUSSINESQ (1877), LEMOINE (1948), SERRE (1953), BENJAMIN and LIGHTHILL (1954) and PEREGRINE (1966). More recently, some unsteady turbulence measurements were conducted using PIV and ADV techniques (HORNUNG et al. 1995, KOCH and CHANSON 2009, CHANSON 2010), and the results demonstrated some intense turbulent mixing during the tidal bore front passage.

In this study, the free-surface properties and the turbulence characteristics of breaking tidal bores were investigated physically under controlled flow conditions. Two types of bed roughness were tested systematically. Detailed free-surface measurements were conducted using a non-intrusive technique, while the turbulent velocity measurements were performed with an acoustic Doppler velocimeter sampled at 200 Hz. The unsteady turbulence properties were analysed using two methods: an ensemble-average (EA) technique and a variable interval time average (VITA) method. The two techniques were compared systematically and the results provided some new understanding of the unsteady turbulent field in a breaking tidal bore.

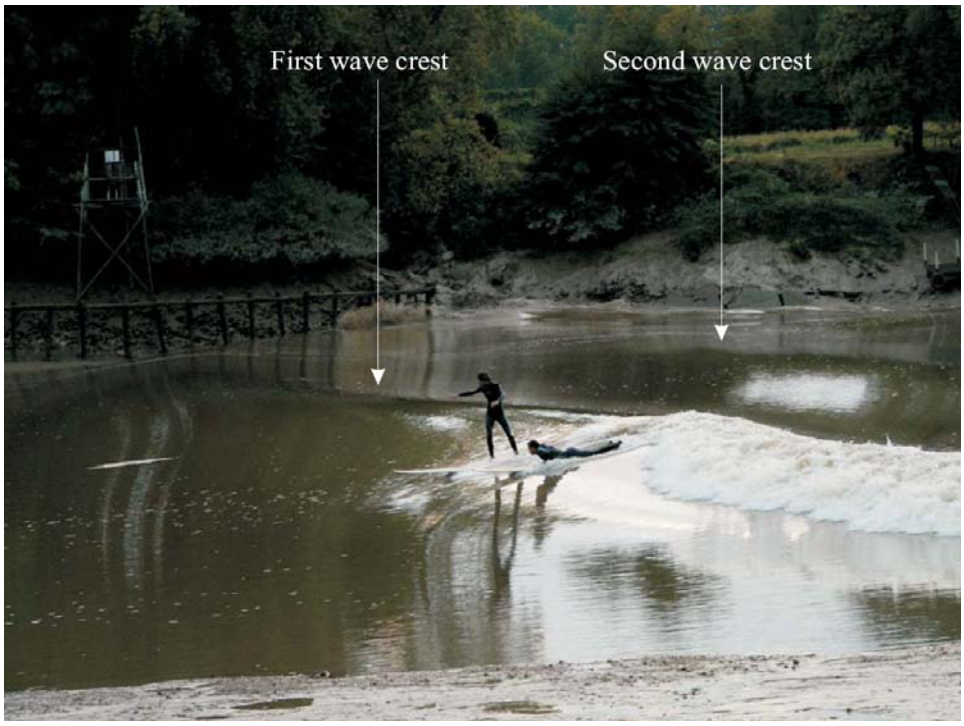

(A) Undular tidal bore of the Garonne River on 1 October 2008 at Béguey (France) - The surfers are riding ahead of the first wave crest with the bore propagating from right to left - Note some wave breaking in the right foreground corresponding to some shallow waters

(B) Breaking tidal bore of the Qiantang River (China) on 20 September 2008 (Courtesy of Pierre WEILL) - Bore propagation from left to right

Fig. 1-1 - Photographs of tidal bores

2. Experimental facilities, instrumentation and procedures

2.1 Experimental setup and facilities

The new experiments were performed in a relatively large tilting flume at the University of Queensland (Fig. 2-1). The channel was 12 m long 0.5 m wide. It was made of smooth PVC bed and glass walls. The waters were supplied by a constant head tank feeding a large intake basin (2.1 m long, 1.1 m wide, 1.1 m deep) leading to the test section through a bed and sidewall convergent. A tainter gate was located next to the downstream end (x = 11.15 m) where x is the distance from the channel upstream end.

The water discharge was measured with two orifice meters that were designed based upon the British Standards (British Standard 1943) and calibrated on site with a volume per time technique. The percentage of error was expected to be less than 2%. In steady flows, the water depths were measured using rail mounted pointer gauges. The unsteady water depths were recorded with a series of acoustic displacement meters. A Microsonic™ Mic+35/IU/TC unit was located at x = 10.8 m immediately upstream of the tainter gate. A further four acoustic displacement meters Microsonic™ Mic+25/IU/TC were spaced along the channel at x = 8, 6, 5 and 4 m. Some information on the sensor characteristics is reported in Table 2-1. The acoustic displacement meters were calibrated against the pointer gauges in steady flows.

In steady and unsteady flows, the velocity measurements were conducted with an acoustic Doppler velocimeter Nortek™ Vectrino+ (Serial No. VNO 0436) equipped with a three-dimensional side-looking head (Fig. 2-2). For the experiments, the velocity range was 1.0 m/s and the sampling rate was 200 Hz. The data accuracy was 1% of the velocity range. The ADV was set up with a transmit length of 0.3 mm and a sampling volume of 6 mm diameter and 1.5 mm height. Both the acoustic displacement meters and acoustic Doppler velocimeter were synchronised within +/- 1 ms, and were sampled simultaneously at 200 Hz using a high-speed data acquisition system NI DAQCard-6024E ([1]).

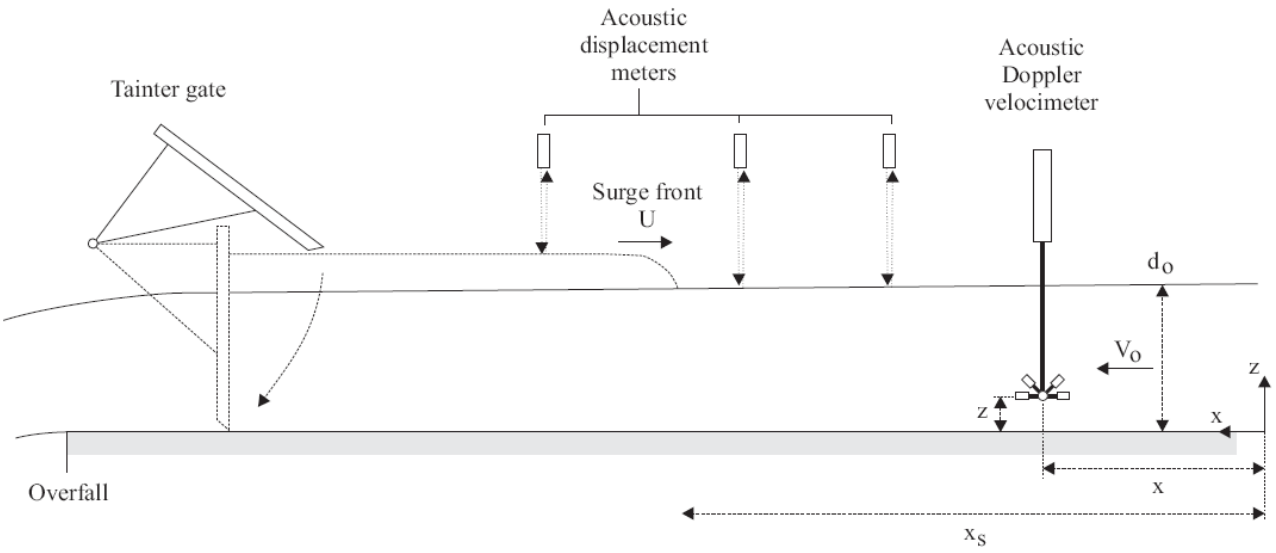

Fig. 2-1 - Sketch of the experimental facility

[1] Maximum sampling rate: 200 kHz.

Table 2-1 - Characteristics of the ultrasonic acoustic displacement meters

Characteristic (1)	Microsonic™ Mic+25/IU/TC (2)	Microsonic™ Mic+35/IU/TC (3)	Units (4)
Accuracy	0.18	0.18	mm
Response time	50	70	ms
Ultrasonic frequency	320	400	Hz
Wave length (at 20 C)	1.1	0.9	mm
Detection zone radius at operating range	22	37.5	mm
Blind zone :	30	60	mm
Operating range	250	350	mm
Maximum range :	350	600	mm

Note: Reference: Microsonic™ webpage {http://www.microsonic.de}

The translation of the ADV probe in the vertical direction was controlled by a fine adjustment travelling mechanism connected to a Mitutoyo™ digimatic scale unit. The error on the vertical position of the probe was $\Delta z < 0.025$ mm. The accuracy on the longitudinal position was estimated as $\Delta x < +/- 2$ mm. The accuracy on the transverse position of the probe was less than 1 mm. Herein all the measurements were taken on the channel centreline since the earlier work of KOCH and CHANSON (2005,2008) showed little transverse differences but close to the sidewall where the acoustic Doppler velocimetry was adversely affected by the sidewall proximity (CHANSON et al. 2007).
Additional information was obtained with some digital still cameras Olympus™ FE320, Panasonic™ Lumix DMC-FZ20GN and Pentax™ K-7. Several photographs of the experiments are presented in Appendix A.

2.2 Acoustic Doppler velocimetry and data post processing

The acoustic Doppler velocimetry (ADV) measurements were based upon the measurements of particle velocities in a remote sampling volume based upon the Doppler shift effect (VOULGARIS and TROWBRIDGE 1998, McLELLAND and NICHOLAS 2000). For each velocity component measurement, the acoustic Doppler velocimeter (ADV) unit recorded further the level of signal strength, a correlation value and a signal to noise ratio. These three parameters were indicative of the accuracy and reliability of velocity measurements (McLELLAND and NICHOLAS 2000, CHANSON 2008b). Past and present experiences demonstrated many problems because the ADV signal outputs combined the effects of velocity fluctuations, Doppler noise, signal aliasing, turbulent shear and other disturbances (LEMMIN and LHERMITTE 1999, GORING and NIKORA 2002, CHANSON et al. 2007,2008a, DOROUDIAN et al. 2007).
For all experiments, the present experience highlighted recurrent problems with the velocity data, including low correlations and low signal to noise ratios. This was primarily due to some inadequate seeding of the channel. Hence the channel was seeded herein with approximately 100 g of Clay Ceram ([2]) for every hour of channel operation. The clay powder was introduced in the intake structure and was dispersed progressively

[2] Clay Ceram is a product of Unimin Australia.

with time.

(A) Pointer gauge (left) and ADV head (right) above the free-surface during a fixed gravel bed experiment

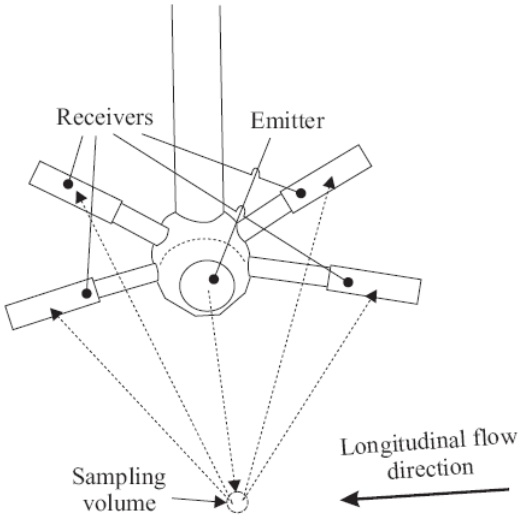

(B) Sketch of the Nortek^{TM} ADV side-looking head

Fig. 2-2 - Acoustic Doppler velocimeter (ADV)

The post processing of the ADV data was conducted with the software WinADV^{TM} version 2.025 using a similar method to KOCH and CHANSON (2009) and CHANSON (2010b). In steady flows, the ADV post processing included the removal of communication errors, the removal of average signal to noise ratio data less than 5 dB and the removal of average correlation values less than 60%. In addition, the phase-space thresholding technique developed by GORING and NIKORA (2002) was used to remove spurious points in the data set. In unsteady flow conditions, however, the above post-processing technique was not applicable (e.g. NIKORA 2004, *Person. Comm.*, CHANSON 2008b,2010b, KOCH and CHANSON 2009). Herein the

unsteady flow post-processing was limited to a removal of communication errors, and it is acknowledged that the vertical velocity component V_z data might be affected adversely by the bed proximity for $z < 0.030$ m (CHANSON 2008b,2010b). This is further discussed and documented in Appendix B.

2.3 Bed roughness

Two types of bed roughness were tested (Table 2-2). Some experiments were performed with the smooth PVC invert. For other experiments, the smooth PVC channel bed was covered with a series of 1.2 m long, 0.5 m wide, 8 mm thick plywood sheets for $2.0 < x < 10.55$ m where x is the longitudinal distance from the channel intake. Each sheet were covered by natural blue granite gravels which were sieved between 4.75 mm and 6.70 mm, glued in resin and covered by a spray gloss surface finish (Fig. 2-2A & 2-3, Inset). The bed was covered continuously with the rough bed for a 8.55 m length.

The hydraulic roughness of the fixed gravel bed was tested for a range of steady flow conditions. The gradually-varied flow profiles were recorded in the fully-developed flow region for steady flow rates ranging from 0.003 to 0.07 m^3/s. Note herein that the water depths were measured above the top of the gravel bed using a semi-circular footing with a 25.1 cm^2 area seen in Figure 2-3 (inset). The bed shear stress was deduced from the measured free-surface profiles and friction slopes. The equivalent Darcy friction factor of the fixed gravel bed sheets ranged from $f_{screen} = 0.031$ to 0.045 (Fig. 2-3). The results were basically independent of Reynolds number and relative roughness. In average, they yielded $f = 0.036$ corresponding to an equivalent sand roughness height $k_s = 3.4$ mm that was comparable to the typical gravel size $d_s = 5.7$ mm.

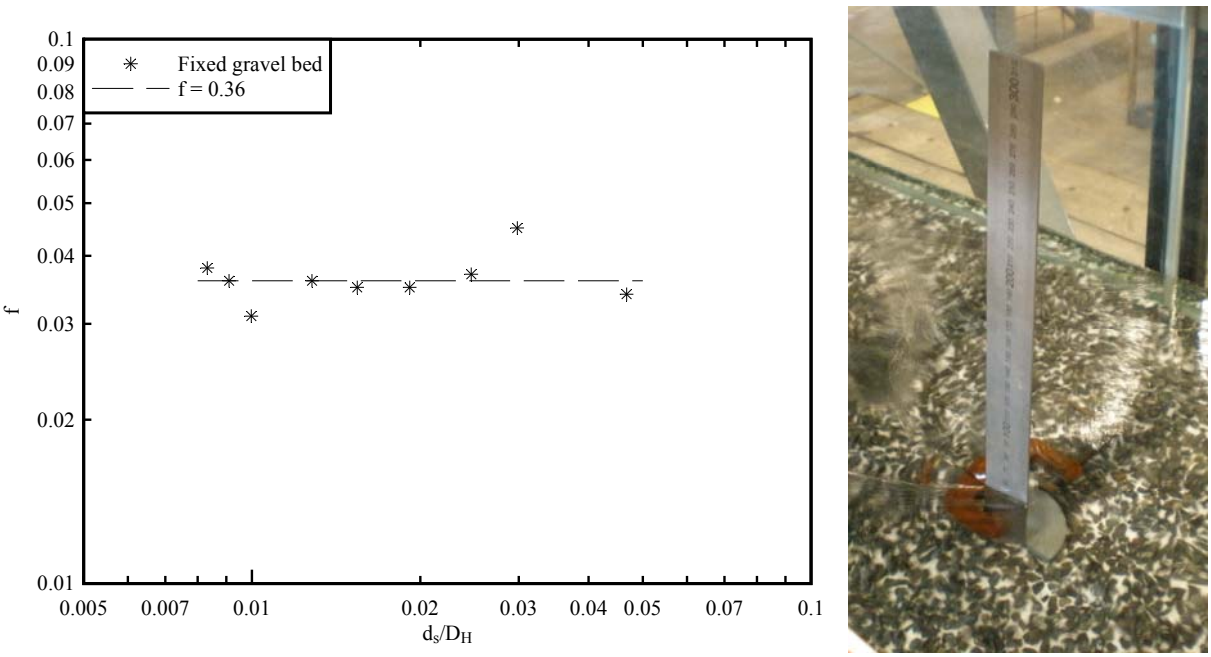

Fig. 2-3 - Darcy-Weisbach friction factor data of the fixed gravel bed ($d_s = 5.7$ mm) - Inset: details of the semi-circular footing used to measure the water depth above the gravels (flow from bottom right to top left)

2.4 Inflow conditions

Some detailed velocity measurements were performed in steady flows at x = 5 m. The results are presented in Figure 2-4 in which each graph corresponds to the initial flow conditions of the tidal bore passing x = 5 m. The data showed that the flow was partially-developed at x = 5 m for all investigated flow conditions (Fig. 2-4). The experimental observations showed a marked effect of the bed roughness on the steady velocity distributions with substantial differences between the smooth bed and fixed gravel bed data for the same flow rate and similar inflow depth (Fig. 2-4). Some larger turbulent velocity fluctuations were observed above the fixed gravel bed, while the vertical distribution of longitudinal velocity exhibited a flatter shape (Fig. 2-4B).

The relative boundary layer thickness δ/d_o was 0.475 and 0.64 for the smooth PVC bed and fixed gravel bed respectively. The findings were close to and consistent with the earlier results of KOCH and CHANSON (2009) and CHANSON (2010b) for different flow rates (Table 2-2).

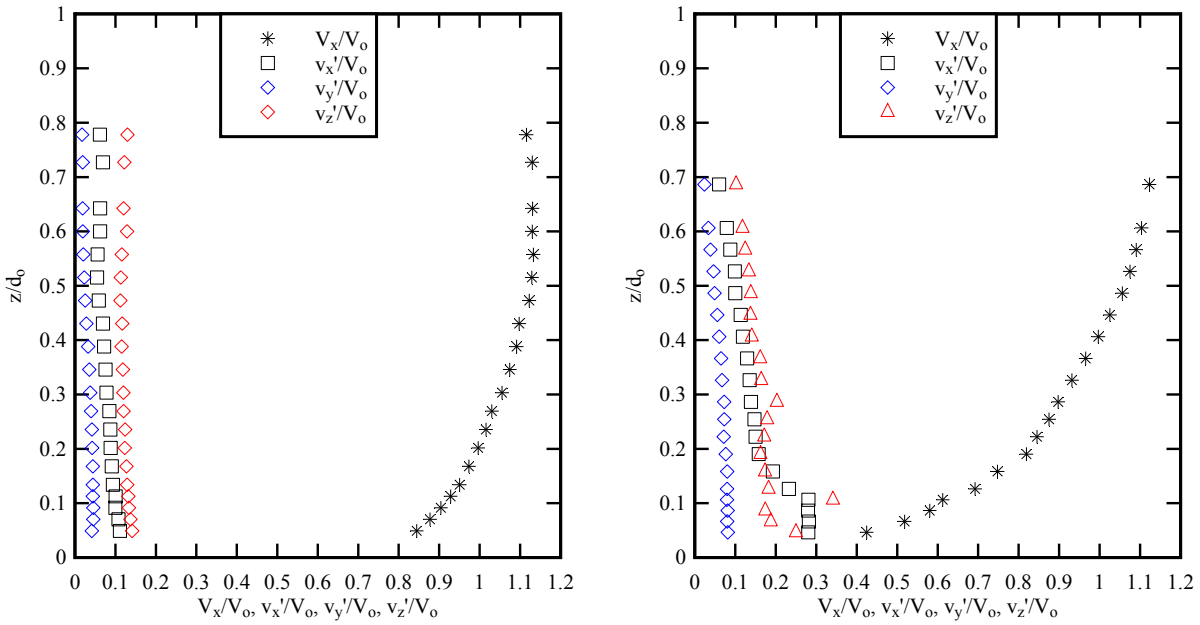

(A, Left) Smooth PVC bed, d_o = 0.118 m (B, Right) Fixed gravel bed, d_o = 0.125 m

Fig. 2-4 - Dimensionless vertical distributions of the time-averaged longitudinal velocity component V_x, and standard deviations of the horizontal, transverse and vertical velocity components v_x', v_y' and v_z' measured at x = 5 m for Q = 0.050 m^3/s, $d_o \approx 0.12$ m

Table 2-2 - Experimental studies of tidal bores: inflow conditions and relative boundary layer thickness

Reference (1)	Q (m^3/s) (2)	B (m) (3)	S_o (4)	d_o (*) (m) (5)	δ/d_o (6)	Bed roughness (7)
KOCH & CHANSON (2009)	0.040	0.50	0	0.079	0.61	Smooth PVC
CHANSON (2010b)	0.058	0.50	0	0.137	0.32	Smooth PVC
				0.142 ($^+$)	0.48	Plastic screens (k_s = 6.6 mm)
Present study	0.0499	0.50	0	0.118	0.475	Smooth PVC
			0.002	0.125 ($^+$)	0.64	Fixed gravel bed (k_s = 3.4 mm)

Notes: B: channel width; d_o: initial water depth; Fr: tidal bore Froude number; k_s: equivalent sand roughness height; Q: initial flow rate; S_o: bed slope; (*) measured at x = 5 m; ($^+$): measured above the roughness.

2.5 Tidal bore generation

The experimental setup and flow conditions were selected to generate both undular bores and breaking surges with the same initial flow rate Q. The main dependant parameters were the bed roughness and the downstream gate opening after closure h. The steady gradually-varied flow conditions were established for at least 5 minutes prior to the measurement start and the data acquisition was started 60 s prior to gate closure. The tidal bore was generated by the rapid partial closure of the downstream tainter gate. The gate was similar to that used by KOCH and CHANSON (2009) and CHANSON (2010b). The gate closure time was between 0.1 and 0.15 s, and less than 0.2 s. LUBIN et al. (2010) presented a computational modelling of the gate closure process.

After closure, the bore propagated upstream and each experiment was stopped before the bore front reached the intake structure to avoid any wave reflection interference. The acoustic displacement meters were located on the channel centreline at x = 10.8 m, 8.0 m, 6.0 m, 5.0 m, and 4.0 m. The sensor at x = 5 .0 m sampled the free-surface elevation immediately above the ADV sampling volume. Note that, at the downstream gate (x = 11.15 m), the channel bed was smooth; the fixed gravel were installed between 2.0 < x < 10.55 m.

The experimental measurements in tidal bores were conducted with one discharge, two bed roughness and two types of surges. For each experiment, the ADV unit was located at x = 5 m and y = 0 (on channel centreline), and most flow patterns observations were conducted between x = 4 and 6 m (Table 2-3).

2.6 Remarks

The present study focused on some basic laboratory experiments performed under controlled flow conditions in a relatively large size flume based upon a Froude similitude. It is understood that the physical modelling could have some limitations including scale effects. These could be particularly significant in narrow channels (sidewall effects) and with small initial depths associated with low Reynolds numbers (viscous effects). Herein the experimental configuration was selected to minimise potential scaling effects based upon

a Froude similitude with the selection of large initial depths and velocities, a relatively wide and long channel, and large Reynolds numbers : i.e., d_o = 0.12 m, V_o = 0.8 to 0.85 m/s, B = 0.5 m, Re = 4×10^5.
Lastly the experiments were performed with freshwater (tap water) as all earlier experiments listed in Table 2-3. In a natural system, the tidal bore propagates upstream in brackish waters.

Table 2-3 - Experimental studies of tidal bores

Reference (1)	Q (m^3/s) (2)	B (m) (3)	S_o (4)	d_o (*) (m) (5)	Fr (6)	Bed roughness (7)	Instrumentation (8)
HORNUNG et al. (1995)	0	--	0	--	1.5 to 6	Smooth bed	DPIV, sampling: 15 Hz, 500×650 pixels, 1 pixel = 0.2×0.2 mm^2.
KOCH & CHANSON (2009)	0.040	0.50	0	0.079	1.31 to 1.93	Smooth PVC	MicroADV (16 MHz), sampling: 50 Hz, sampling volume: 4.2×4.2×6.2 mm^3.
CHANSON (2010b)	0.058	0.50	0	0.137	1.17 to 1.49	Smooth PVC	Vectrino+ ADV (10 MHz), sampling: 200 Hz, sampling volume: 6×6×1.5 mm^3.
				0.142 ($^+$)	1.13 to 1.47	Plastic screens	
Present study	0.0499	0.50	0	0.118	1.08 to 1.59	Smooth PVC	Vectrino+ ADV (10 MHz), sampling: 200 Hz, sampling volume: 6×6×1.5 mm^3.
			0.002	0.125 ($^+$)	1.01 to 1.52	Fixed gravel bed	

Notes: B: channel width; d_o: initial water depth; Fr: tidal bore Froude number; Q: initial flow rate; S_o: bed slope; ($^+$): measured above the roughness; (*) measured at x = 5 m.

3. Basic flow patterns and free-surface characteristics

3.1 Presentation

Some visual observations and free-surface measurements were conducted for a range of flow conditions with initially-steady subcritical open channel flow (Table 2-3). Several flow patterns were observed depending upon the tidal bore Froude number Fr defined as:

$$Fr = \frac{V_o + U}{\sqrt{g \times d_o}} \quad (3\text{-}1)$$

where V_o and d_o are the initial flow velocity and depth respectively, g is the gravity acceleration and U is the surge front celerity for an observer standing on the bank, positive upstream ([3]). For a Froude number between unity and 1.5 to 1.6, the tidal bore was undular: that is, the tidal bore front was followed by a train of secondary, quasi-periodic waves called undulations (Fig. 3-1). For larger Froude numbers, a breaking bore with a marked roller was observed (Fig. 3-2). The basic flow pattern observations were consistent with the earlier findings of FAVRE (1935), BENET and CUNGE (1971), TRESKE (1994) and KOCH and CHANSON (2008). Some photographs of undular and breaking tidal bore profiles are shown in Figures 3-1 and 3-2, and further illustrations are presented in Appendix A.

The undular tidal bore had a smooth, quasi-two-dimensional free-surface profile for Fr < 1.2 to 1.4 for smooth PVC and rough gravel bed respectively. For 1.2 to 1.4 < Fr, some slight cross-waves (shock waves) were observed, starting next to the sidewalls upstream of the first wave crest and intersecting next to the first crest on the channel centreline. The shock waves are seen in Figure 3-1C next to the sidewalls. For 1.3 to 1.45 < Fr < 1.5, some slight breaking was observed at the first wave crest next to the channel centreline, and the secondary waves became flatter (Fig. 3-1C). The size and strength of the roller increased with increasing Froude number until the roller occupied the entire channel width.

At the largest bore Froude numbers (i.e. Fr > 1.5), the bore had a marked roller, and appeared to be quasi-two-dimensional (Fig. 3-2). There was no shock wave. Behind the roller, the free-surface was about horizontal although some large free-surface fluctuations were seen. Some air entrainment and intense turbulent mixing were observed in the bore roller.

Overall the present findings were comparable to those of earlier studies (Table 3-1). Importantly the tidal bore flow patterns were basically independent of the initially steady flow Froude number $V_o / \sqrt{g \times d_o}$, and they were independent of the bed roughness.

[3] Herein U was the average bore front celerity measured between x = 4 and 6 m, as previously used by KOCH and CHANSON (2009) and CHANSON (2010b).

Table 3-1 - Experimental observations of change in tidal bore flow patterns

Reference	Q (m^3/s)	S_o	Bed roughness		Fr	
				Undular bore (no breaking)	Undular bore (with breaking)	Breaking bore
(1)	(2)	(3)	(4)	(5)	(6)	(7)
HORNUNG et al. (1995)	0	0	Smooth bed	< 1.6	1.6 - 1.9	1.9 <
KOCH and CHANSON (2009)	0.040	0	Smooth PVC	< 1.53	1.53 - 1.77	1.77 <
CHANSON (2010b)	0.058	0	Smooth PVC	< 1.3	1.3 -1.45	1.45 <
	0.058	0	Rough screens (k_s = 6.6 mm)	< 1.3	1.3 - 1.5	1.5 <
Present study	0.050	0	Smooth PVC	< 1.3	1.3-1.5	1.5
	0.050	0.002	Fixed gravels (k_s = 3.4 mm)	< 1.4	1.45-1.55	--

Notes: k_s: equivalent sand roughness height; Q: initial flow rate; S_o: bed slope; (--): data not available.

(A) Propagation of a smooth, two-dimensional undular tidal bore above the fixed gravel bed (Filename: IMGP0455b.jpg) - Q = 0.050 m^3/s, d_o = 0.139 m, h = 0.050 m, fixed gravel bed, shutter speed: 1/50 s, lens: Voigtlander Nokton 58mm f1.4

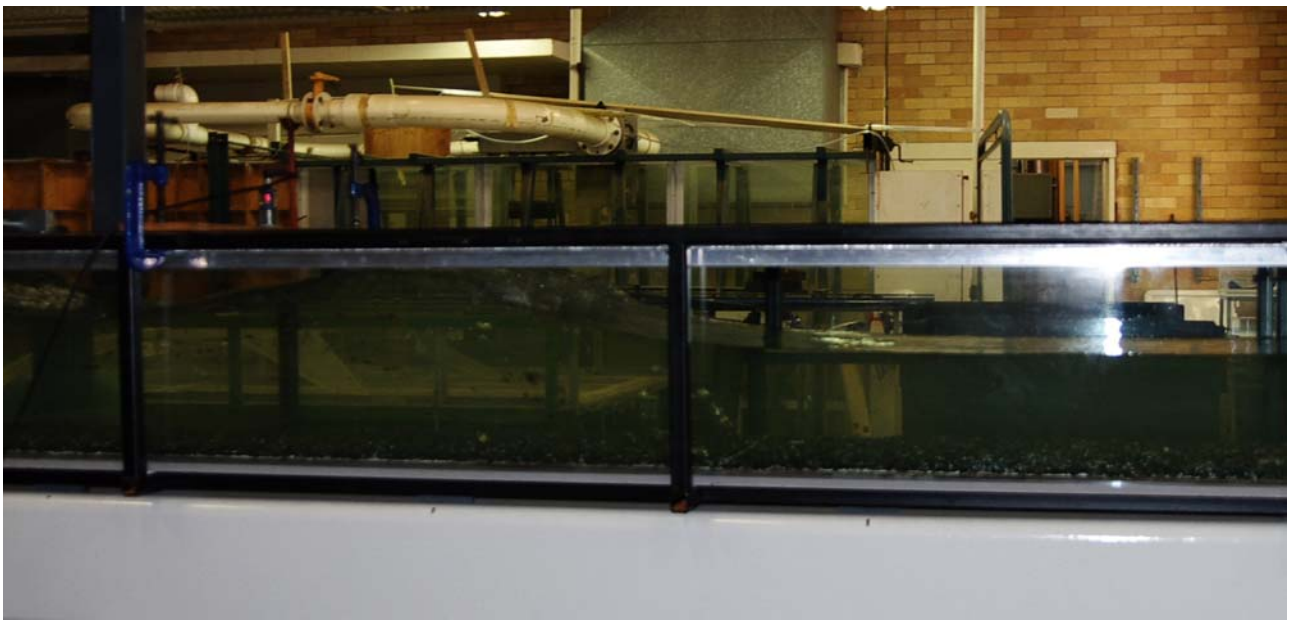

(B) Undular bore propagation above the fixed gravel bed at x = 4 m (Filename: IMGP0451b.jpg) - Q = 0.050 m^3/s, d_o = 0.139 m, fixed gravel bed, shutter speed: 1/50 s, lens: Voigtlander Nokton 58mm f1.4 - Note some breaking at the first wave crest

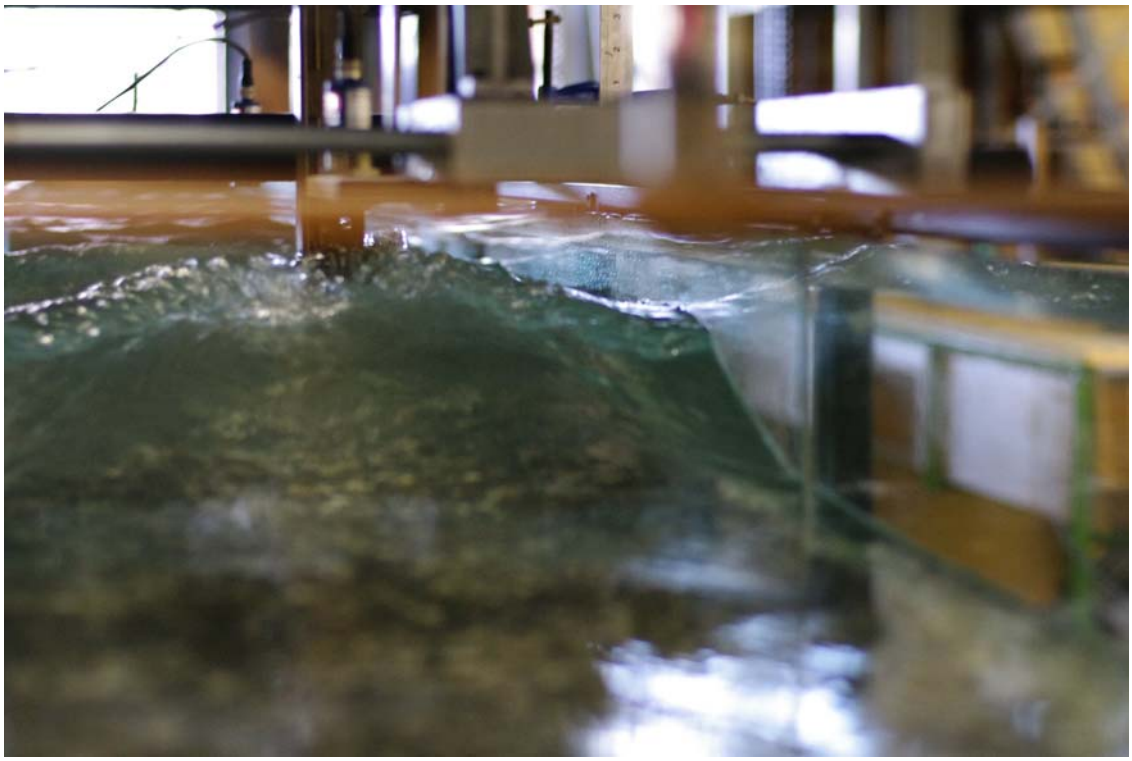

(C) Looking downstream at an incoming undular tidal bore roller with shock waves and breaking roller (Filename: IMGP0486b.jpg) - Q = 0.050 m^3/s, d_o = 0.120 m, h = 0.010 m, Fr = 1.5, fixed gravel bed, shutter speed: 1/60 s, lens: Voigtlander Nokton 58mm f1.4

Fig. 3-1 - Photographs of undular tidal bores

(A) Looking downstream at the incoming tidal bore roller (Filename: P1160051b.jpg) - Q = 0.0515 m^3/s, d_o = 0.144 m, U = 0.96 m/s, Fr = 1.41, shutter speed: 1/80 s

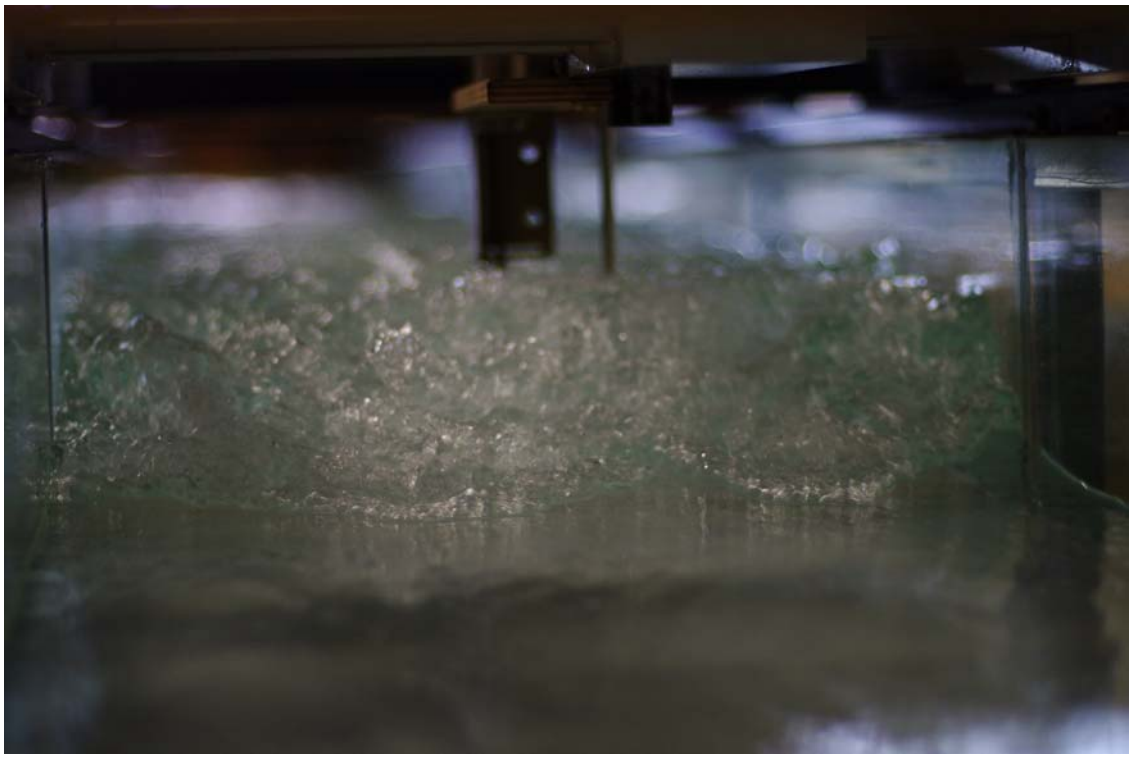

(B) Looking downstream at the incoming tidal bore roller (Filename: IMGP0326b.jpg) - Q = 0.050 m^3/s, d_o = 0.116 m, U = 0.85 m/s, Fr = 1.6, shutter speed: 1/100 s, lens: Voigtlander Nokton 58mm f1.4

Fig. 3-2 - Photographs of breaking tidal bores

3.2 Free-surface characteristics

In a tidal bore, the flow properties immediately upstream and downstream of the bore front must satisfy the continuity and momentum principles (HENDERSON 1966, LIGGETT 1994, CHANSON 2004). Considering a tidal bore travelling in a river section, the bore front propagates upstream with a celerity U. In the quasi-steady system of co-ordinates for an observer following the bore front, the integral form of the equations of conservation of mass and momentum gives a series of relationships between the flow properties in front of and behind the bore front:

$$(V_o + U) \times d_o = (V_{conj} + U) \times d_{conj} \quad (3\text{-}2)$$

$$\frac{1}{2} \times \rho \times g \times ({d_{conj}}^2 - {d_o}^2) = \rho \times (V_o + U) \times d_1 \times ((V_o + U) - (V_{conj} + U)) \quad (3\text{-}3)$$

where ρ is the water density, g is the gravity acceleration, V is the flow velocity positive downstream towards the river mouth, d is the water depth, the subscript o refers to the initial flow conditions and the subscript conj refers to the conjugate flow conditions or new flow conditions immediately after the tidal bore passage. Herein d_o and d_{conj} are respectively the flow depths immediately before and after the tidal bore passage (Fig. 3-3). Note that Equation (3-3) is based the assumption of hydrostatic pressure distribution in front of and behind the bore front, the channel is quasi-horizontal and the friction losses are neglected. For a rectangular channel, Equations (3-2) and (3-3) yield two dimensionless relationships:

$$\frac{d_{conj}}{d_o} = \frac{1}{2} \times \left(\sqrt{1 + 8 \times Fr^2} - 1 \right) \quad (3\text{-}4)$$

$$\frac{V_{conj} + U}{\sqrt{g \times d_{conj}}} = \frac{2^{3/2} \times Fr}{\left(\sqrt{1 + 8 \times Fr^2} - 1 \right)^{3/2}} \quad (3\text{-}5)$$

The Froude number of the tidal bore Fr is always greater than unity and the term (Fr-1) gives a measure of the strength of the bore. For the present experiments, the ratio of the conjugate depths d_{conj}/d_o is presented as a function of the tidal bore Froude number in Figure 3-4. The present data are compared with Equation (3-4) as well as with earlier prototype and laboratory data. The results highlighted a good agreement between the data and theory, including for the rough bed configurations (CHANSON 2010b, Present study). The finding is somehow challenging since Equations (3-3), (3-4) and (3-5) were developed neglecting boundary friction, but this is consistent with earlier observations (HENDERSON 1966, MONTES 1998, CHANSON 2004).

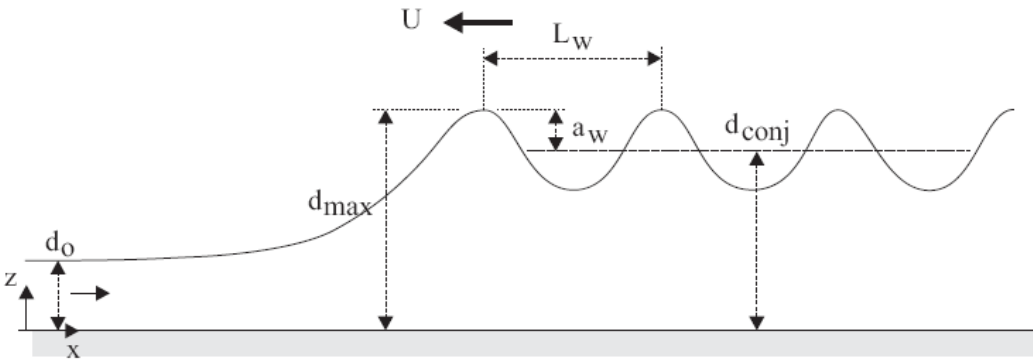

Fig. 3-3 - Definition sketch of an undular tidal bore

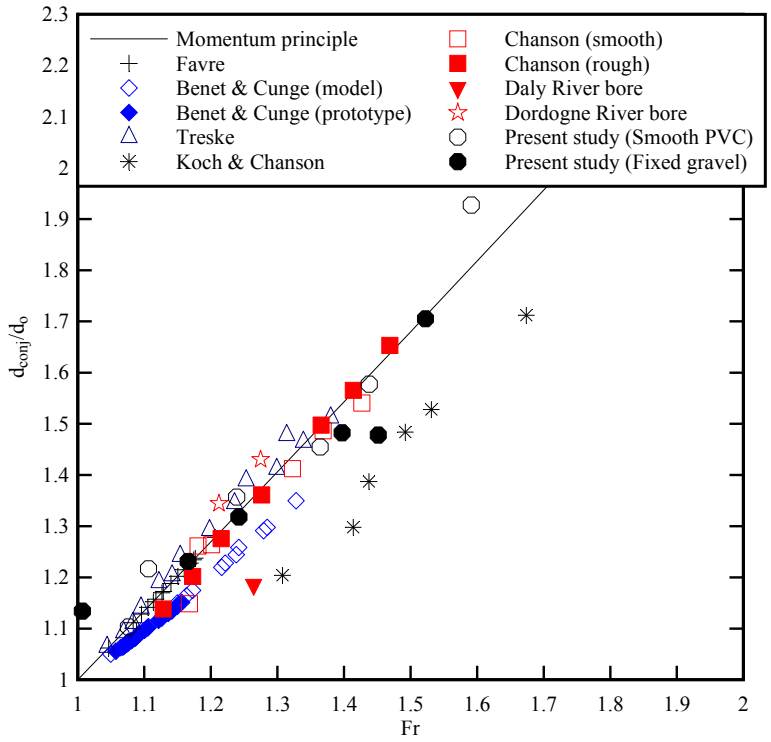

Fig. 3-4 - Dimensionless conjugate depth d_{conj}/d_o as a function of the tidal bore Froude number - Comparison between the present data, earlier laboratory studies (FAVRE 1935, BENET and CUNGE 1971, TRESKE 1994, KOCH and CHANSON 2009, CHANSON 2010b), prototype data (BENET and CUNGE 1975, NAVARRE 1995 [Dordogne River], WOLANSKI et al. 2004 [Daly River]), and the Bélanger equation (Eq. (3-4))

For tidal bore Froude numbers less than 1.5, the bore consisted of first wave followed by a train of well-formed undulations (Fig. 3-1 & 3-3). The free-surface profile of the secondary waves had a quasi-periodic shape, but neither the linear wave theory nor the cnoidal wave equation captured the asymmetrical wave shape nor the fine details of the free-surface profiles, as noted by CHANSON (2010a,c). The dimensionless wave amplitude and steepness are presented in Figures 3-5 and 3-6, while the entire data set is reported in Table 3-1. In Figures 3-5 and 3-6, the data were compared with both field and laboratory observations. The measurements were compared further with the analytical solutions of LEMOINE (1948) and ANDERSEN (1978) respectively based upon the linear wave theory and the Boussinesq equations. For a bore Froude number slightly larger than unity, the wave amplitude a_w/d_o and wave steepness a_w/L_w increased monotically with an increasing Froude number Fr. However, both a_w/d_o and a_w/L_w presented a local maximum followed by a sharp decrease immediately before the disappearance of free-surface undulations. It is believed that the flow conditions associated with the maximum wave amplitude and steepness took place shortly before the appearance of some slight breaking at the first wave crest for Fr ~ 1.3 to 1.45.

Overall the present results were close to and overlap with the previous results of KOCH and CHANSON (2009) and CHANSON (2010b), and they were close to past field observations (LEWIS 1972, BENET and CUNGE 1971, NAVARRE 1995, WOLANSKI et al. 2004).

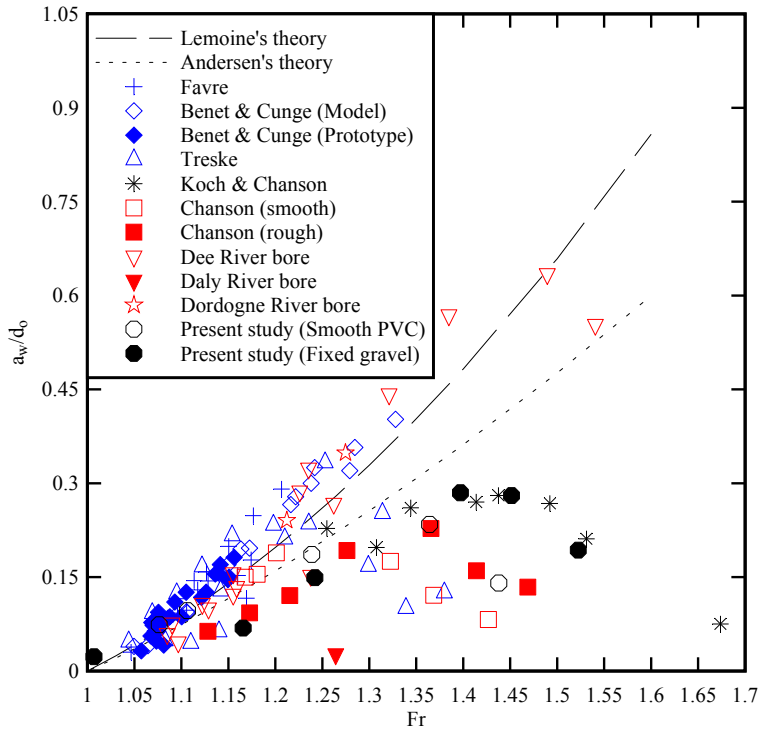

Fig. 3-5 - Dimensionless wave amplitude a_w/d_o as a function of the undular tidal bore Froude number - Comparison between the present undular bore data, earlier laboratory studies (FAVRE 1935, BENET and CUNGE 1971, TRESKE 1994, KOCH and CHANSON 2009, CHANSON 2010b), prototype data (LEWIS 1972 [Dee River], BENET and CUNGE 1971, NAVARRE 1995 [Dordogne River], WOLANSKI et al. 2004 [Daly River]), the linear wave theory (LEMOINE 1948) and cnoidal wave theory (ANDERSEN 1978)

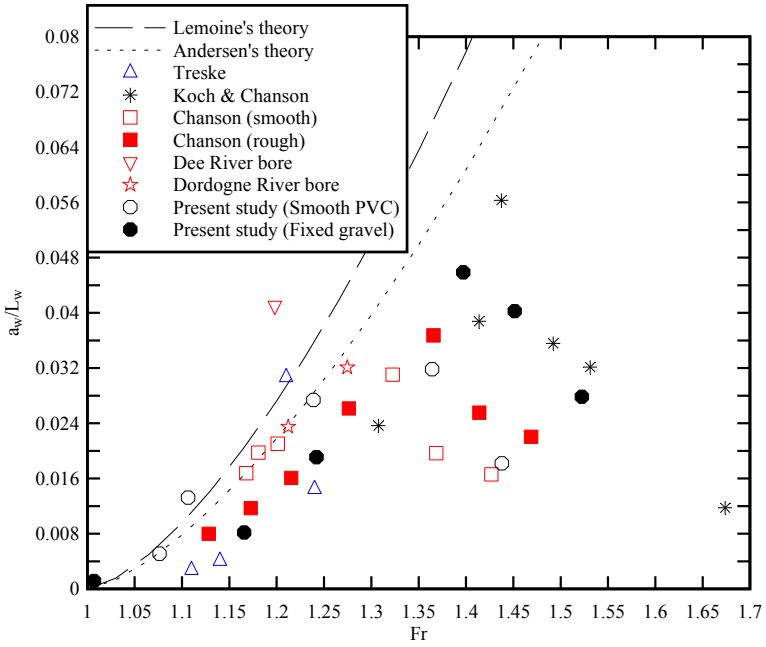

Fig. 3-6 - Dimensionless wave steepness a_w/L_w as a function of the undular tidal bore Froude number - Comparison between the present undular bore data, earlier laboratory studies (TRESKE 1994, KOCH and CHANSON 2009, CHANSON 2010b), prototype data (LEWIS 1972 [Dee River], NAVARRE 1995 [Dordogne River]), the linear wave theory (LEMOINE 1948) and cnoidal wave theory (ANDERSEN 1978)

Table 3-1 - Free-surface properties of tidal bores (Present study)

Bed roughness	Q (m^3/s)	d_o (m)	Fr	Type of tidal bore	d_{conj}/d_o	d_{max}/d_o	a_w/d_o	a_w/L_w
(1)	(2)	(3)	(4)	(5)	(6)	(7)	(8)	(9)
Smooth PVC bed	0.050	0.117	1.59	Breaking	1.93	N/A	N/A	N/A
		0.117	1.44	Undular/Breaking	1.58	1.72	0.141	0.018
		0.117	1.36	Undular	1.45	1.71	0.234	0.032
		0.116	1.24	Undular	1.36	1.61	0.186	0.027
		0.117	1.11	Undular	1.22	1.33	0.096	0.013
		0.117	1.08	Undular	1.10	1.18	0.074	0.005
Fixed gravel bed	0.050	0.125	1.52	Undular/Breaking	1.71	1.93	0.193	0.028
		0.125	1.45	Undular	1.48	1.75	0.280	0.040
		0.125	1.40	Undular	1.48	1.77	0.285	0.046
		0.125	1.24	Undular	1.32	1.45	0.149	0.019
		0.125	1.17	Undular	1.23	1.29	0.069	0.008
		0.125	1.01	Undular	1.13	1.13	0.023	0.001

Notes: a_w: wave amplitude of first wave length; d_o: initial water depth; d_{conj}: conjugate depth; d_{max}: water depth of first wave crest; Fr: tidal bore Froude number; L_w first wave length; Q: discharge; All data were recorded at x = 5 m.

3.3 Turbulent free-surface properties of a tidal bore with marked roller

In a turbulent breaking bore, a time-average is not meaningful because the hydrodynamic shock and the short-term fluctuations must be treated separately. A solution consists in repeating the experiments many times; the average of the instantaneous data (i.e. the ensemble-average) is the relevant mean property at a point at an instant. For a tidal bore with a marked roller (Fr = 1.5-1.6), the free-surface properties were systematically investigated at x = 5 m: a total of 25 identical experiments were repeated and the results were ensemble-averaged. The experimental flow conditions are summarised in Table 3-2.

Figure 3-7 presents the original data of instantaneous water depth as a function of time ([4]). Both the free-surface data and the visual observations of breaking bores showed that the free-surface elevation rose first slowly, immediately prior to the roller (Fig. 3-7). This is illustrated in Figures 3-7 to 3-9. In Figure 3-8, the period between the characteristic times t_1 and t_2 corresponded to the duration of the gentle rise h_s of the free-surface. The data are summarised in Table 3-2 (columns 7 & 8). The gradual rise in free-surface ahead of the turbulent roller was previously observed by HORNUNG et al. (1995), KOCH and CHANSON (2009) and CHANSON (2010b). Immediately after the gentle rise of the free-surface, the turbulent roller caused by a sharp rise in water depth that was basically a discontinuity (Fig. 3-7). This corresponded to the period between the characteristic times t_2 and t_3 in Figure 3-8. Note that, on the fixed gravel bed, the roller was followed by some weak secondary waves seen in Figure 3-7B. The present discussion focused on the passage of the roller and the effect of the undulations will not be discussed thereafter.

Figure 3-10 present the ensemble-averaged median water depth as a function of time. Each graph includes the ensemble-averaged median water depth d_{median}, the differences between 3rd and 4th quartiles (d_{75}-d_{25}) and 90% and 10% percentiles (d_{90}-d_{10}), and the maximum height between minimum and maximum water depth measurements (d_{max}-d_{min}). The data showed that the free-surface fluctuations were the largest next to the roller toe and impingement point, and they decayed quasi-exponentially with increasing time as the bore roller passed beneath the sensor. The characteristic time t_{peak} for which the fluctuations in free-surface elevations were the largest is summarised in Table 3-2 (column 9). Typically the maximum free-surface fluctuations were observed during the first third of the bore roller (Fig. 3-10).

The overall data trend was consistent with the findings of MOUAZE et al. (2005) and MURZYN and CHANSON (2009) in stationary hydraulic jumps.

Table 3-2 - Gradual free-surface elevation h_s in front of the roller (breaking tidal bore on horizontal channel)

Reference (1)	Q (m^3/s) (2)	d_o (*) (m) (3)	Fr (4)	Bed roughness (5)	h_s (m) (6)	t_2-t_1 (s) (7)	t_3-t_2 (s) (8)	t_{peak}-t_2 (s) (9)
KOCH & CHANSON (2009)	0.040	0.079	1.75-1.9	Smooth PVC	$0.1 \times d_o$	--	--	--
CHANSON (2010b)	0.058	0.137	1.50	Smooth PVC	0.01585	0.32	0.24	--
		0.142 ($^+$)	1.46	Plastic screens (k_s = 6.6 mm)	0.0152	0.41	*0.26*	--
Present study	0.050	0.119	1.65	Smooth PVC	**0.0095**	**0.35**	**0.48**	**0.18**
		0.127 ($^+$)	1.50	Fixed gravel bed (k_s = 3.4 mm)	**0.0192**	**0.32**	**0.36**	**0.22**

Notes: ($^+$): measured above the roughness; (*) measured at x = 5 m; **Bold data**: ensemble-averaged data; *Italic data*: uncertain data; (--): data not available.

[4] For all the experiments, the time scale t' was generated using the characteristic time t_2 (Fig. 3-8) as a reference time.

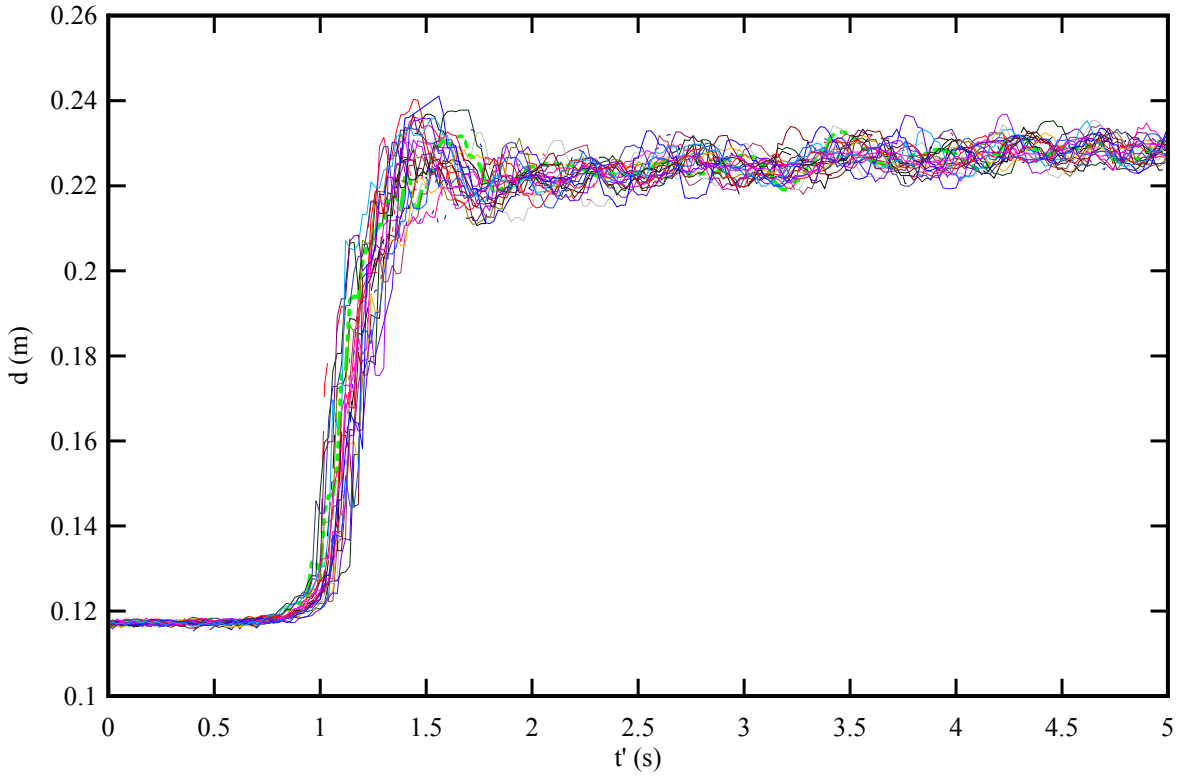

(A) Smooth PVC bed data: Q = 0.050 m^3/s, d_o = 0.119 m, Fr = 1.65

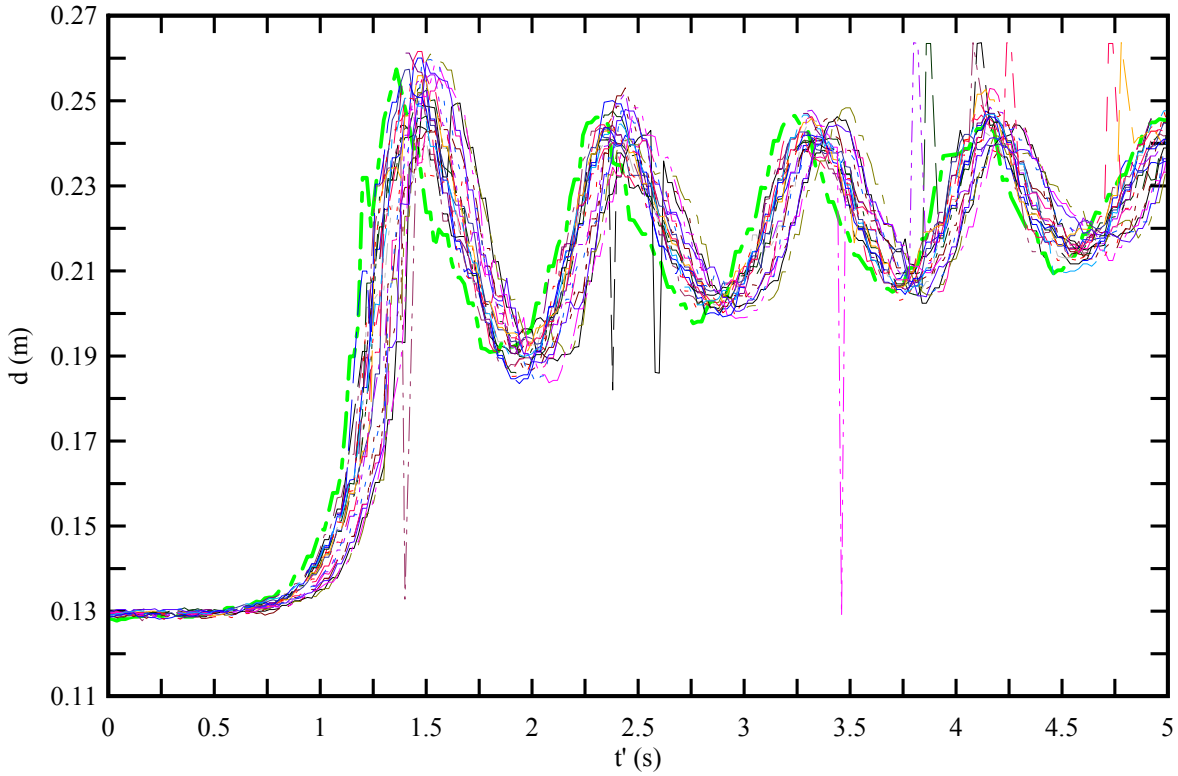

(B) Fixed gravel bed data: Q = 0.050 m^3/s, d_o = 0.127 m, Fr = 1.50

Fig. 3-7 - Time-variations of the water depth at x = 5 m: superposition of all 25 experiments

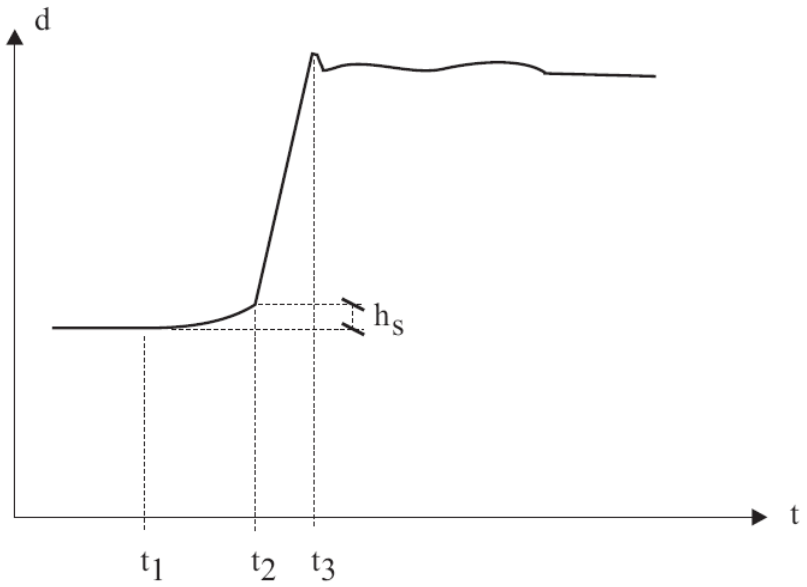

Fig. 3-8 - Sketch of instantaneous water depth measurement next to the breaking bore front

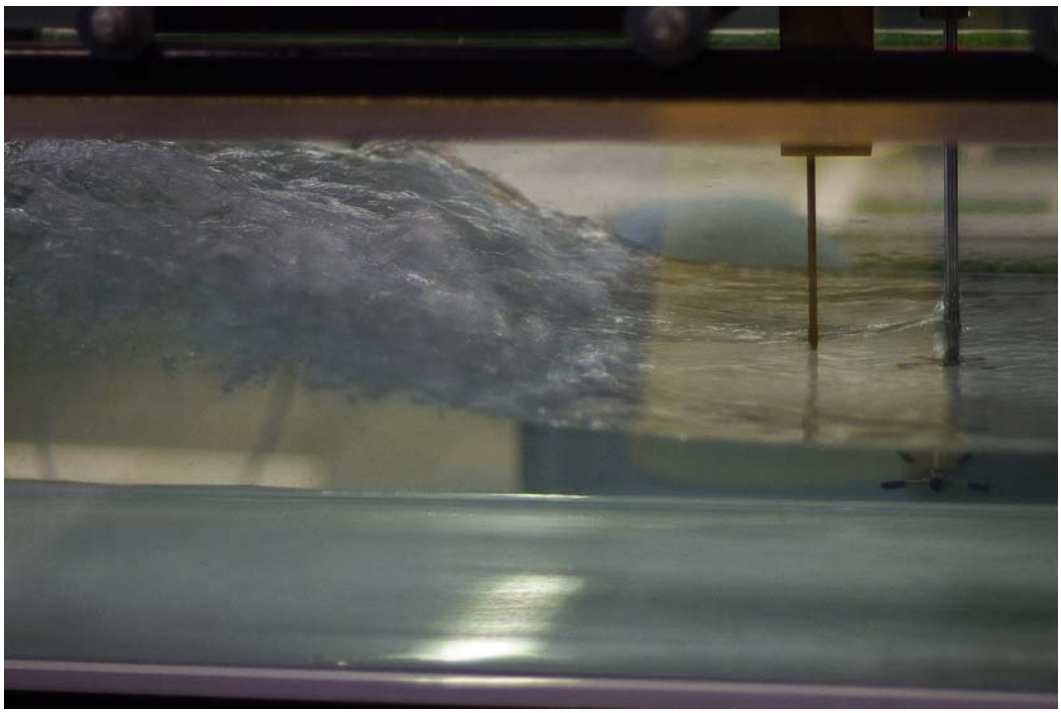

Fig. 3-9 - Details of the free-surface in a breaking tidal bore - Q = 0.050 m^3/s, d_o = 0.116 m, U = 0.847 m, Fr = 1.6, smooth PVC bed, shutter speed: 1/100 s - Note the gentle rise in free-surface elevation in front of the roller with the bore propagation from left to right

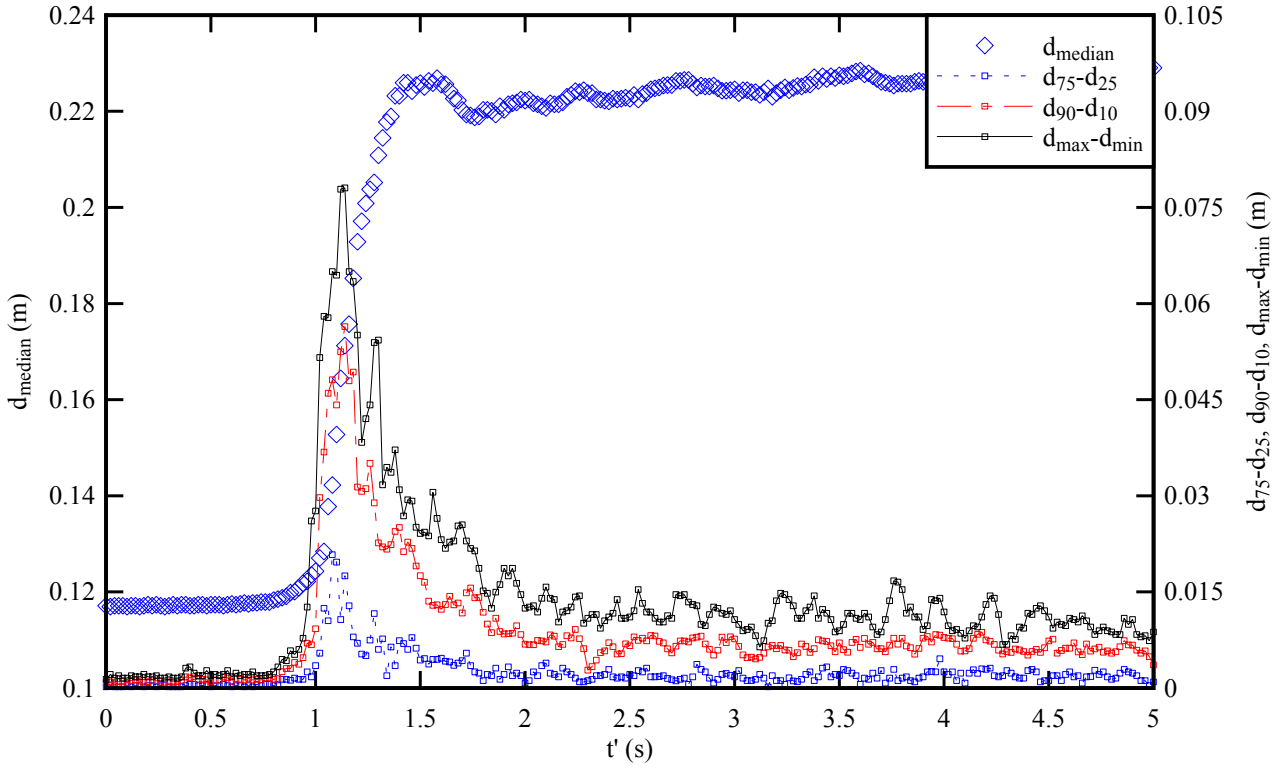

(A) Smooth PVC bed data: Q = 0.0499 m^3/s, d_o = 0.119 m, Fr = 1.66

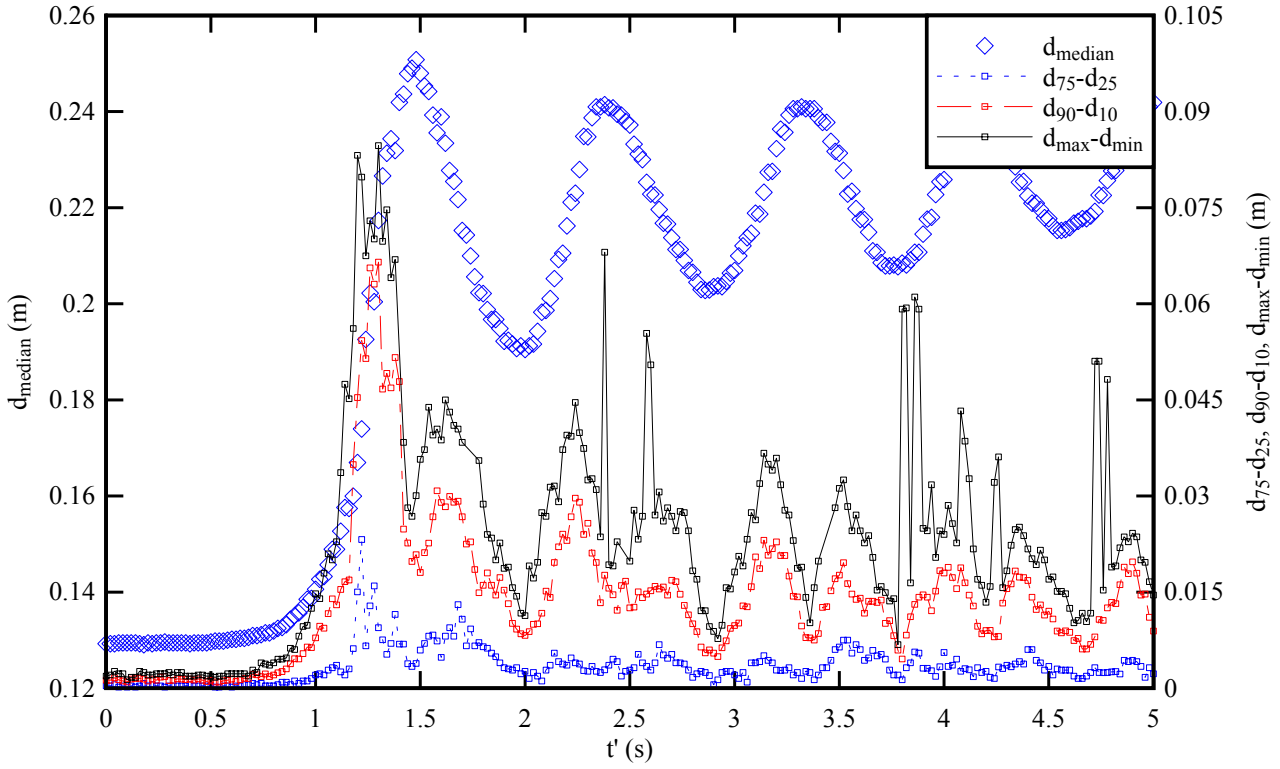

(B) Fixed gravel bed data: Q = 0.0500 m^3/s, d_o = 0.127 m, Fr = 1.50

Fig. 3-10 - Ensemble-average median water depth d_{median}, difference between 3rd and 4th quartiles (d_{75}-d_{25}) and 90% and 10% percentiles (d_{90}-d_{10}), and range of maximum to minimum water depth (d_{max}-d_{min})

4. Turbulent velocity measurements

4.1 Presentation

In a tidal bore with a marked roller, some instantaneous velocity measurements were performed with the acoustic Doppler velocimeter (ADV) at several vertical elevations. The data were sampled at 200 Hz on the channel centreline at x = 5 m for 0.0058 < z < 0.9 m where z is the vertical elevation above the bed ([5]). Table 4-1 presents the experimental flow conditions for both smooth PVC and fixed gravel bed experments. Figures 4-1 and 4-2 present some typical results in the form of the dimensionless time variations of the turbulent velocity components. Herein the instantaneous velocity components V_x, V_y and V_z were positive downstream, towards the left sidewall and upwards respectively.

Table 4-1 - Experimental flow conditions for turbulent velocity measurements in tidal bores

Q (m^3/s) (1)	S_o (2)	Bed roughness (3)	d_o (m) (4)	V_o (m/s) (5)	Bore type (6)	Fr (7)	U (m/s) (8)
0.050	0.000	Smooth PVC	0.118	0.848	Breaking	1.59	0.867
	0.002	Fixed gravel bed (k_s = 3.4 mm)	0.126	0.794	Undular/Breaking	1.49	0.866

Note: tainter gate opening after closure: h = 0.

The turbulent velocity data showed a number of flow patterns typical of tidal bores with a marked roller: i.e., a breaking bore, or an undular/breaking bore with a marked roller followed by residual secondary waves. First, for both bed roughness configurations, the longitudinal velocity component highlighted some flow deceleration during the passage of the bore front. As the bore front reached the sampling volume at x = 5 m, the water depth increased first gradually with time between the characteristic times t_1 and t_2 (Fig. 3-8). The gradual rise in the free surface was associated with a gradual longitudinal deceleration (Fig. 4-1 & 4-2). Later a sudden increase in the free surface elevation took place during the roller passage, corresponding to $t_2 < t < t_3$. The sudden rise in water depth was associated with a sharp decrease in longitudinal velocity component seen in Figures 4-1 and 4-2. The observations were consistent with the earlier results of HORNUNG et al. (1995), KOCH and CHANSON (2009) and CHANSON (2010b).

Second some transient negative longitudinal velocities V_x were observed next the invert on both smooth PVC and fixed gravel beds. For $z/d_o < 0.31$ on the smooth PVC bed and $z/d_o < 0.56$ on the fixed gravel bed, the longitudinal velocity component became negative during and shortly after the bore front. This is seen in Figures 4-1A and 4-2A. Above, for $z/d_o > 0.31$ and 0.56 on smooth PVC and fixed gravel bed respectively, the longitudinal velocity component tended to remain positive for the entire tidal bore passage record (Fig. 4-1B & 4-2B). The observations implied the existence of a transient recirculation pattern next to the bed during

[5] On the fixed gravel bed, the vertical elevation z was measured above the top of the gravel bed using a semi-circular

the bore propagation. Such a transient recirculation was associated with some large turbulent stresses in the water column and would induce some major impact in a natural system in terms of sediment processes and particulate dispersion. The present observations were consistent with the earlier findings of KOCH and CHANSON (2009) and CHANSON (2010b) in breaking bores.

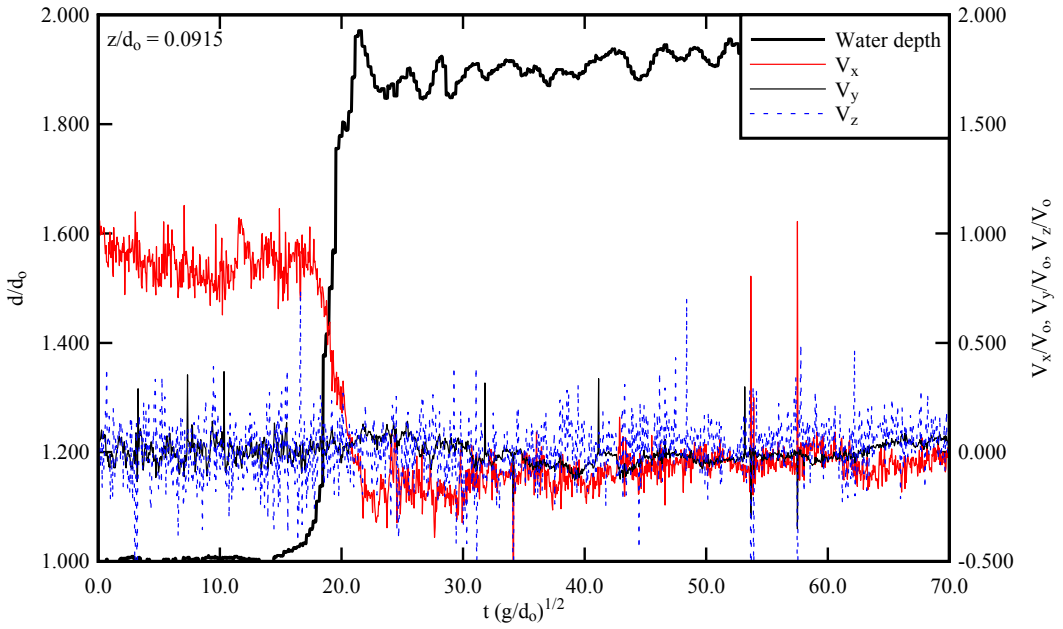

(A) $z/d_o = 0.091$

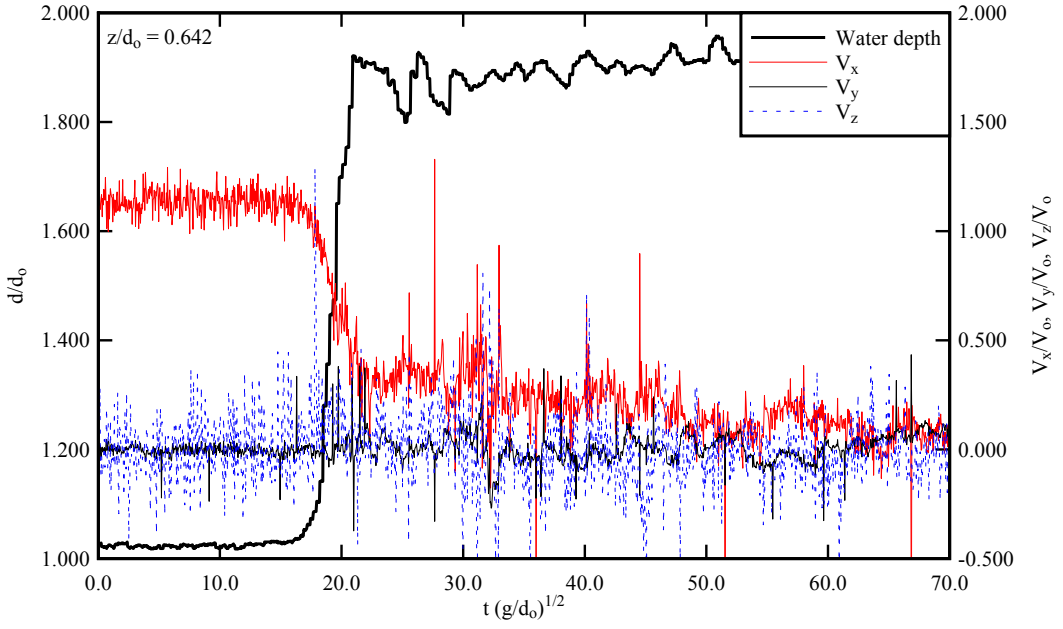

(B) $z/d_o = 0.642$

Fig. 4-1 - Instantaneous turbulent velocities in a breaking tidal bore on smooth PVC bed - Q = 0.050 m^3/s, d_o = 0.118 m, U = 0.87 m/s, Fr = 1.59

---

footing with a 25.1 cm^2 area seen in Figure 2-3 (inset).

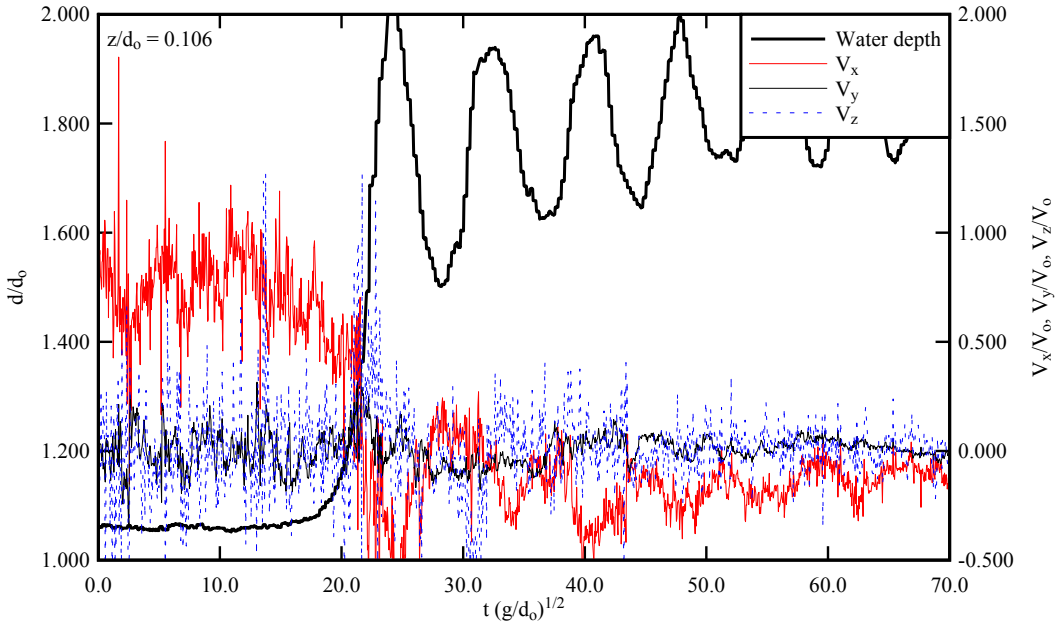

(A) $z/d_o = 0.106$

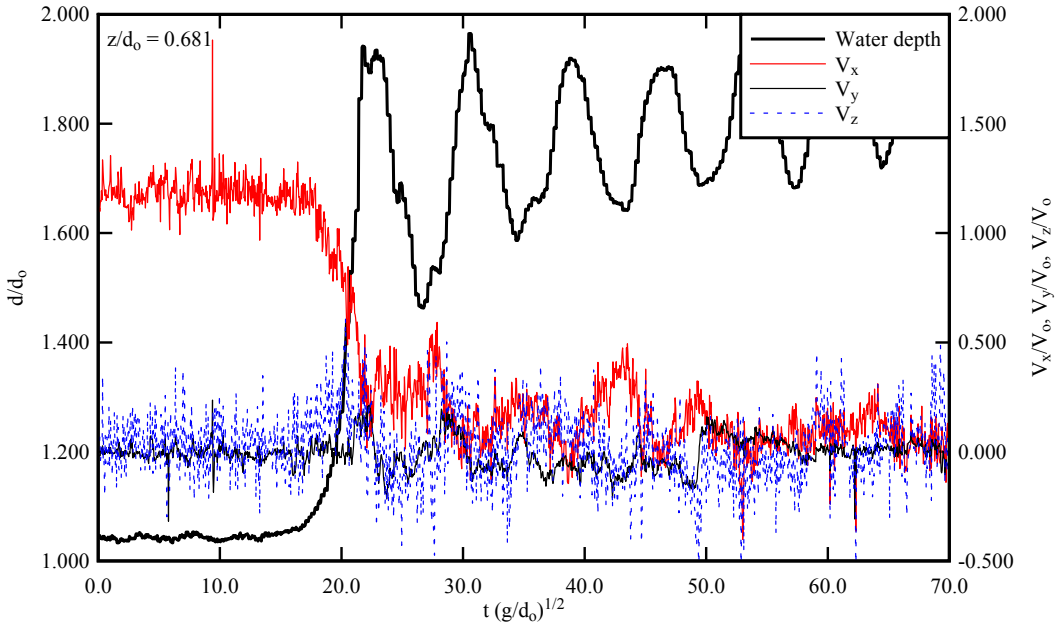

(B) $z/d_o = 0.681$

Fig. 4-2 - Instantaneous turbulent velocities in a breaking tidal bore on fixed gravel bed - Q = 0.050 m^3/s, d_o = 0.126 m, U = 0.87 m/s, Fr = 1.49 - Note that the water depths were measured above the top of the gravel bed

Third, the vertical velocity component tended to be positive in average during the bore front passage for $z/d_o \geq 0.4$ on both smooth and fixed gravel beds (Fig. 4-2B). For $z/d_o \geq 0.39$ on smooth PVC bed and $z/d_o \geq 0.36$ on fixed gravel bed, the vertical velocity tended to reach a local maximum during the roller passage, indicating an upward motion.

Most characteristic features of the longitudinal and vertical velocity components were similar for both the smooth PVC and fixed gravel beds, although the bed roughness had a noticeable effect on the recirculation

patterns in the flow.

4.2 Ensemble-averaged velocity properties

In a tidal bore with a marked roller, a series of twenty instantaneous velocity records were repeated at three vertical elevations above both smooth PVC and fixed gravel beds (Table 4-2). The acoustic Doppler velocimeter (ADV) sampled the instantaneous velocity components on the channel centreline at x = 5 m, and three sampling locations were selected: z/d_o = 0.135, 0.434 and 0.733. Between each repeat, the initial flow conditions were left unchanged for five minutes to achieve the same well defined initially steady flow conditions. An ensemble-median of each instantaneous velocity component was produced for each vertical elevation on both smooth PVC and fixed gravel beds. All the data were synchronised in terms of the characteristic time t_2 (Fig. 3-8). Some typical experimental results are shown in Figures 4-3 and 4-4 in terms of the ensemble-averaged median velocity components as a function of the time. Each graph includes the ensemble-averaged median velocity component (V_x, V_y or V_z), the differences between 3rd and 4th quartiles (V_{75}-V_{25}) and 90% and 10% percentiles (V_{90}-V_{10}), and the ensemble-averaged median water depth d_{median}. The full data sets are reported in Appendix C.

The experimental results showed consistently several characteristic trends on both smooth PVC and fixed gravel beds. The longitudinal velocity data V_x highlighted some maximum fluctuations during the tidal bore front passage, in particular beneath the roller. This is seen by the large values of the differences between 3rd and 4th quartiles (V_{75}-V_{25}) and 90% and 10% percentiles (V_{90}-V_{10}) in Figures 4-3A and 4-4A. The maximum horizontal velocity fluctuations occurred about the same time as when the maximum free-surface fluctuations were observed (section 3.3). Further the transverse velocity data V_y presented some large fluctuations after the bore front for $z/d_o \geq 0.43$, typically 5 to 10 times $\sqrt{g/d_o}$ after the front passage (Fig. 4-3B and 4-4B). The findings implied some intense secondary motion in the wake of the tidal bore front. Interestingly, the vertical velocity data V_z presented a substantial positive value during the front passage for $z/d_o \geq 0.43$ (Fig. 4-3C and 4-4C). It is believed to be closely linked with the streamline curvature immediately prior to the bore roller ($t_1 < t < t_2$) and possibly during the roller propagation ($t_2 < t < t_3$). Since the free-surface is a streamline, the surface slope is related to the vertical velocity component at the free-surface:

$$\frac{V_z(z=d)}{V_x(z=d)} = \frac{\partial d}{\partial x} \quad (4\text{-}1)$$

where $V_x(z=d)$ is the horizontal velocity component at the surface while, at the bottom, $V_z(z=0) = 0$ for an impervious boundary. For a solitary wave, BOUSSINESQ (1871) assumed a linear distribution of vertical velocity:

$$\frac{V_z}{V_z(z=d)} = \frac{z}{d} \quad (4\text{-}2)$$

The result may be applied to open channel flows with streamline curvature (MONTES 1998, p. 25). In the present study, the magnitude of the maximum median vertical velocity component $(V_z)_{max}$ increased with increasing distance from the bed (Fig. 4-5). This is illustrated in Figure 4-5 showing the maximum median vertical velocity component as a function of the vertical elevation. On the same graph, the free-surface

elevation rate $(\partial d/\partial t)_{z=d}$ is shown in addition. Since $V_z(z=0) = 0$ at the bed and $V_z(z=d) = (\partial d/\partial t)_{z=d}$ at the free-surface, an entire data trend can be extrapolated and the present data were best correlated by:

$$\left(\frac{V_z}{V_o}\right)_{max} = 0.215 \times \frac{z}{d_o} \quad \text{for } 0 < z/d < 1 \text{ (Smooth PVC bed)} \quad (4\text{-}3)$$

$$\left(\frac{V_z}{V_o}\right)_{max} = 0.466 \times \left(\frac{z}{d_o}\right)^{1.54} \quad \text{for } 0 < z/d < 1 \text{ (Fixed gravel bed)} \quad (4\text{-}4)$$

with a normalised correlation coefficient of 0.982 and 0.999 for Equations (4-3) and (4-4) respectively. First the results showed a trend comparable to BOUSSINESQ's (1871) approximation (Eq. (4-2)) as seen in Figure 4-5. The experimental results highlighted however a marked quantitative difference between the smooth and rough bed. These might be linked with slightly different flow conditions (Table 4-2), but may also be associated with some effects of the bed roughness on the turbulent flow field, especially close to the bed.

Table 4-2 - Experimental flow conditions for ensemble-average of turbulent velocity measurements in breaking tidal bores (Tainter gate opening after closure: h = 0)

Q (m^3/s) (1)	S_o (2)	Bed roughness (3)	d_o (m) (4)	V_o (m/s) (5)	Bore type (6)	Fr (7)	U (m/s) (8)	z/d_o (9)
0.050	0.000	Smooth PVC	0.117	0.855	Breaking	1.61	0.869	0.135 0.434 0.733
	0.002	Fixed gravel bed (k_s = 3.4 mm)	0.126	0.794	Undular/Breaking	1.50	0.877	0.135 0.434 0.733

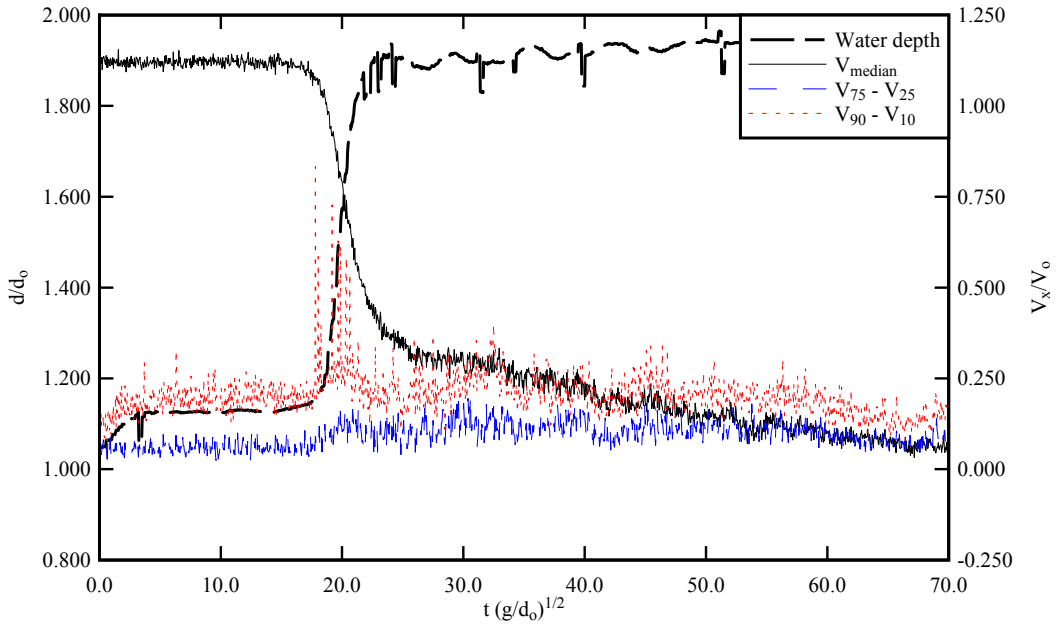

(A) Longitudinal velocity component V_x

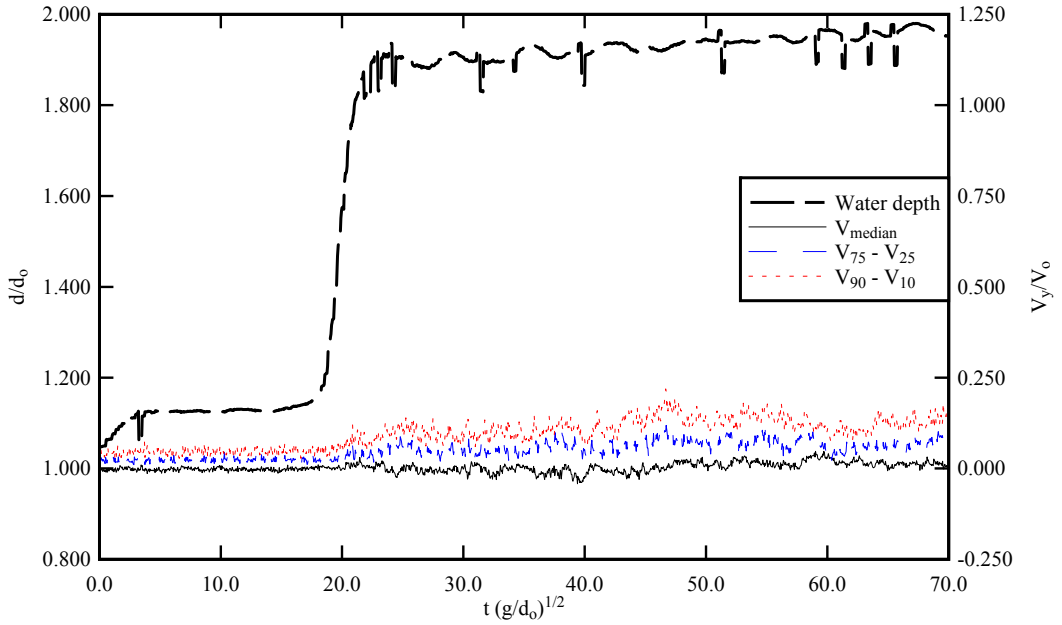

(B) Transverse velocity component V_y

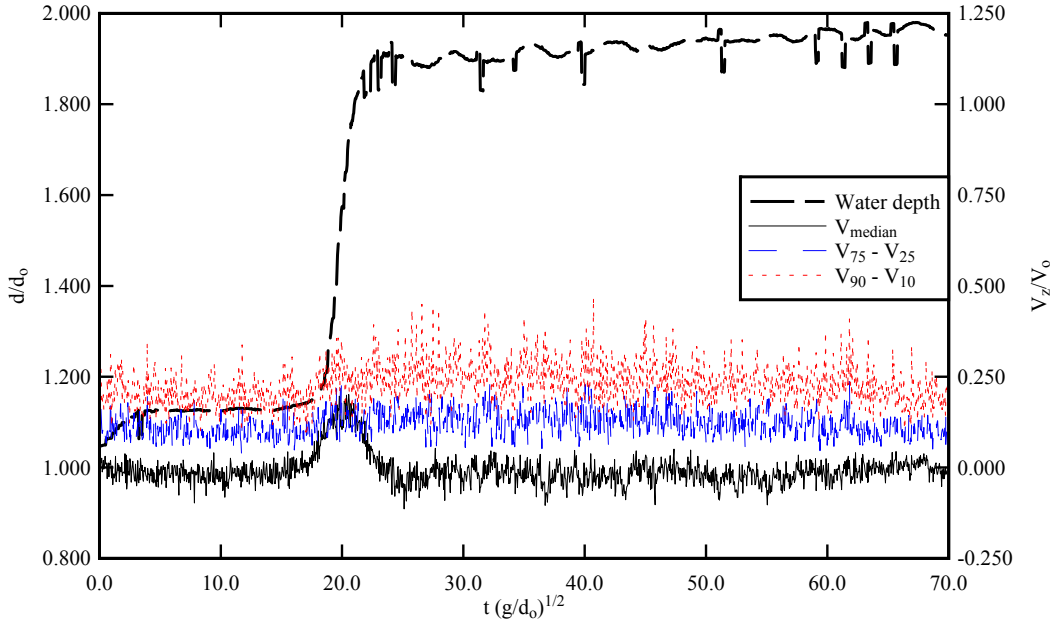

(C) Vertical velocity component V_z

Fig. 4-3 - Ensemble-average median velocity component V_{median}, difference between 3rd and 4th quartiles (V_{75}-V_{25}) and 90% and 10% percentiles (V_{90}-V_{10}), and ensemble-average median water depth d_{median} - Q = 0.050 m^3/s, d_o = 0.117 m, Fr = 1.61, z/d_o = 0.733, Smooth PVC bed

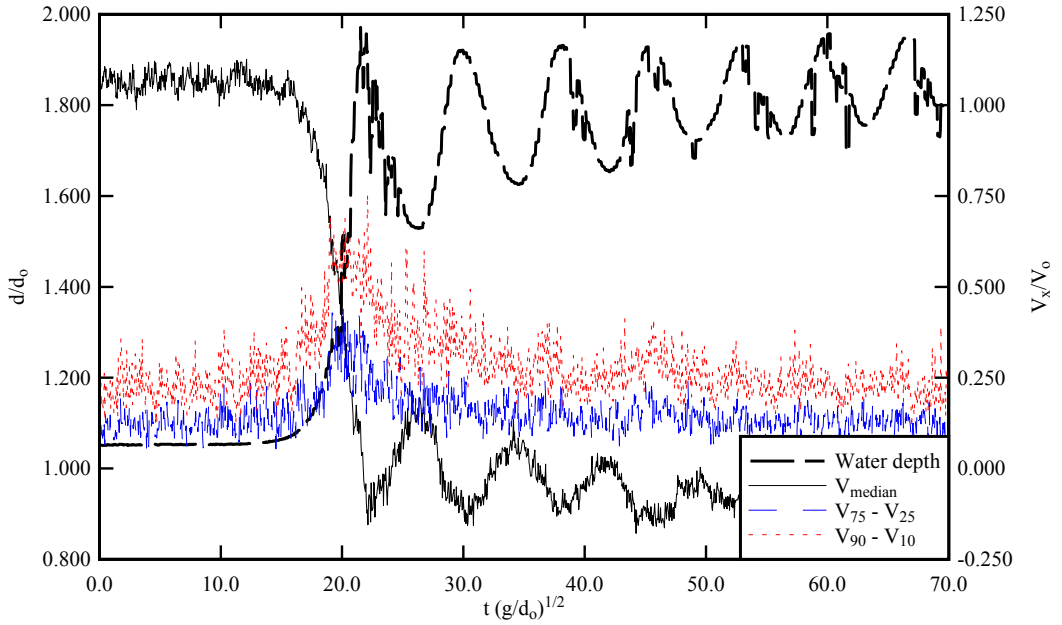

(A) Horizontal velocity component V_x

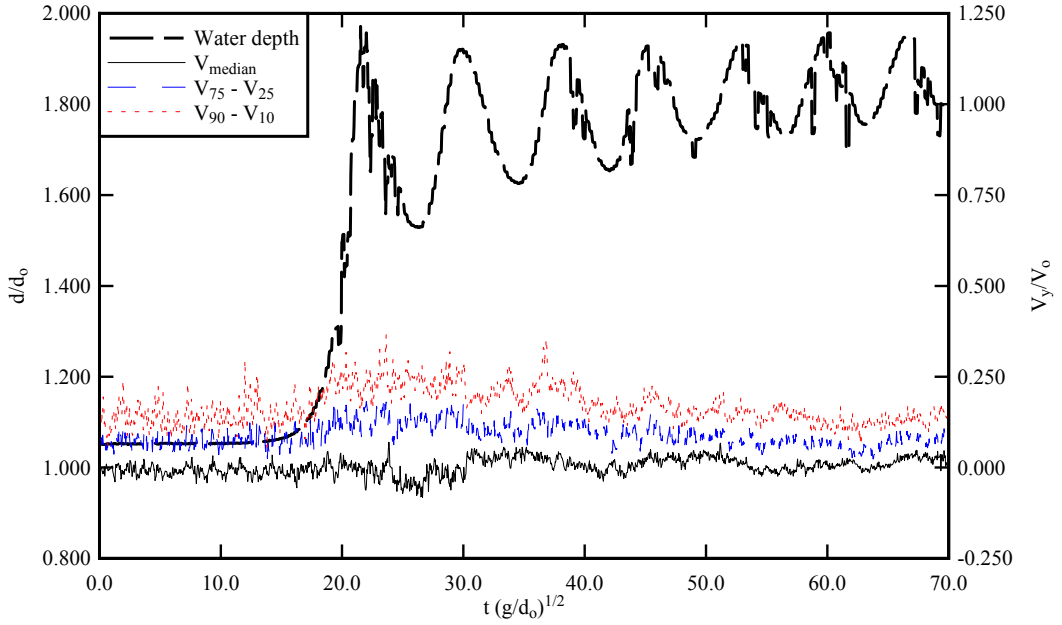

(B) Transverse velocity component V_y

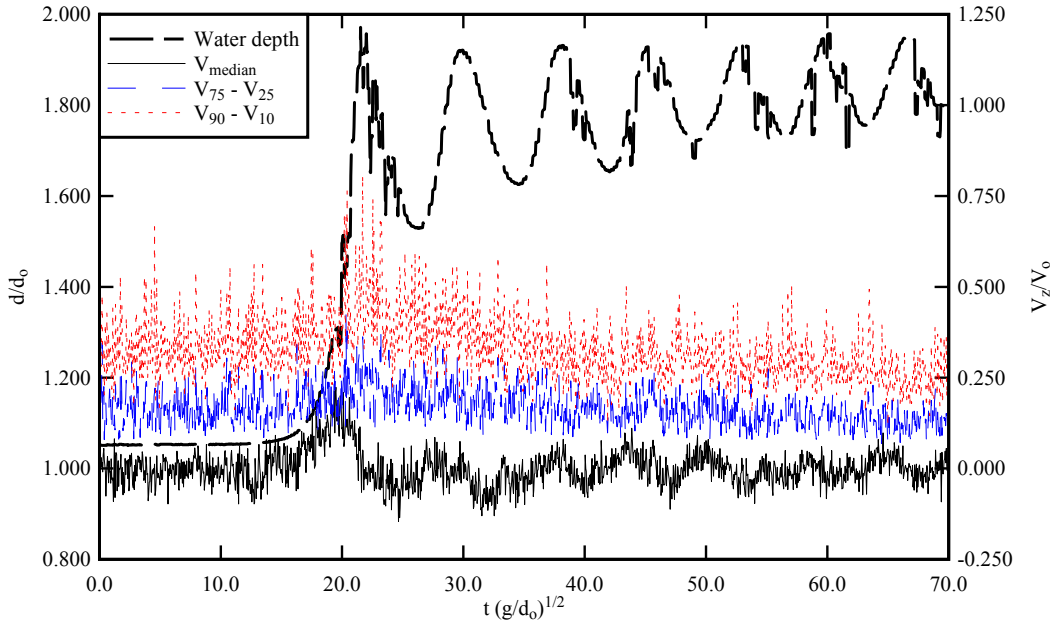

(C) Vertical velocity component V_z

Fig. 4-4 - Ensemble-average median velocity component V_{median}, difference between 3rd and 4th quartiles (V_{75}-V_{25}) and 90% and 10% percentiles (V_{90}-V_{10}), and ensemble-average median water depth d_{median} - Q = 0.050 m^3/s, d_o = 0.126 m, Fr = 1.50, z/d_o = 0.434, Fixed gravel bed

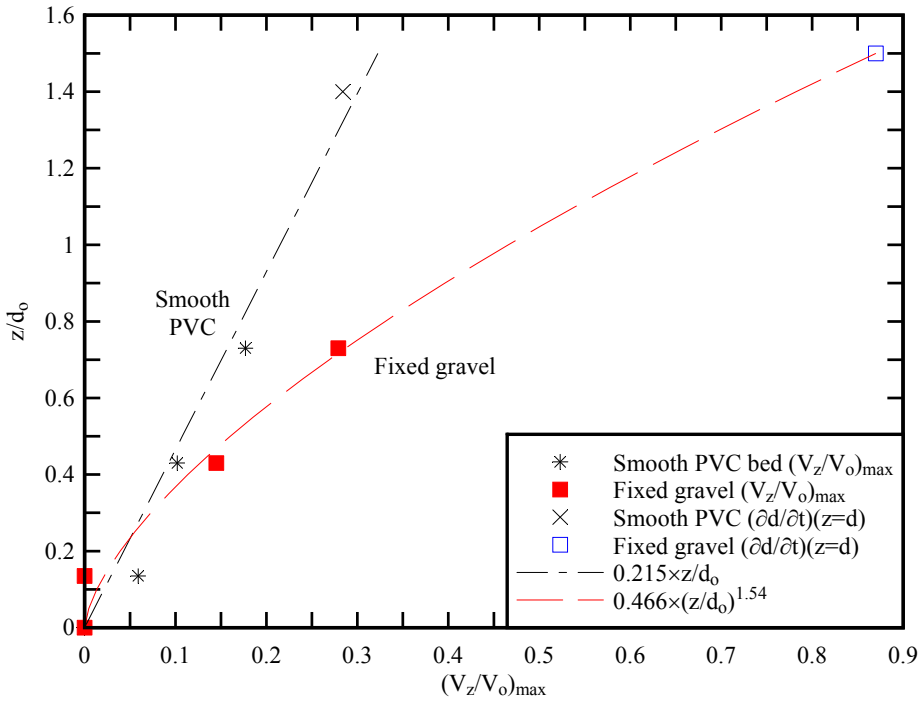

Fig. 4-5 - Maximum median vertical velocity beneath the tidal bore roller and corresponding free-surface vertical velocity on smooth PVC and fixed gravel beds - Comparison with Equations (4-3) and (4-4)

5. Discussion

5.1 Turbulence characterisation

In the present study, two techniques the ensemble-average method (EA) and the variable interval time average technique (VITA), were tested to characterise the unsteady turbulence in breaking tidal bores. A turbulent flow is characterised by its unpredictable behaviour, a broad spectrum of length and time scales, and its strong mixing properties. Turbulent flows have a great mixing potential involving a wide range of eddy length scales (HINZE 1975). In a turbulent flow motion, the velocity and pressure are typically divided into a time-average component plus a turbulent fluctuation component:

$$V = \overline{V} + v \tag{5-1}$$

where V is the instantaneous velocity, $\overline{V}$ is the time-averaged velocity, and v is the instantaneous velocity fluctuation. Similarly:

$$P = \overline{P} + p \tag{5-2}$$

In Equations (5-1) and (5-2), the minuscule refers to the fluctuating parameter and the overbar corresponds to the time-averaged quantity. In a steady flow, the time-average of a parameter V is defined as:

$$\overline{V} = \frac{1}{T} \times \int_{t-T/2}^{t+T/2} V \times dt' \tag{5-3}$$

where the averaging period T is large such that the time-average becomes independent of the time t.

When the flow is unsteady, a time average is not meaningful because the long-term trend and the short-term, turbulent fluctuations must be processed separately. That is, the integration limits in Equation (5-3) must be large in comparison to the turbulent time scales but small compared to the time scale of the flow motion (BRADSHAW 1971, LIGGETT 1994).

If the flow is "gradually-varied" with some distinct long-term and short-term fluctuation frequencies, $\overline{V}$ can be represented by a low-pass filtered component, or variable-interval time average VITA (PIQUET 1999). A cutoff frequency F_{cutoff} is required such that the characteristic time $1/ F_{cutoff}$ is greater than the characteristic period of turbulent fluctuations, and small with respect to the characteristic period for the time-evolution of the mean properties (PIQUET 1999, GARCIA and GARCIA 2006, KOCH and CHANSON 2008). $\overline{V}$ is called the VITA. The instantaneous fluctuation v becomes the high-pass filtered component of the measured quantity V. In a transient, highly unsteady flow, the quantities of the mean motion are determined by ensemble-averaging (BRADSHAW 1971, SCHLICHTING and GERSTEN 2001). The same experiment is repeated N times and the ensemble average is defined as:

$$\overline{V}(x, y, z, t) = \frac{1}{N} \times \sum_{i=1}^{N} V_i(x, y, z, t) \tag{5-4a}$$

When the number N of repeats is small, the ensemble-average is better defined in terms of the median value:

$$\overline{V}(x, y, z, t) = \text{Median}\left(V_i(x, y, z, t)\right)_{i=1, N} \tag{5-4b}$$

The turbulent velocity fluctuation v becomes the deviation of the instantaneous velocity V from the ensemble average $\overline{V}$ (BRADSHAW 1971).

Herein, both the ensemble-average method (EA) and the variable interval time average technique (VITA) were tested. The ensemble-average technique was based upon the repetition of 20 identical experiments (section 4.2) and the ensemble-average was calculated using Equation (5-4b). For the VITA method, the final cut-off frequency was selected based upon a sensitivity analysis between an upper limit of the filtered signal was the Nyquist frequency (herein 100 Hz) and a lower limit corresponding to a period of about 0.9 s that was the period of the residual undulations (e.g. Fig. 4-4). The results yielded an optimum threshold of F_{cutoff} = 2 Hz, and the filtering was applied to all velocity components. Note that KOCH and CHANSON (2008) selected similarly a cutoff period 1/ F_{cutoff} that was about half the undulation period, as in the present study.

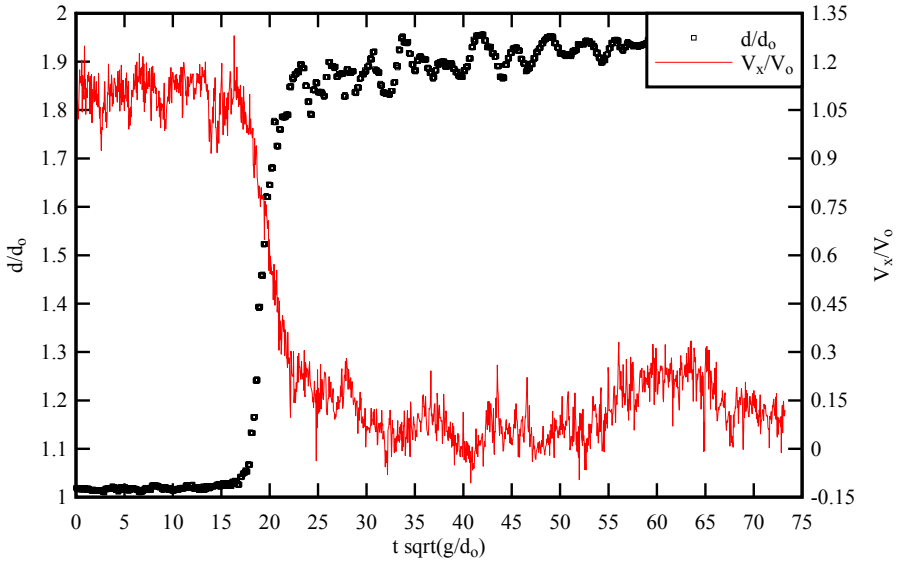

(A) Instantaneous water depth and longitudinal velocity (Run 1)

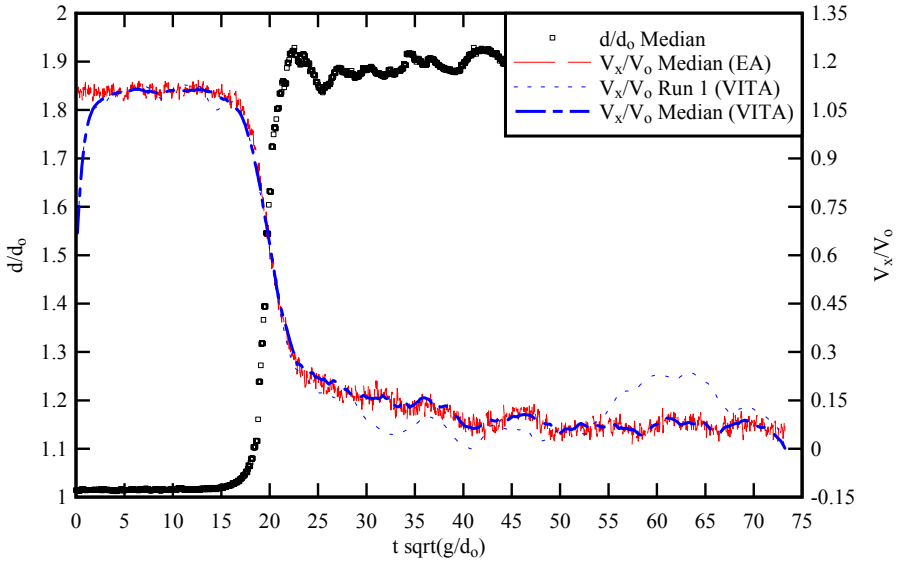

(B) Median water depth (EA 20 runs), median longitudinal velocity (EA 20 runs), low-pass filtered longitudinal velocity (VITA Run 1), median low-pass filtered longitudinal velocity (VITA, 20 Runs)

Fig. 5-1 - Water depth and longitudinal velocity component in a breaking bore - Q = 0.050 m^3/s, d_o = 0.117

m, V_o = 0.855 m/s, Fr = 1.61, z/d_o = 0.434, Smooth PVC bed

5.2 Unsteady turbulence characteristics in tidal bores

The differences in signal processing techniques are discussed herein in the context of breaking tidal bores and a detailed, thorough comparison is presented in Appendix D. Figure 5-1 illustrates the differences in signal processing techniques. Figure 5-1A presents the instantaneous water depth and longitudinal velocity for one experiment (Run 1). For the same flow conditions, Figure 5-1B shows the median water depth d_{median} and longitudinal velocity component $(V_x)_{median}$, both of which were ensemble-averaged (EA) over the 20 runs. In addition, Figure 5-1B includes the low-pass filtered longitudinal velocity, or VITA, for the experiment (Run 1) shown in Figure 5-1A as well as the median VITA value for the 20 Runs. Some preliminary remarks may be derived from Figure 5-1B. The VITA value is meaningless at both ends of the record. Both the median VITA value for the 20 runs and the ensemble average median data yielded very close results in terms of both water depth and longitudinal velocity. However the VITA data based upon a single run highlighted some difference with the EA results (Fig. 5-1B).

Figures 5-2 and 5-3 illustrate further differences between the signal processing techniques. Figures 5-2 and 5-3 present the median water depth d_{median}, the ensemble-average (EA) median velocity component V_{median} (median of 20 runs, thick red dashed line), the median value of VITA velocities (median value of 20 runs, thick blue dashed line), and all the VITA velocity for each of the 20 runs (thin black dotted line). Figure 5-2 shows some data obtained on the smooth PVC invert and Figure 5-3 presents some fixed gravel bed data.

Both the ensemble-averaged (EA) and VITA data showed some key flow features: (a) a rapid flow deceleration during the passage of the tidal bore roller above the sampling volume, (b) some negative longitudinal velocity component next to the bed highlighting some transient recirculation "bubble", (c) some positive vertical velocity component beneath the roller linked with the upward curvature of the free-surface (section 4.2). The experimental results indicated that the ensemble-average (EA) median data were very close to the median VITA value for the 20 runs. The finding is interesting considering that the ensemble-averaging method required significantly less post-processing, and tended to suggest the sound selection of the threshold frequency F_{cutoff} for the VITA technique.

The results highlighted however some differences between the EA and VITA processing techniques. The time-variations of the VITA data for each individual run presented some significant scatter compared to the ensemble-averaged median value (Fig. 5-1 to 5-3). Simply a single experiment could not provide a long-term trend comparable to the ensemble-averaged median value. Lastly note the scatter of the ensemble-averaged data around the long-term tend. It is acknowledged that the number of experimental repeats (20 herein) was small.

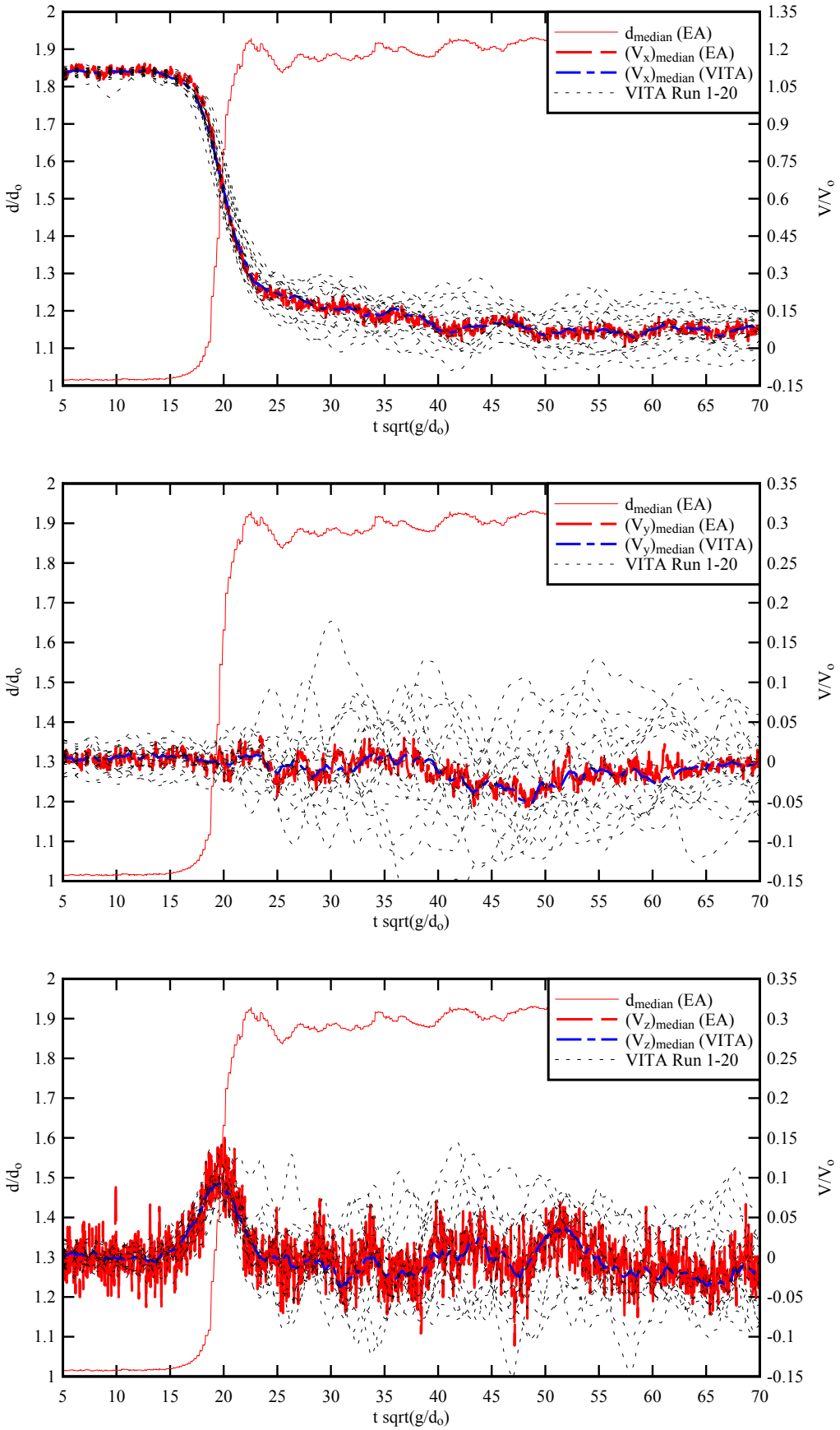

Fig. 5-2 - Dimensionless ensemble-average median water depth d_{median}, ensemble-average median velocity component V_{median}, median value of the variable interval time average (VITA) velocity component (median value of 20 runs), and low-pass filtered velocity components (VITA Runs 1 to 20) at $z/d_o = 0.434$ - Smooth

PVC bed - From top to bottom: V_x, V_y and V_z

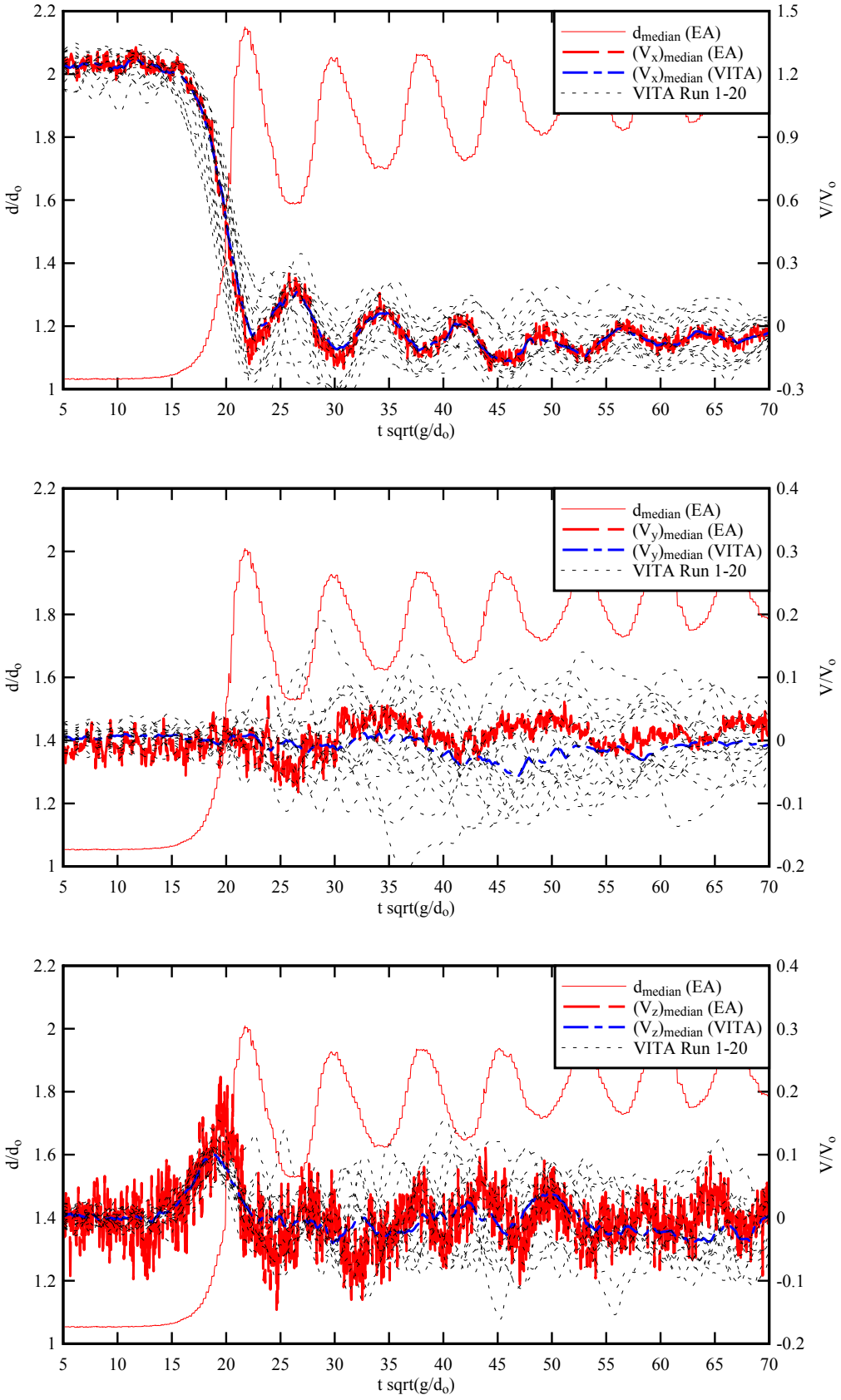

Fig. 5-3 - Dimensionless ensemble-average median water depth d_{median}, ensemble-average median velocity component V_{median}, median value of the variable interval time average (VITA) velocity component (median value of 20 runs), and low-pass filtered velocity components (VITA Runs 1 to 20) at $z/d_o = 0.434$ - Fixed

gravel bed - From top to bottom: V_x, V_y and V_z

Figures 5-4 and 5-5 show some comparison between the free-surface fluctuations (d_{75}-d_{25}), the velocity fluctuations (V_{75}-V_{25}) and the variance of the velocity component v^2. The graphs present the median water depth d_{median} and the difference between 3rd and 4th quartiles for the water depth (d_{75}-d_{25}) for the smooth PVC and fixed gravel beds respectively. Each graph includes further the median velocity component V_{median} (median of 20 runs) and the difference between 3rd and 4th quartiles (V_{75}-V_{25}), as well as the median value of the variable interval time average (VITA) velocity component (median value of 20 runs), and the variance of the velocity component v^2. Herein the median water depth and velocity components were ensemble-averaged over the 20 runs, while the variance was calculated for the 20 runs. The median VITA value was calculated as the median VITA for the 20 Runs.

The experimental results showed that the passage of the roller was always associated in some large free-surface fluctuations, associated with some large longitudinal velocity fluctuations v_x^2 and some upwards flow motion ($V_z > 0$) (Fig. 5-4 & 5-5). The effect of the sampling volume vertical elevation is illustrated in Figures 5-4 and 5-5 in terms of the horizontal and vertical velocity components. The transient recirculation region ("bubble") was restricted to the flow region next to the bed: $z/d_o < 0.31$ and 0.56 for smooth PVC and fixed gravel bed respectively (section 4.1). In the upper flow region, no negative longitudinal velocity was recorded (Fig. 5-4B & 5-5B).

5.3 Turbulent Reynolds stresses in breaking tidal bores

The Reynolds stress tensor is a transport effect resulting from turbulent motion induced by velocity fluctuations with its subsequent increase of momentum exchange and of mixing (PIQUET 1999). Herein the instantaneous turbulent stresses were calculated using the ensemble-averaging (EA) and variable interval time averaging (VITA) techniques for the flow properties summarised in Table 4-2. The complete data sets are reported in Appendix E, and some typical results are presented in Figure 5-6. In Figure 5-6, the median Reynolds stress tensor components were calculated using either the ensemble-averaging (EA) and variable interval time averaging (VITA) methods (median value of 20 runs).

The turbulent stress results showed a number of seminal features. Overall the turbulent stress data suggested that the passage of breaking tidal bores was associated with large turbulent stresses at all vertical elevations. That is, the magnitude of the Reynolds stress tensor components was significantly larger than prior to the bore passage. The finding was consistent with the observations of KOCH and CHANSON (2009), but that study deduced the turbulent stresses from a VITA analysis of a single experiment. KOCH and CHANSON did not present any ensemble-averaged nor VITA median data. Second, both the ensemble-averaging and variable interval time averaging techniques yielded comparable results (Fig. 5-6).

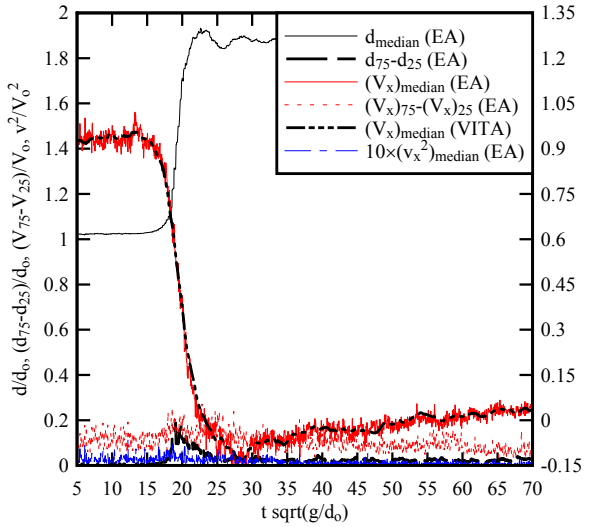

(A) Horizontal velocity component, $z/d_o = 0.135$

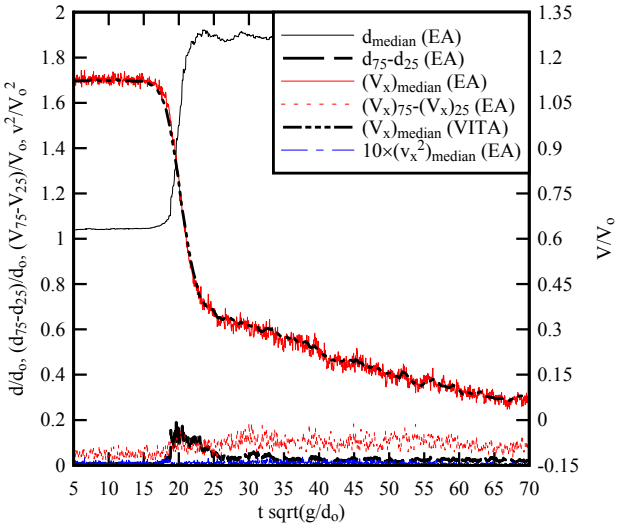

(B) Horizontal velocity component, $z/d_o = 0.733$

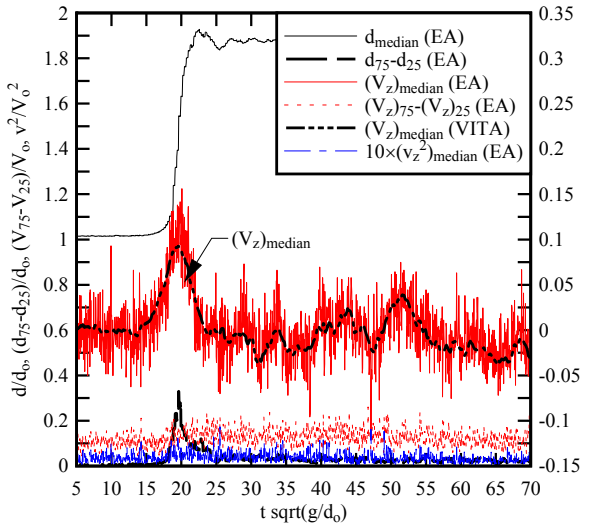

(C) Vertical velocity component, $z/d_o = 0.434$

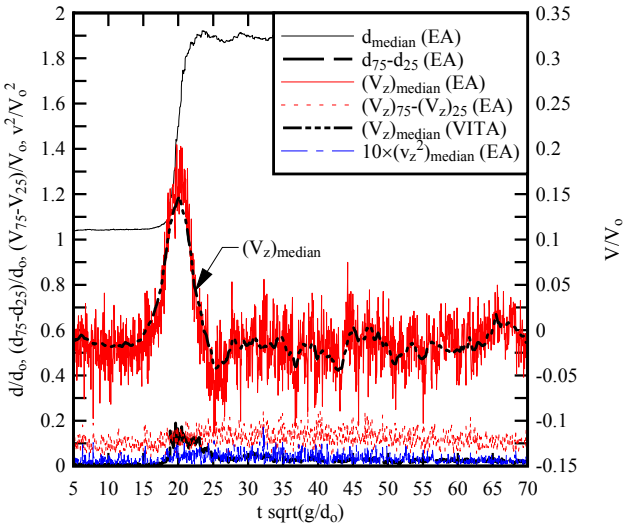

(D) Vertical velocity component, $z/d_o = 0.733$

Fig. 5-4 - Dimensionless ensemble-average (EA) median water depth d_{median}, difference between 3rd and 4th quartiles of the water depth (d_{75}-d_{25}), ensemble-average median velocity component V_{median}, difference between 3rd and 4th quartiles of the velocity component (V_{75}-V_{25}), median value of the variable interval time average (VITA) velocity component (median value of 20 runs), and variance of velocity component v^2 (ensemble-average of 20 runs) - Smooth PVC bed

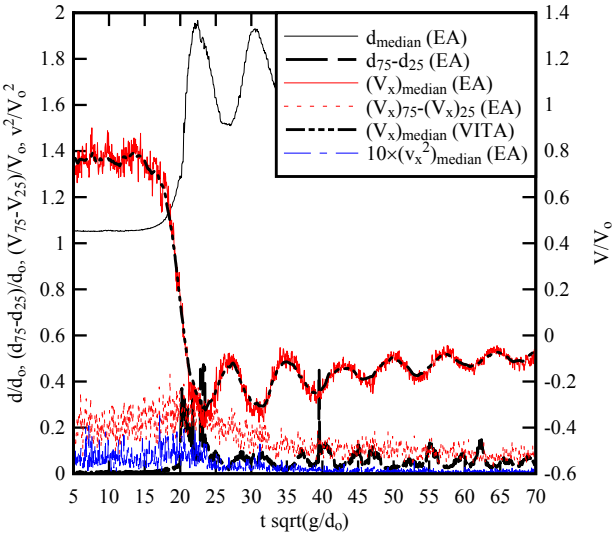

(A) Horizontal velocity component, $z/d_o = 0.135$

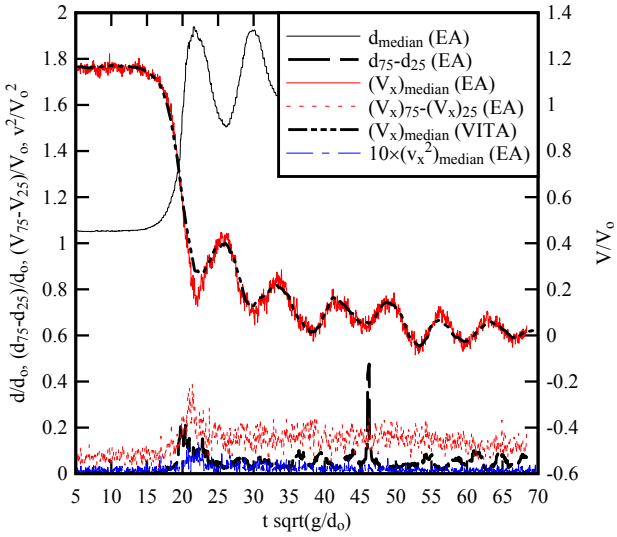

(B) Horizontal velocity component, $z/d_o = 0.733$

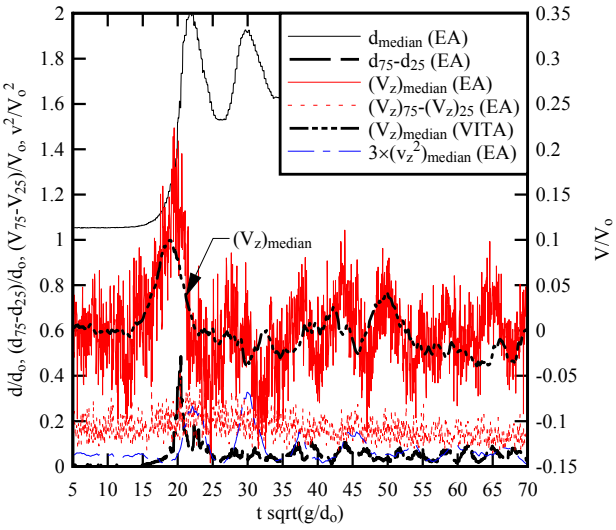

(C) Vertical velocity component, $z/d_o = 0.434$

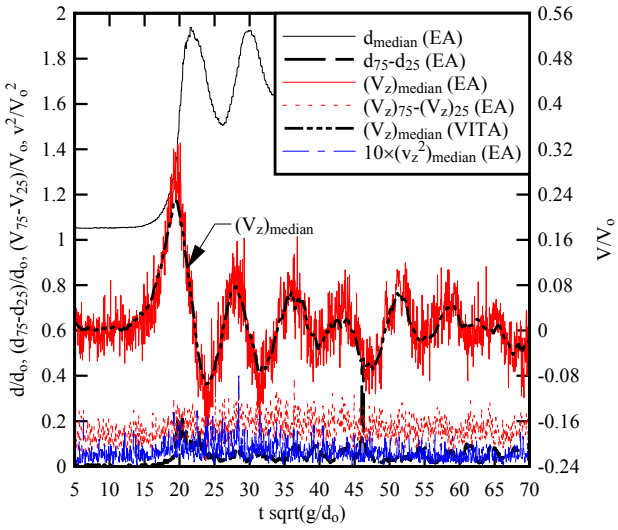

(D) Vertical velocity component, $z/d_o = 0.733$

Fig. 5-5 - Dimensionless ensemble-average (EA) median water depth d_{median}, difference between 3rd and 4th quartiles of the water depth (d_{75}-d_{25}), ensemble-average median velocity component V_{median}, difference between 3rd and 4th quartiles of the velocity component (V_{75}-V_{25}), median value of the variable interval time average (VITA) velocity component (median value of 20 runs), and variance of velocity component v^2 (ensemble-average of 20 runs) - Fixed gravel bed

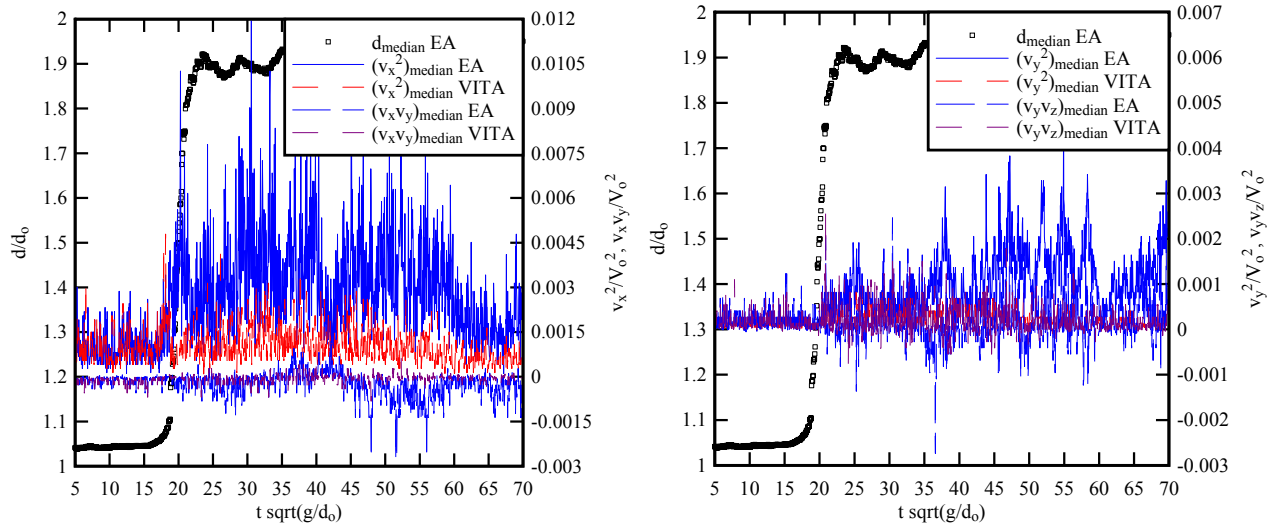

(A) $z/d_o = 0.733$, Smooth PVC bed

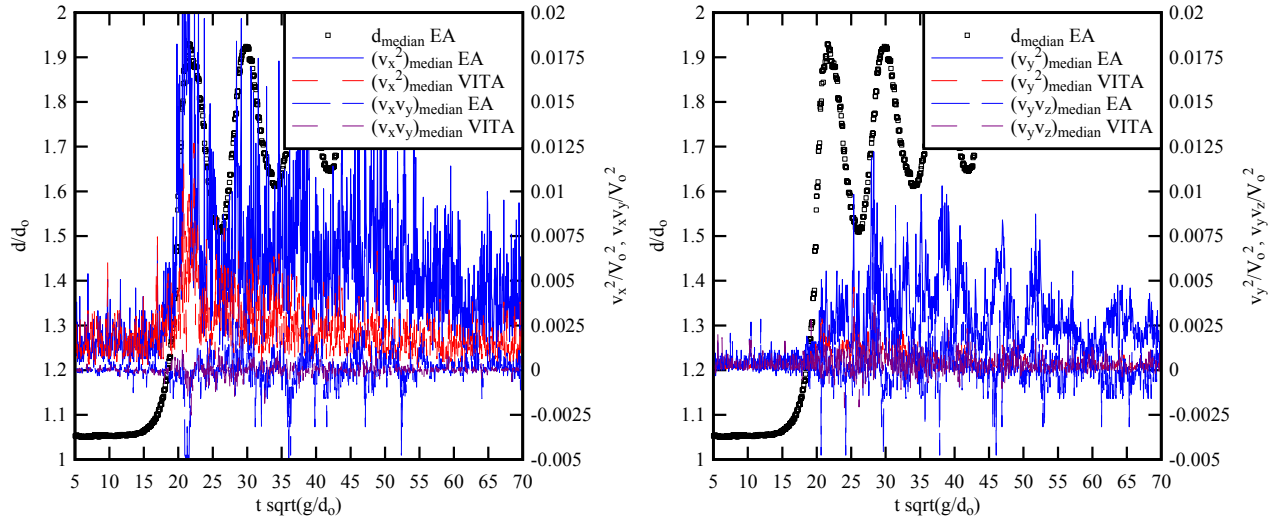

(B) $z/d_o = 0.733$, Fixed gravel bed

Fig. 5-6 - Dimensionless ensemble-average median water depth d_{median}/d_o and median Reynolds stresses v_x^2/V_o^2 and $v_x \times v_y/V_o^2$ (Left), and v_y^2/V_o^2 and $v_y \times v_z/V_o^2$ (Right) on smooth PVC and fixed gravel beds - Comparison between ensemble-averaged and VITA calculations

5.4 Concluding remarks

Both the ensemble average (EA) and variable interval time average (VITA) methods were tested to characterise the turbulence properties in breaking tidal bores. The experimental results showed a number of key features of the EA and VITA techniques:

- The VITA data based upon a single run presented some non-negligible differences with the EA median results in terms of all velocity components.

- The median value for the 20 VITA data and the ensemble average (EA) median yielded very close results in terms of both water depth and velocity components. The finding tended to support the selection of an appropriate cutoff frequency $F_{cutoff} = 2$ Hz.

- Both the EA and VITA methods showed some comparable long-term trends superposed to some rapid

turbulent fluctuations. The result is valuable indicating that the method with less post-processing (EA technique) gave valid results.

- The turbulent stress data showed comparable results with both EA and VITA techniques. Again the result highlighted the validity of the EA method with less post-processing.

6. Conclusion

The propagation of tidal bores induces some substantial turbulent mixing in natural estuaries. Herein the turbulence in breaking tidal bores was investigated experimentally under controlled flow conditions. Some detailed measurements of free-surface fluctuations were recorded using a non-intrusive method based upon acoustic displacement meters. Some Eulerian velocity measurements were sampled with a high temporal and spatial resolution using acoustic Doppler velocimetry (200 Hz, sampling volume: $6\times6\times1.5$ mm^3). Further two types of bed roughness were tested: smooth PVC and fixed gravel bed (k_s = 3.4 mm).

Some qualitative observations were conducted with tidal bore Froude numbers between 1 and 1.7. Both undular and breaking bores were observed. The tidal bore flow patterns were independent of the bed roughness, as well as of the initial steady flow conditions. The free-surface properties were close to earlier findings. Using an ensemble-averaging technique, the free-surface fluctuations of breaking tidal bores were characterised. Immediately prior to the roller, the free-surface curved gradually upwards and the gentle surface elevation rise was about $0.1\times d_o$ where d_o is the initial water depth. The passage of the bore roller was associated with some large water depth fluctuations; the largest free-surface fluctuations were observed during the first third of the bore roller.

Some detailed turbulent velocity measurements were performed at several vertical elevations during and shortly after the breaking bore passage. Both the instantaneous and ensemble-averaged velocity data highlighted some seminal features of breaking tidal bores. Namely a strong flow deceleration was observed at all elevations during the tidal bore passage. Close to the bed, the longitudinal velocity component became negative immediately after the roller passage implying the existence of a transient recirculation "bubble". The height and duration of the transient was a function of the bed roughness, with a longer, higher recirculation region above the fixed gravel bed. The vertical velocity data presented some positive, upward motion during the bore passage with increasing maximum vertical velocity with increasing distance from the bed. The vertical motion was believed to be linked with some streamline curvature. The transverse velocity data presented some large fluctuations with non-zero ensemble-average after the roller passage that highlighted some intense secondary motion advected behind the bore front.

A comparison between the ensemble-average (EA) and variable interval time average (VITA) velocity calculations was developed. Both the EA and VITA results showed some comparable velocity pattern with some relatively-long-term data trend superposed to some high-frequency turbulent fluctuations. While both methods should converge to the same asymptotic trend, the data showed that the VITA calculations over a single experiment presented some non-negligible difference with the EA median value for all velocity components. The EA median value and the median of 20 VITA data sets yielded very close results suggesting that the selection of cutoff frequency was sound. The results showed further that the EA method with the least post-processing gave valid results. The turbulent stress data highlighted larger median Reynolds stresses during and shortly after the tidal bore passage than prior to.

Overall the study demonstrated the intensive turbulence and turbulent mixing under a breaking tidal bore.

7. Acknowledgements

The authors acknowledge the technical assistance of Graham ILLIDGE and Clive BOOTH (The University of Queensland). The authors thank further Prof. Laurent DAVID (University of Poitiers, France) and Dr David REUNGOAT (University of Bordeaux, France) for their detailed reviews of the report and valuable comments. Prof. C.J. APELT (University of Queensland) provided some helpful advice.

Appendix A - Photographs of the tidal bore experiments

A.1 Presentation

New experiments were performed in the Gordon McKAY Hydraulics Laboratory at the University of Queensland. The channel was horizontal, 12 long and 0.5 m wide. The sidewalls were made of 0.45 m high glass panels and the bed was made of 12 mm thick PVC sheets. For some experiments, a rough gravel bed was installed.

Notation

B	channel width (m);
d_o	initial flow depth (m) measured at x = 5 m;
Fr	tidal Froude number: $Fr = (V_o + U) / \sqrt{g \times d_o}$;
g	gravity acceleration (m/s^2): g = 9.80 m/s^2 in Brisbane (Australia);
h	tainter gate opening (m) after fast closure;
Q	water discharge (m^3/s);
t'	time (s);
U	tidal bore celerity (m/s) for an observer standing on the bank and positive upstream;
V_o	initial flow velocity (m/s): $V_o = Q/(B \times d_o)$;
x	longitudinal distance from the channel upstream end (m);

Subscript

o	initial flow conditions.

Fig. A-1 - Details of the small roller of an advancing undular bore with a breaking front (Filename: P1160033.jpg) - Q = 0.0435 m^3/s, d_o = 0.138 m, U = 0.95 m/s, Fr = 1.34, bore propagation from left to right,

shutter speed: 1/80 s

Fig. A-2 - Looking beneath the roller of an advancing bore (Filename: P1160045.jpg) - Q = 0.0515 m^3/s, d_o = 0.144 m, U = 0.96 m/s, Fr = 1.41, bore propagation from left to right, shutter speed: 1/80 s

Fig. A-3 - Looking downstream at the incoming tidal bore roller (Filename: P1160051b.jpg) - Q = 0.0515 m^3/s, d_o = 0.144 m, U = 0.96 m/s, Fr = 1.41, shutter speed: 1/80 s

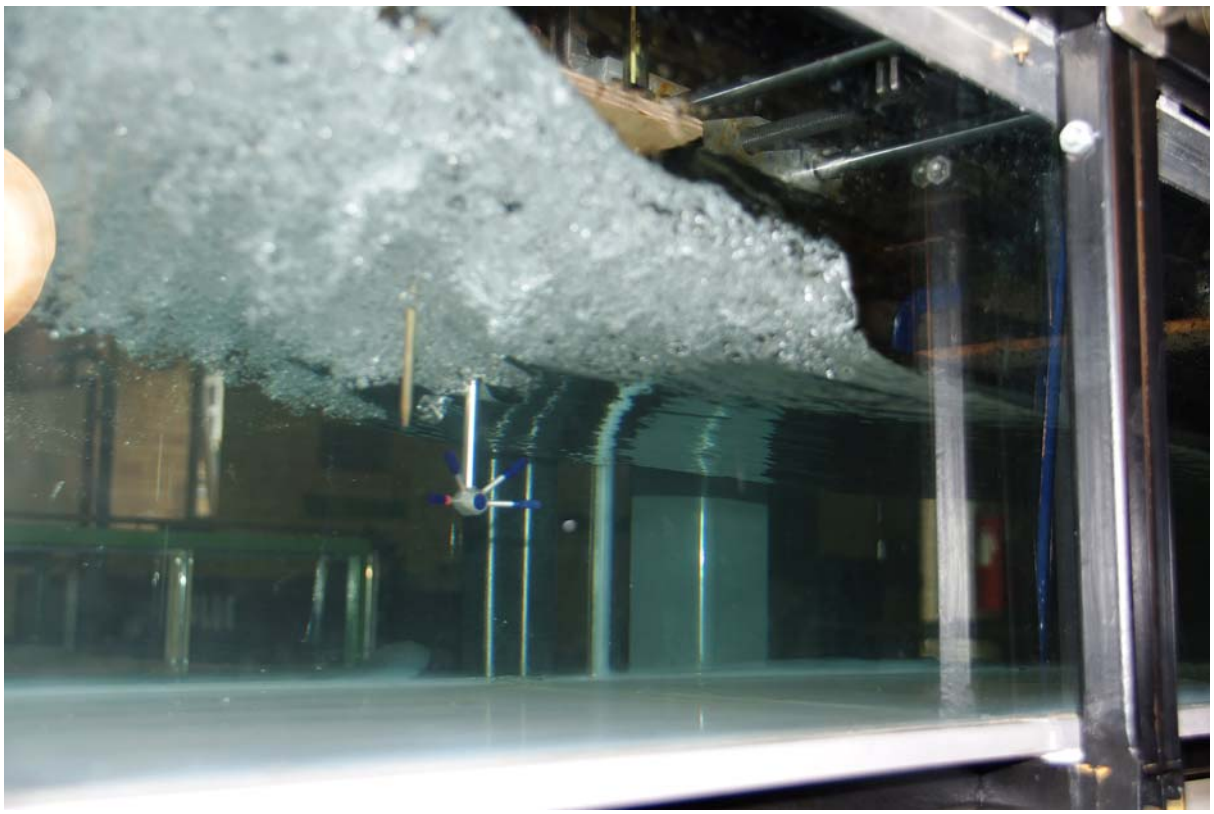

Fig. A-4 - Looking beneath the roller of an advancing bore (Filename: IMGP0255b.jpg) - Q = 0.050 m^3/s, d_o = 0.116 m, U = 0.85 m/s, Fr = 1.6, bore propagation from left to right - Note the ADV sidelooking-head and submerged point gauge, shutter speed: 1/60 s

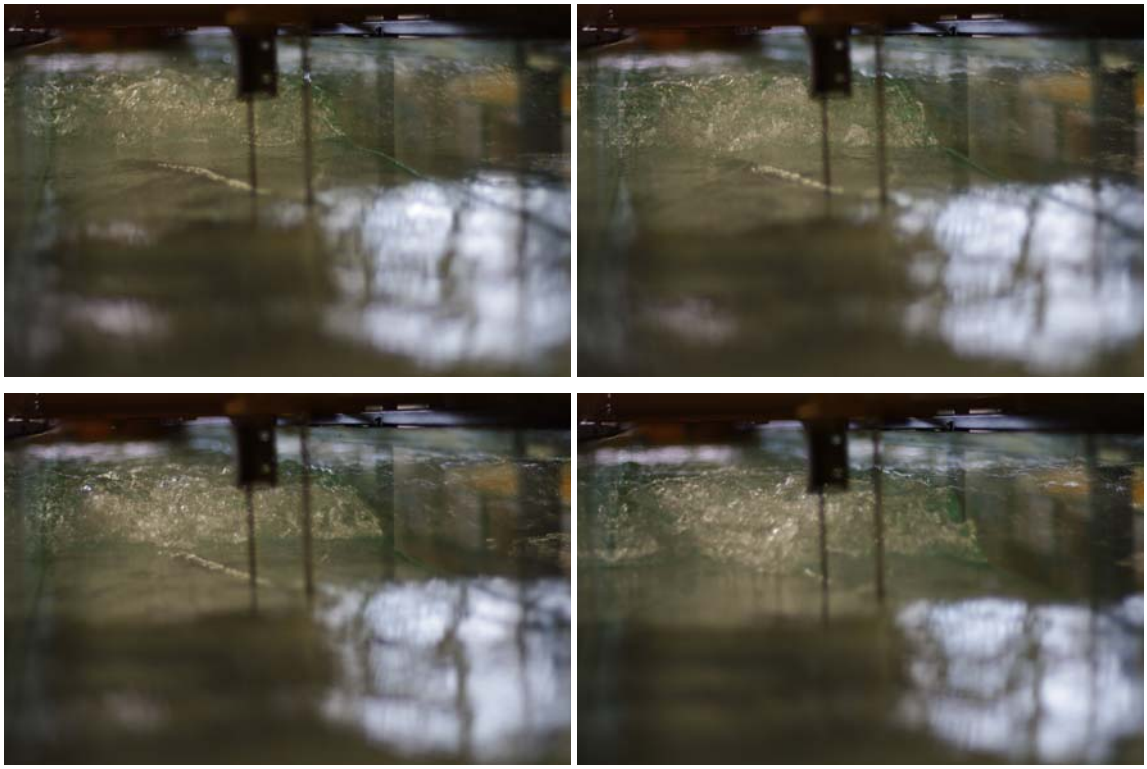

Fig. A-5 - Looking downstream at the incoming tidal bore roller (Filenames: IMGP0314b.jpg to IMGP0317b.jpg) - Q = 0.050 m^3/s, d_o = 0.116 m, U = 0.85 m/s, Fr = 1.6, shutter speed: 1/100 s, continuous shooting at 5.2 fps (from left to right, top to bottom) with Voigtlander Nokton 58mm f1.4 lens

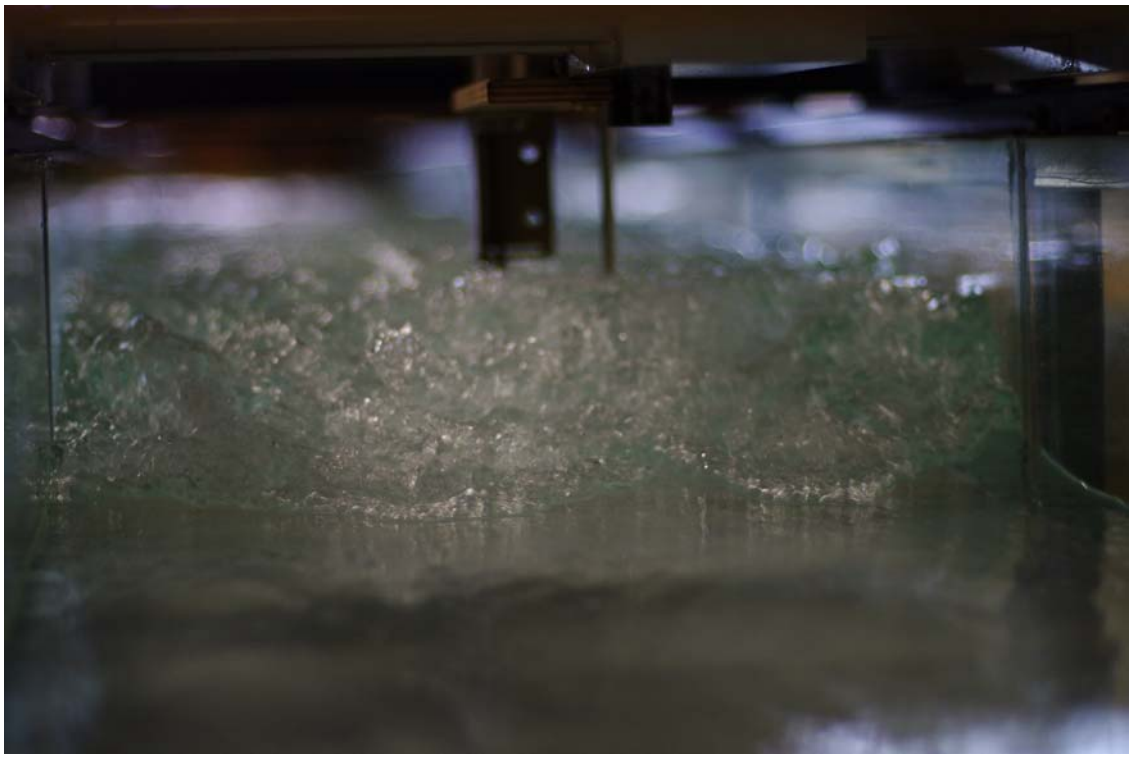

Fig. A-6 - Looking downstream at the incoming tidal bore roller (Filename: IMGP0326b.jpg) - Q = 0.050 m^3/s, d_o = 0.116 m, U = 0.85 m/s, Fr = 1.6, shutter speed: 1/100 s, lens: Voigtlander Nokton 58mm f1.4

Fig. A-7 - Looking downstream at the incoming tidal bore roller (Filename: IMGP0331b.jpg) - Q = 0.050 m^3/s, d_o = 0.116 m, U = 0.85 m/s, Fr = 1.6, shutter speed: 1/100 s, lens: Voigtlander Nokton 58mm f1.4

Fig. A-8 - Tidal bore generation immediately after the tainter gate closure (h = 0) and bore propagation at x = 8 m and 4 m above the fixed gravel bed (Filenames: IMGP0449b.jpg to IMGP0451b.jpg) - Q = 0.050 m^3/s, d_o = 0.139 m, fixed gravel bed, shutter speed: 1/50 s, lens: Voigtlander Nokton 58mm f1.4

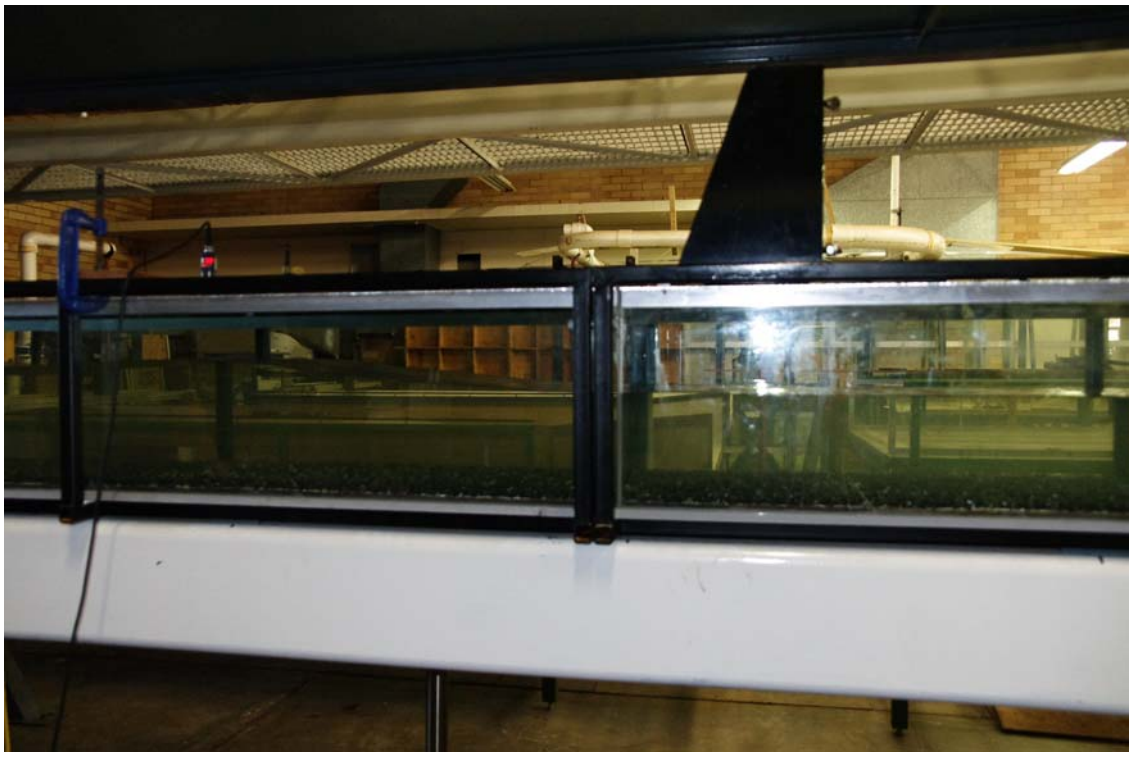

Fig. A-9 - Propagation of a smooth, two-dimensional undular tidal bore above the fixed gravel bed (Filenames: IMGP0453b.jpg to IMGP0456b.jpg) - Q = 0.050 m^3/s, d_o = 0.139 m, h = 0.050 m, fixed gravel bed, shutter speed: 1/50 s, lens: Voigtlander Nokton 58mm f1.4 - Propagation times: t' = 0, 6, 12 and 14 s from top to bottom

Fig. A-10 - Advancing undular tidal bore (Filename: IMGP0463b.jpg) - Q = 0.050 m^3/s, d_o = 0.139 m, h = 0.050 m, fixed gravel bed, shutter speed: 1/50 s, lens: Voigtlander Nokton 58mm f1.4 - The wave crest was about x = 1 m and the photograph was taken upstream of the fixed gravel bed section

Fig. A-11 - Advancing breaking tidal bore roller (Filename: P1160216.jpg) - Q = 0.050 m^3/s, d_o = 0.120 m, Fr = 1.58, fixed gravel bed, shutter speed: 1/80 s - The ADV stem (on right) is visible behind the roller

Fig. A-12 - Advancing breaking tidal bore roller (Filename: IMGP0505.jpg) - Q = 0.050 m^3/s, d_o = 0.120 m, Fr = 1.58, fixed gravel bed, shutter speed: 1/60 s, lens: Voigtlander Nokton 58mm f1.4

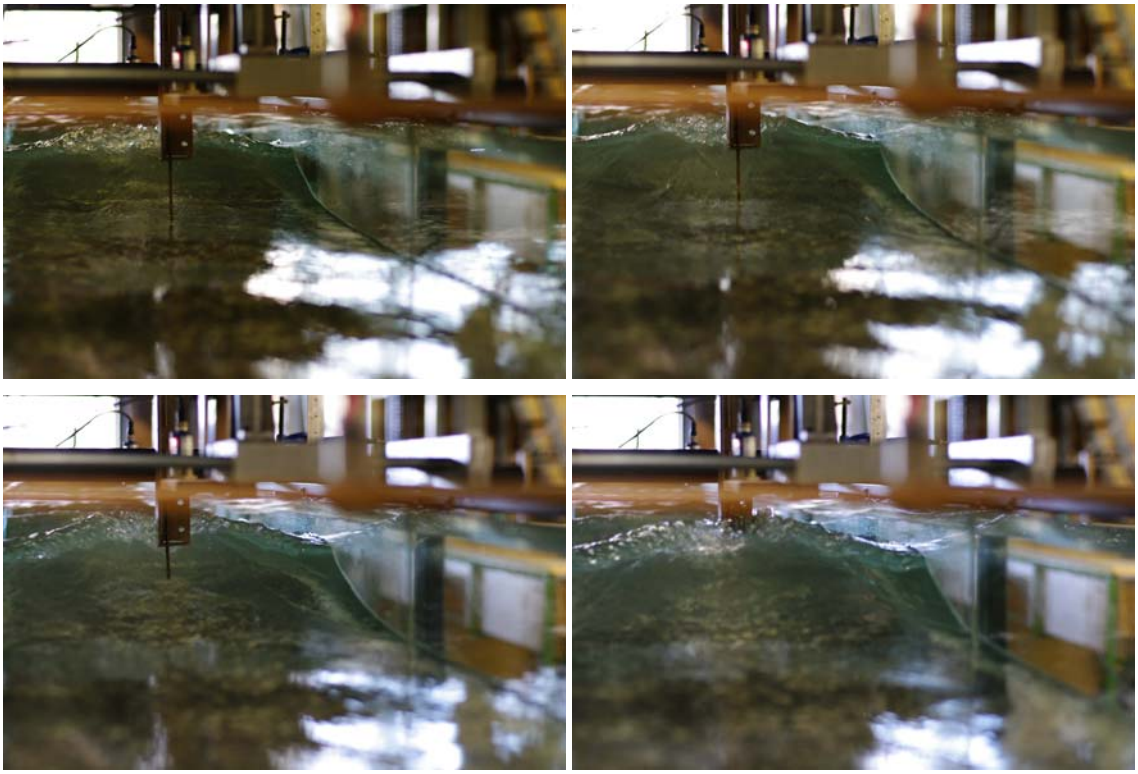

Fig. A-13 - Advancing undular tidal bore roller with shock waves and breaking roller (Filenames: IMGP0483b.jpg to IMGP0486b.jpg) - Q = 0.050 m^3/s, d_o = 0.120 m, h = 0.010 m, Fr = 1.5, fixed gravel bed, shutter speed: 1/60 s, continuous shooting at 5.2 fps (from left to right, top to bottom) with Voigtlander Nokton 58mm f1.4 lens

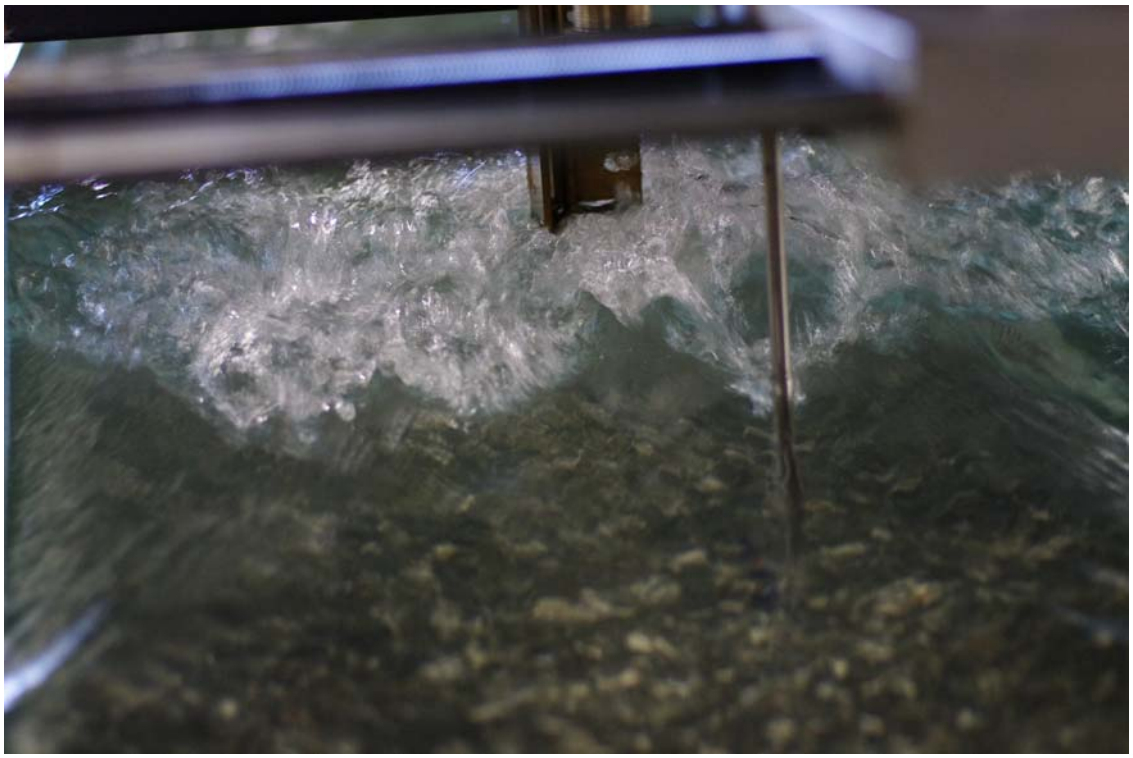

Fig. A-14 - Advancing undular tidal bore with a roller (Filename: IMGP0659b.jpg) - Q = 0.050 m^3/s, d_o = 0.125 m, Fr = 1.5, fixed gravel bed, shutter speed: 1/60 s, lens: Voigtlander Nokton 58mm f1.4 - The bore roller almost reached the ADV stem

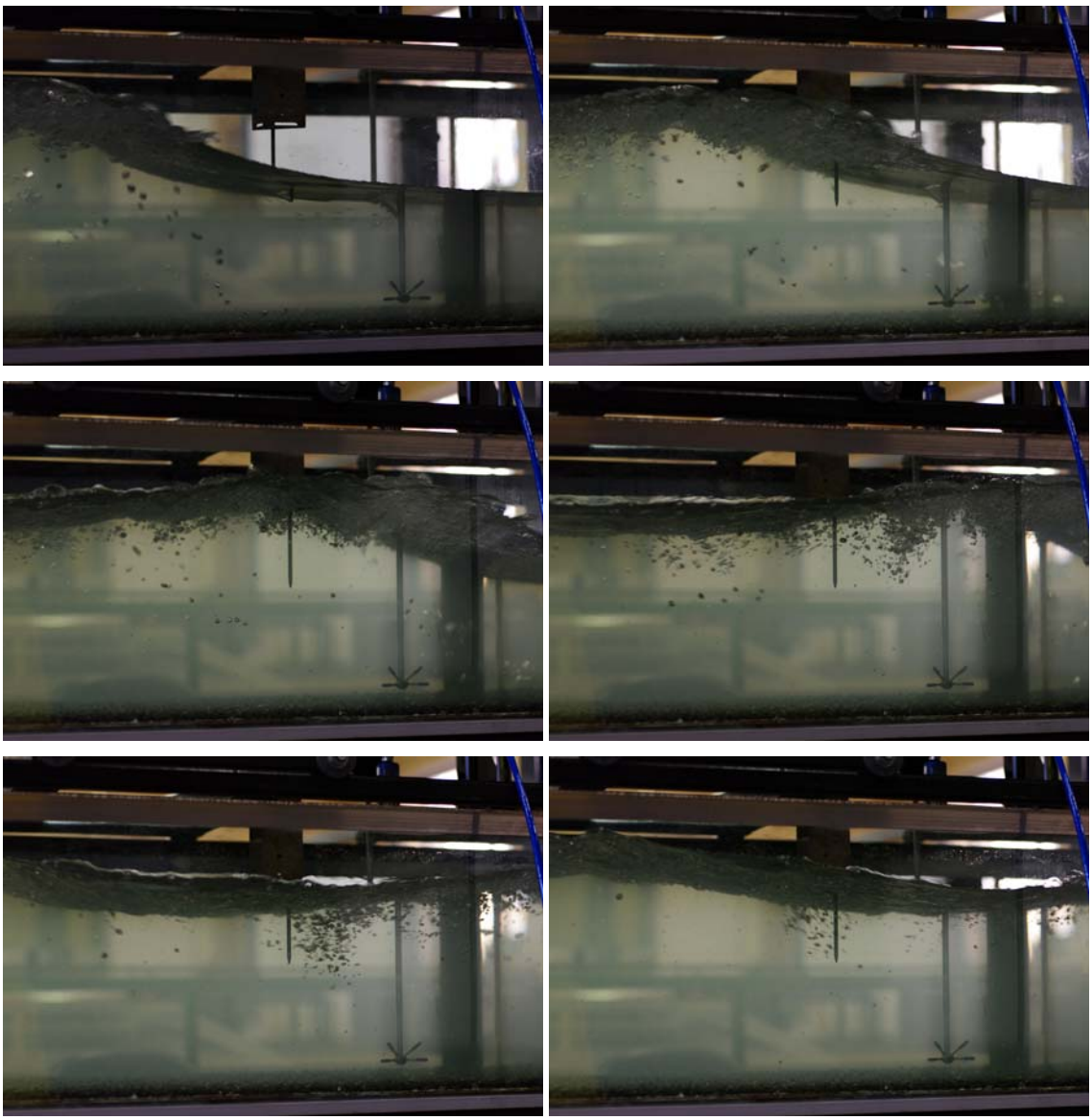

Fig. A-15 - Advancing undular tidal bore roller with shock waves and breaking roller (Filenames: IMGP0632b.jpg to IMGP0637b.jpg) - Q = 0.050 m^3/s, d_o = 0.125 m, Fr = 1.5, fixed gravel bed, shutter speed: 1/100 s, continuous shooting at 5.2 fps (from left to right, top to bottom) with Voigtlander Nokton 58mm f1.4 lens - Note the underwater bubble "trail" behind the bore roller

Appendix B - Effect of bed proximity on the ADV signal

B.1 Presentation

The acoustic Doppler velocimetry (ADV) is designed to record instantaneous velocity components at a single-point with a relatively high frequency. Measurements are performed by measuring the velocity of particles in a remote sampling volume based upon the Doppler shift effect (VOULGARIS and TROWBRIDGE 1998, McLELLAND and NICHOLAS 2000). The probe head includes one transmitter and between two to four receivers (Fig. B-1). Figure 1 show an example of ADV head equipped with four receivers. The remote sampling volume is located typically 5 or 10 cm from the tip of the transmitter (5 cm herein), but some studies showed that the distance might change slightly. The sampling volume size is determined by the sampling conditions and manual setup. In a standard configuration, the sampling volume is about a cylinder of water with a diameter of 6 mm and a height of 9 mm, although some newer laboratory ADVs may be configured with a smaller sampling volume (e.g. Sontek microADV, Nortek Vectrino+).

A typical ADV system equipped with N receivers records simultaneously 4×N values with each sample. That is, for each receiver, a velocity component, a signal strength value (or amplitude), a signal-to-noise (SNR) and a correlation value. The signal strength, SNR and correlation values are used primarily to determine the quality and accuracy of the velocity data, although the signal strength (acoustic backscatter intensity) may related to the instantaneous suspended sediment concentration in the sampling volume with proper calibration (CHANSON et al. 2008b). The velocity component is measured along the line connecting the sampling volume to each receiver (dotted line sin Fig. B-1). The velocity data must be transformed into a Cartesian system of coordinates and the trigonometric transformation may cause some velocity resolution errors.

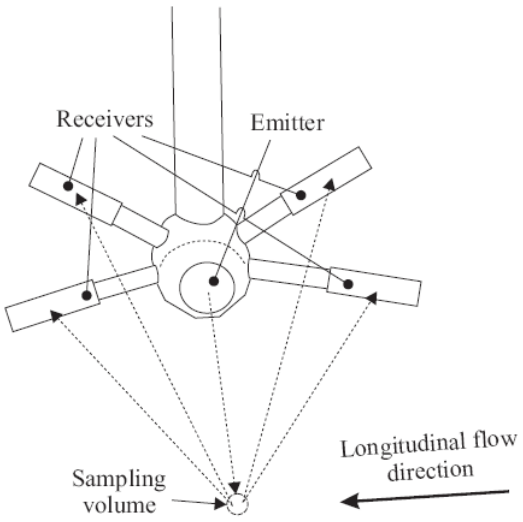

Fig. B-1 - Sketch of the Nortek™ Vectrino+ ADV side-looking head equipped with 4 receivers

Although the acoustic Doppler velocimetry (ADV) has become a popular technique in laboratory and field applications, several researchers pointed out accurately that the ADV signal outputs include the combined effects of turbulent velocity fluctuations, Doppler noise, signal aliasing, turbulent shear and other

disturbances. Evidences included by high levels of noise and spikes in all velocity components (NIKORA and GORING 1998, McLELLAND and NICHOLAS 2000, CHANSON 2008b). In turbulent flows, the ADV velocity outputs are a combination of Doppler noise, signal aliasing, velocity fluctuations, installation vibrations and other disturbances. The signal may be further affected adversely by velocity shear across the sampling volume and boundary proximity (CHANSON et al. 2007). LEMMIN and LHERMITTE (1999), CHANSON et al. (2002), and BLANCKAERT and LEMMIN (2006) discussed the inherent Doppler noise of an ADV system. Spikes may be caused by aliasing of the Doppler signal. McLELLAND and NICHOLAS (2000) explained the physical processes while NIKORA and GORING (1998), GORING and NIKORA (2002) and WAHL (2003) developed techniques to eliminate aliasing errors called "spikes". These methods were developed for steady flow situations and tested in man-made channels. Not all of them are reliable, and the phase-space thresholding despiking technique appears to be a robust method in steady and gradually-varied flows (WAHL 2003, CHANSON et al. 2008a). Simply the "raw" ADV velocity data are not "true" turbulent velocities and they should never be used without adequate post-processing (e.g. NIKORA and GORING 1998, CHANSON 2008b).

B.2 Effect of bed proximity

The proximity of a solid boundary may affect adversely the ADV probe output, especially in small flumes. Several studies discussed the effects of boundary proximity on sampling volume characteristics and the impact on the time-averaged velocity (CHANSON et al. 2007, CHANSON 2008b). The findings highlighted that the acoustic Doppler velocimeters underestimated the streamwise velocity component when the solid boundary was less than 30 to 45 mm from the probe sampling volume. Some correction correlations were proposed by LIU et al. (2002) and KOCH and CHANSON (2005) for Sontek microADV units.

Figures B-2 and B-3 illustrates the effect of solid boundaries on the Nortek Vectrino+ ADV signals at three vertical elevations with a fixed gravel bed ([1]). Close to the wall (z = 0.0166 m), the effects of wall proximity on the ADV velocity signal were characterised by some acoustic beams reflection on the fixed gravel bed, with the presence of a secondary peak in SNR and amplitude about 100 mm from the emitter (Fig. B-2 Top & B-3 Top). Note the other peaks at 50 mm and 300 mm from the emitter. The former (50 mm) was the location of the sampling volume while the latter (300 mm) corresponded to the left sidewall. The effects of wall proximity on the ADV velocity signal were characterised by a significant drop in average signal correlations, in average signal-to-noise ratios and in average signal amplitudes next to the wall.

Lastly, past and present comparative studies were restricted to limited comparisons of the time-average streamwise velocity component. No comparative test was performed to assess independently the effect of boundary proximity on instantaneous velocities, turbulent velocity fluctuations, Reynolds stresses nor other turbulence characteristics.

[1] The vertical elevation z was measured above the top of the gravel bed using a semi-circular footing with a 25.1 cm^2 area seen in Figure 2-3 (inset).

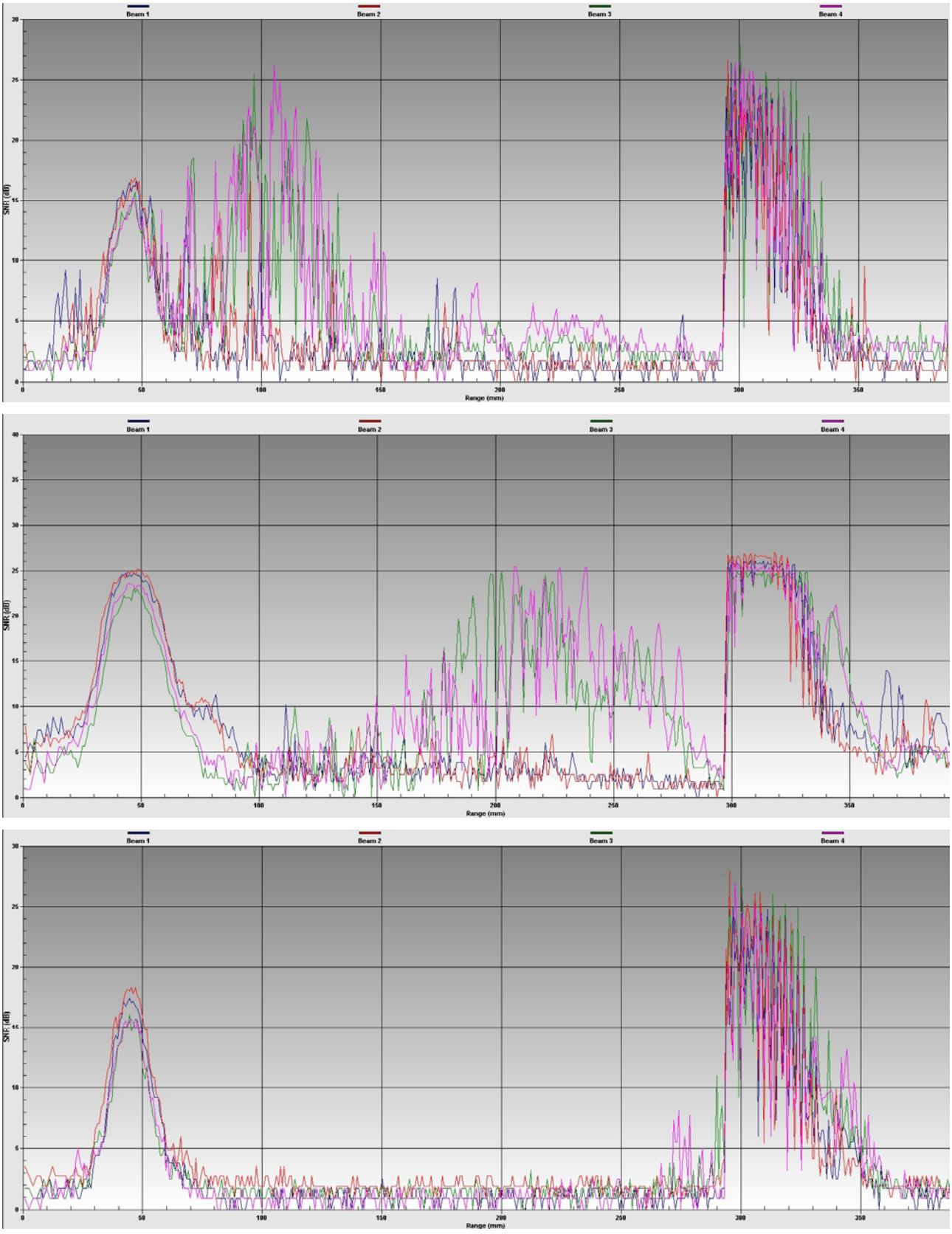

Fig. B-2 - Instantaneous signal-to-noise ratio (SNR) as a function of the distance from the emitter at z = 0.0166, 0.0547 and 0.0927 m (Top to bottom) with a Vectrino+ ADV using a side-looking head equipped with 4 receivers - Data: Q = 0.050 m^3/s, x = 5 m, d_o = 0.126 m, sampling rate: 200 Hz, velocity range: 1 m/s, fixed gravel bed

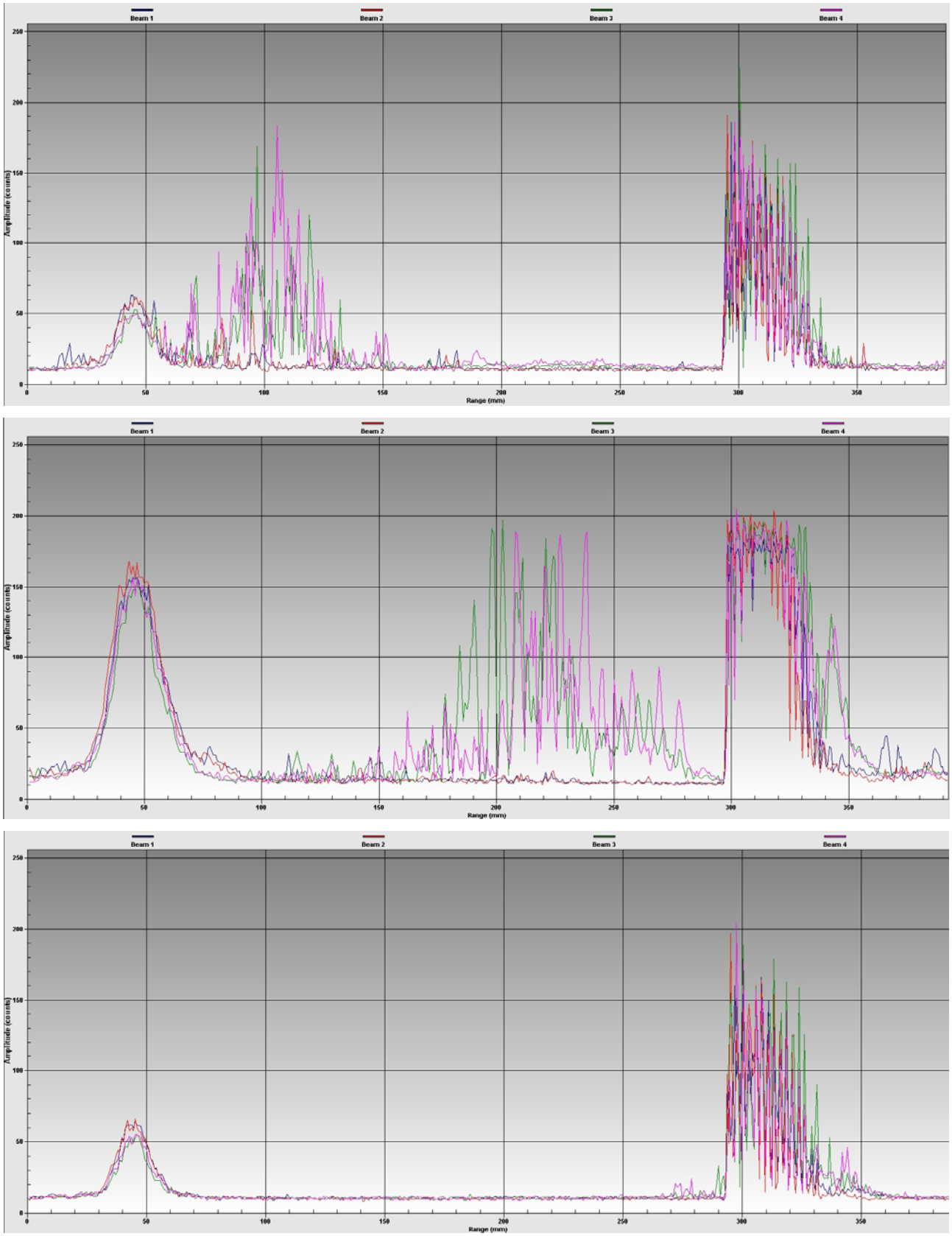

Fig. B-3 - Instantaneous signal amplitude (counts) as a function of the distance from the emitter at z = 0.0166, 0.0547 and 0.0927 m (Top to bottom) with a Vectrino+ ADV using a side-looking head equipped with 4 receivers - Data: Q = 0.050 m^3/s, x = 5 m, d_o = 0.126 m, sampling rate: 200 Hz, velocity range: 1 m/s, fixed gravel bed

Appendix C - Ensemble-averaged velocity data in a breaking bore

C.1 Presentation

In a tidal bore with a marked roller, a series of twenty instantaneous velocity records were repeated at three vertical elevations above both smooth PVC and fixed gravel beds (Table C-1). The acoustic Doppler velocimeter (ADV) sampled the instantaneous velocity components on the channel centreline at x = 5m, and the three sampling locations were z/d_o = 0.135, 0.434 and 0.733. Between each repeat, the initial flow conditions were left unchanged for five minutes to achieve the same well-defined initially-steady flow conditions. An ensemble-median of each instantaneous velocity component was produced for each vertical elevation on both smooth PVC and fixed gravel beds. All data were synchronised in terms of the characteristic time t_2 (Fig. 3-8).

Table C-1 - Experimental flow conditions for ensemble-average of turbulent velocity measurements in breaking tidal bores

Q (m^3/s) (1)	S_o (2)	Bed roughness (3)	d_o (m) (4)	V_o (m/s) (5)	Bore type (6)	Fr (7)	U (m/s) (8)	z/d_o (9)
0.050	0.000	Smooth PVC	0.117	0.855	Breaking	1.61	0.869	0.135 0.434 0.733
	0.002	Fixed gravel bed (k_s = 3.4 mm)	0.126	0.794	Undular/Breaking	1.50	0.877	0.135 0.434 0.733

Note: tainter gate opening after closure: h = 0.

Notation

d	(a) flow depth (m) measured normal to the invert; (b) flow depth (m) measured above the fixed gravel bed;
d_o	initial flow depth (m) measured normal to the chute invert;
Fr	tidal bore Froude number defined as: $Fr = (V_o + U) / \sqrt{g \times d_o}$;
g	gravity constant (m/s^2): g = 9.80 m/s^2 in Brisbane, Australia;
Q	volume flow rate (m^3/s);
S_o	bed slope: $S_o = \sin\theta$;
U	tidal bore front celerity (m/s) for an observer standing on the bank, positive upstream;
V_x	longitudinal velocity (m/s) positive downstream;
V_y	transverse velocity (m/s) positive towards the left sidewall;
V_z	vertical velocity (m/s) positive upwards;
V_o	initial flow velocity (m/s) positive downstream: $V_o = q/d_o$;
x	longitudinal distance (m) measured from the channel upstream end, positive downstream;

z distance (m) normal to the bed; it is the vertical distance (m) for a horizontal channel; for the fixed ravel bed, z is measured above the top of the gravel bed;

θ bed slope angle with the horizontal, positive downwards;

Subscript

median median value;

x longitudinal component positive downstream;

y component transverse to the channel centreline;

z component normal to the invert;

o initial flow conditions : i.e., upstream of the positive surge front;

10 10% percentile;

25 25% percentile;

75 75% percentile;

90 90% percentile.

C.2 Experimental results

The experimental results are shown in terms of the ensemble-averaged median velocity component as a function of the time. Each graph includes the ensemble-averaged median velocity component (V_x, V_y or V_z), the differences between 3rd and 4th quartiles (V_{75}-V_{25}) and 90% and 10% percentiles (V_{90}-V_{10}), and the ensemble-averaged median water depth d_{median}.

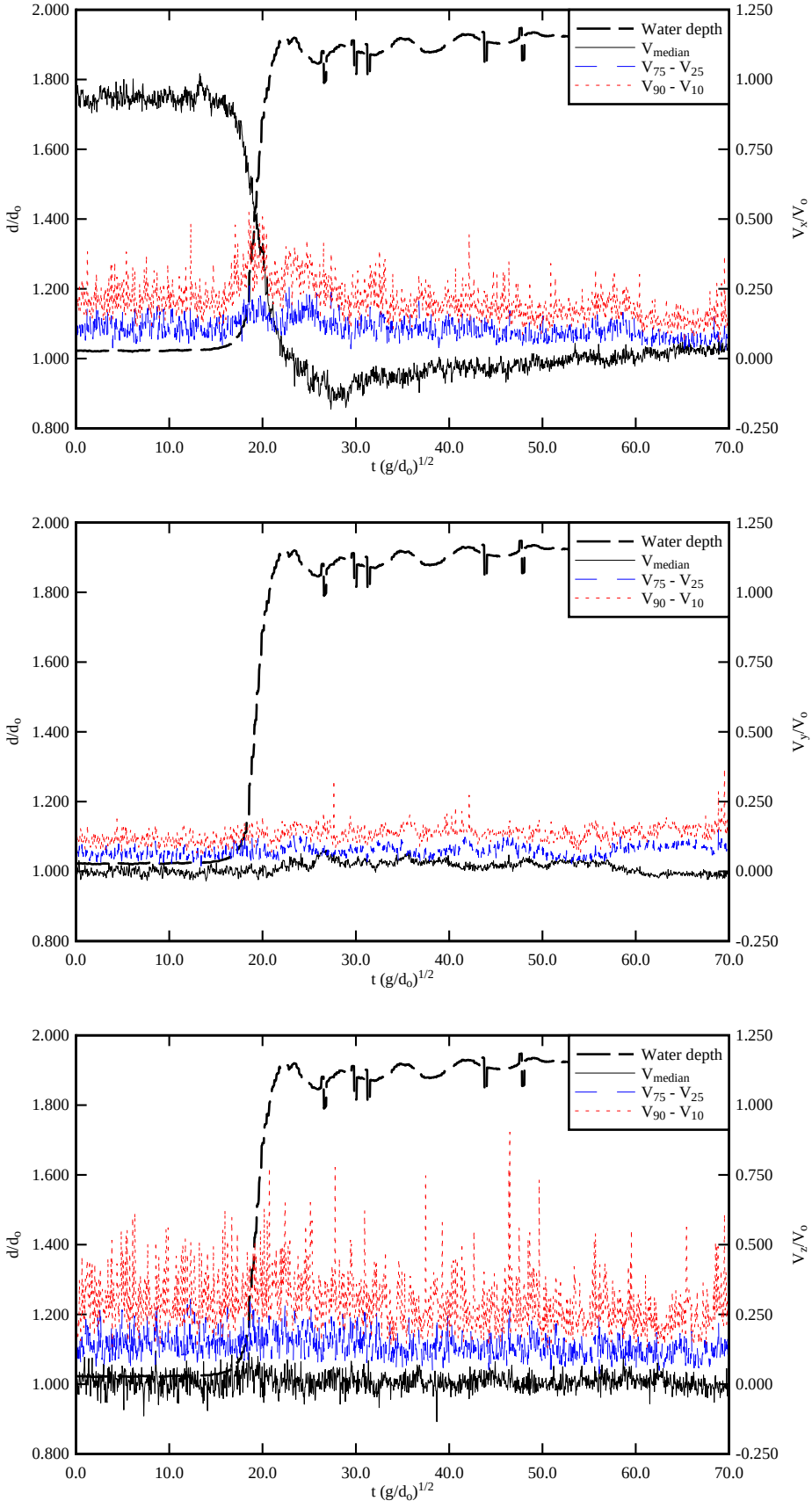
Water depth
V_{median}
$V_{75} - V_{25}$
$V_{90} - V_{10}$
d/d_o
V_x/V_o
V_y/V_o
V_z/V_o
$t (g/d_o)^{1/2}$
2.000
1.800
1.600
1.400
1.200
1.000
0.800
1.250
1.000
0.750
0.500
0.250
0.000
-0.250
0.0
10.0
20.0
30.0
40.0
50.0
60.0
70.0

(A) $z/d_o = 0.135$

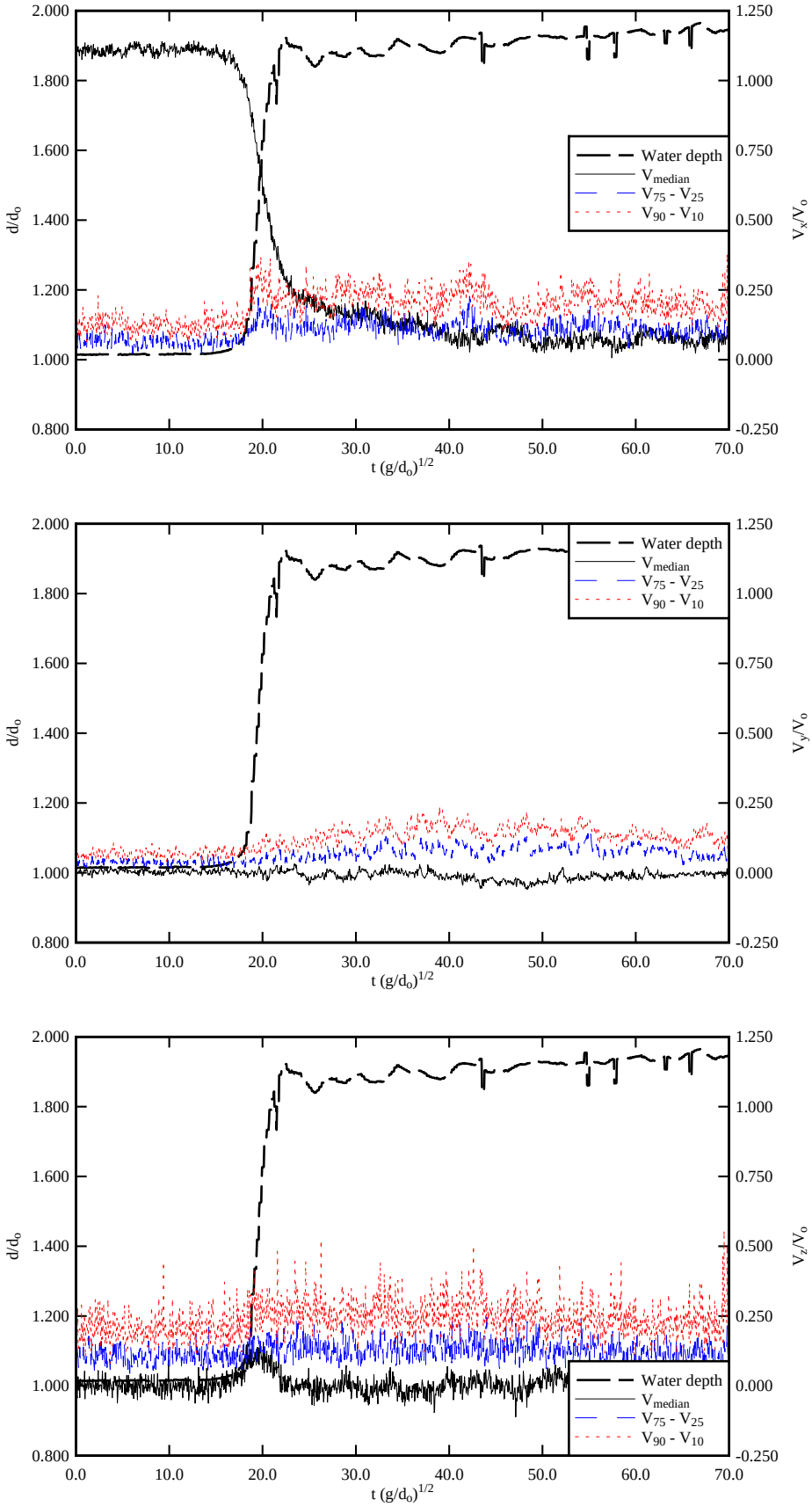
2.000
1.800
1.600
1.400
1.200
1.000
0.800
d/d$_o$
1.250
1.000
0.750
0.500
0.250
0.000
-0.250
V$_x$/V$_o$
Water depth
V$_{median}$
V$_{75}$ - V$_{25}$
V$_{90}$ - V$_{10}$
0.0
10.0
20.0
30.0
40.0
50.0
60.0
70.0
t (g/d$_o$)$^{1/2}$
V$_y$/V$_o$
V$_z$/V$_o$

(B) $z/d_o = 0.434$

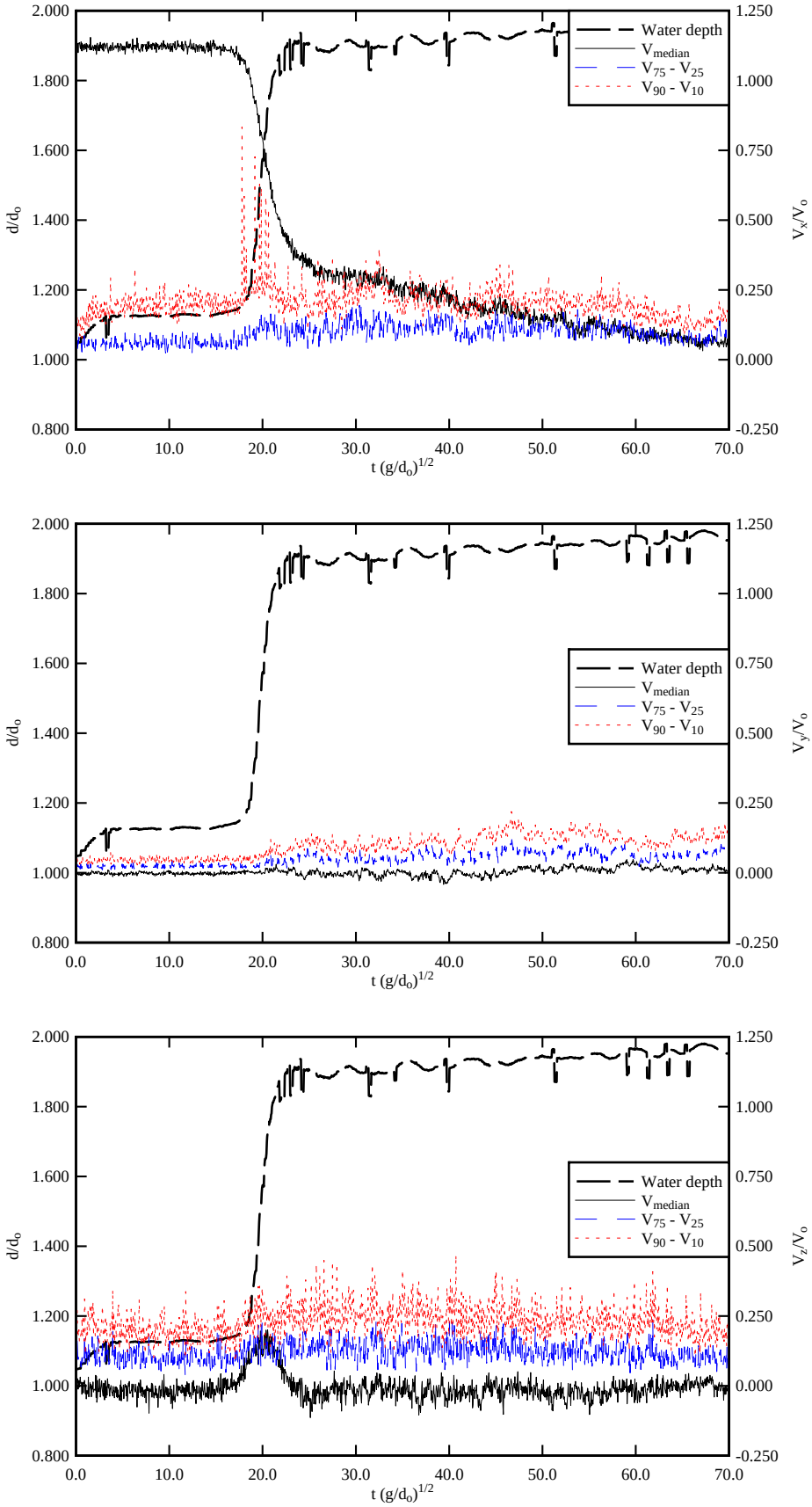

(C) $z/d_o = 0.733$

Fig. C-1 - Ensemble-average median velocity component V_{median}, difference between 3rd and 4th quartiles (V_{75}-V_{25}) and 90% and 10% percentiles (V_{90}-V_{10}), and ensemble-average median water depth d_{median} - Smooth PVC bed - From top to bottom: V_x, V_y, V_z

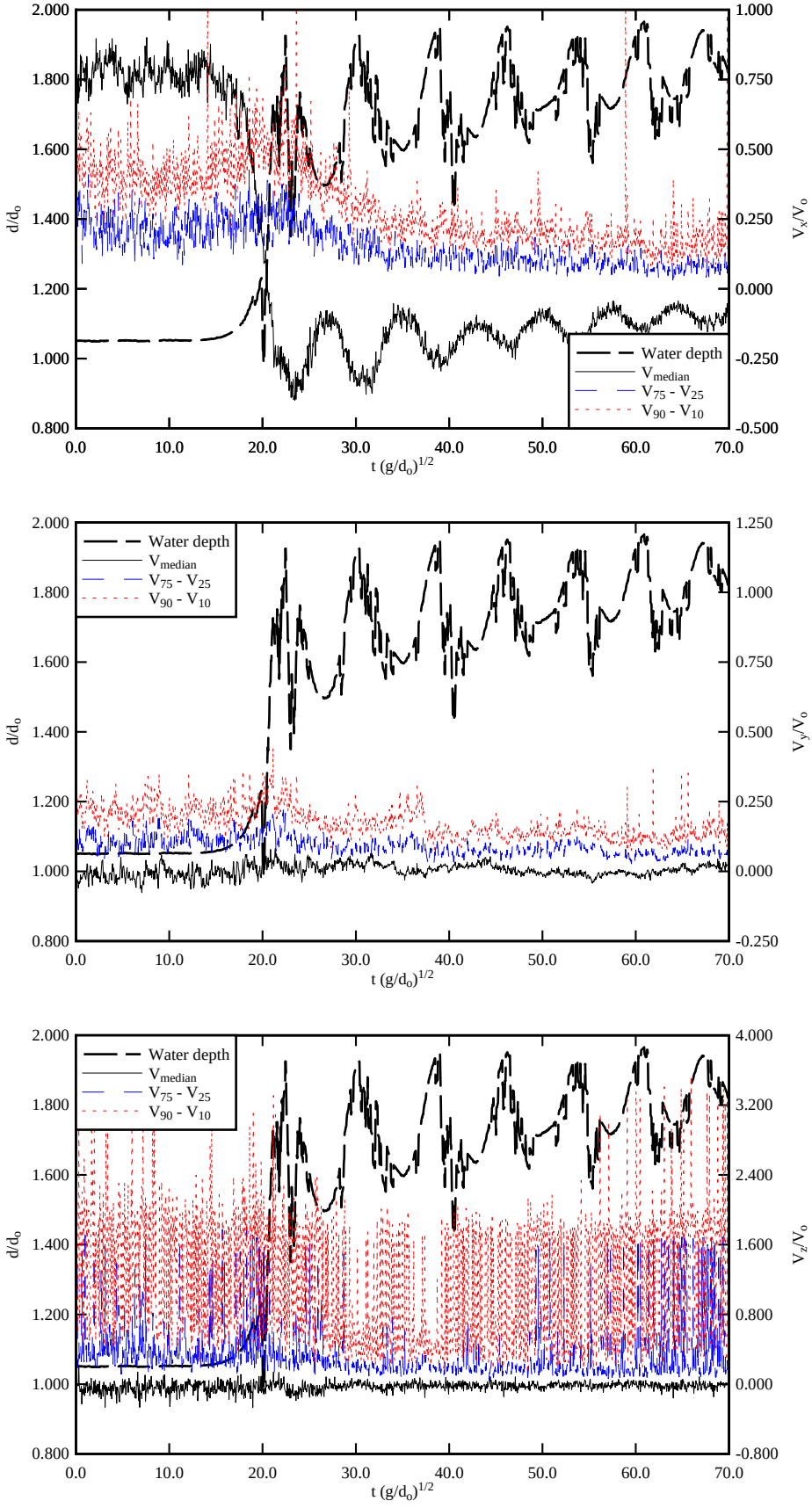
2.000
1.800
1.600
1.400
1.200
1.000
0.800
d/d$_o$
1.000
0.750
0.500
0.250
0.000
-0.250
-0.500
V$_x$/V$_o$
Water depth
V$_{median}$
V$_{75}$ - V$_{25}$
V$_{90}$ - V$_{10}$
0.0
10.0
20.0
30.0
40.0
50.0
60.0
70.0
t (g/d$_o$)$^{1/2}$
1.250
1.000
0.750
0.500
0.250
0.000
-0.250
V$_y$/V$_o$
4.000
3.200
2.400
1.600
0.800
0.000
-0.800
V$_z$/V$_o$

(A) $z/d_o = 0.135$

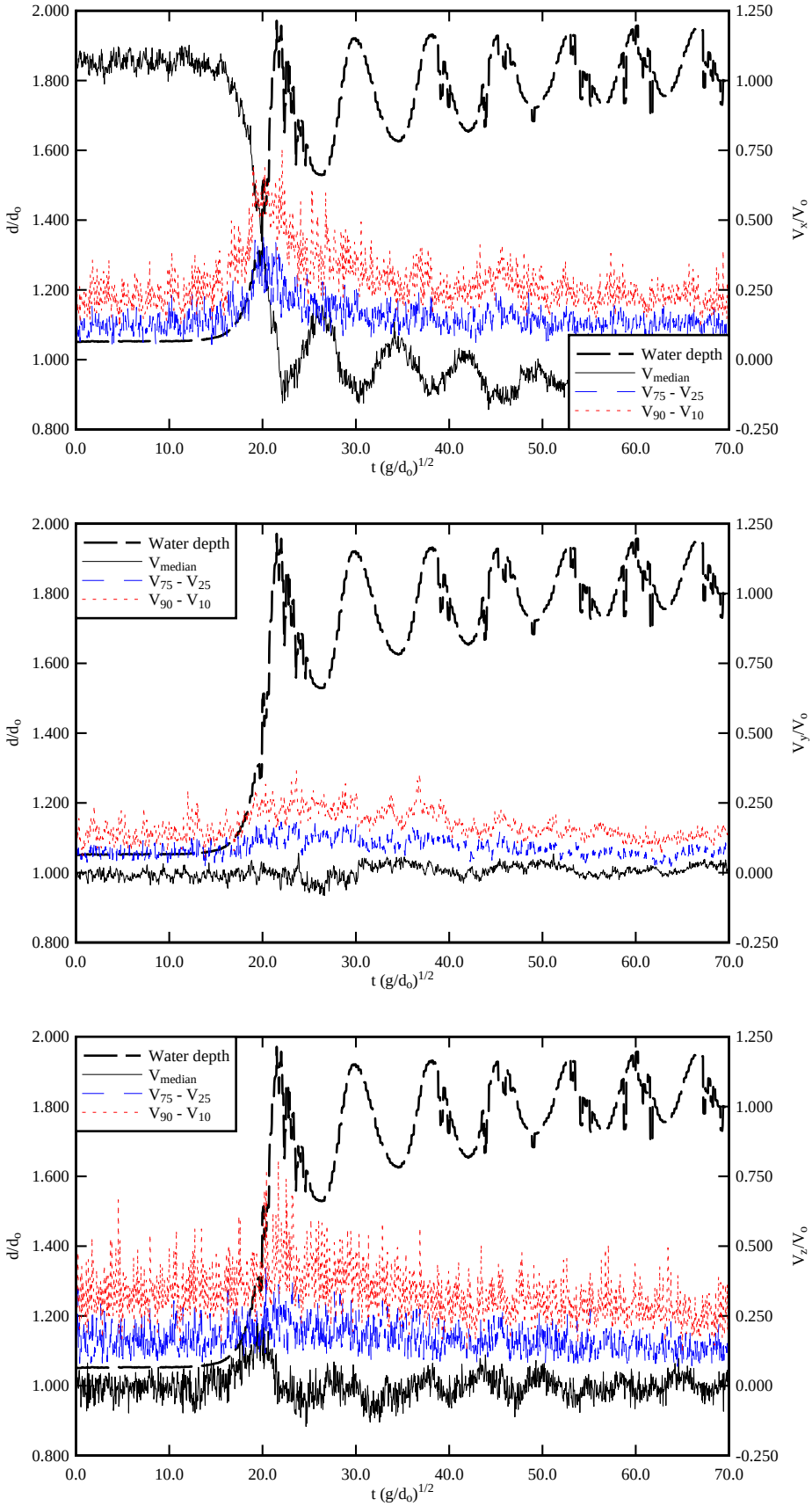
2.000
1.800
1.600
1.400
1.200
1.000
0.800
d/d$_o$
1.250
1.000
0.750
0.500
0.250
0.000
-0.250
V$_x$/V$_o$
0.0
10.0
20.0
30.0
40.0
50.0
60.0
70.0
t (g/d$_o$)$^{1/2}$
Water depth
V$_{median}$
V$_{75}$ - V$_{25}$
V$_{90}$ - V$_{10}$
V$_y$/V$_o$
V$_z$/V$_o$

(B) $z/d_o = 0.434$

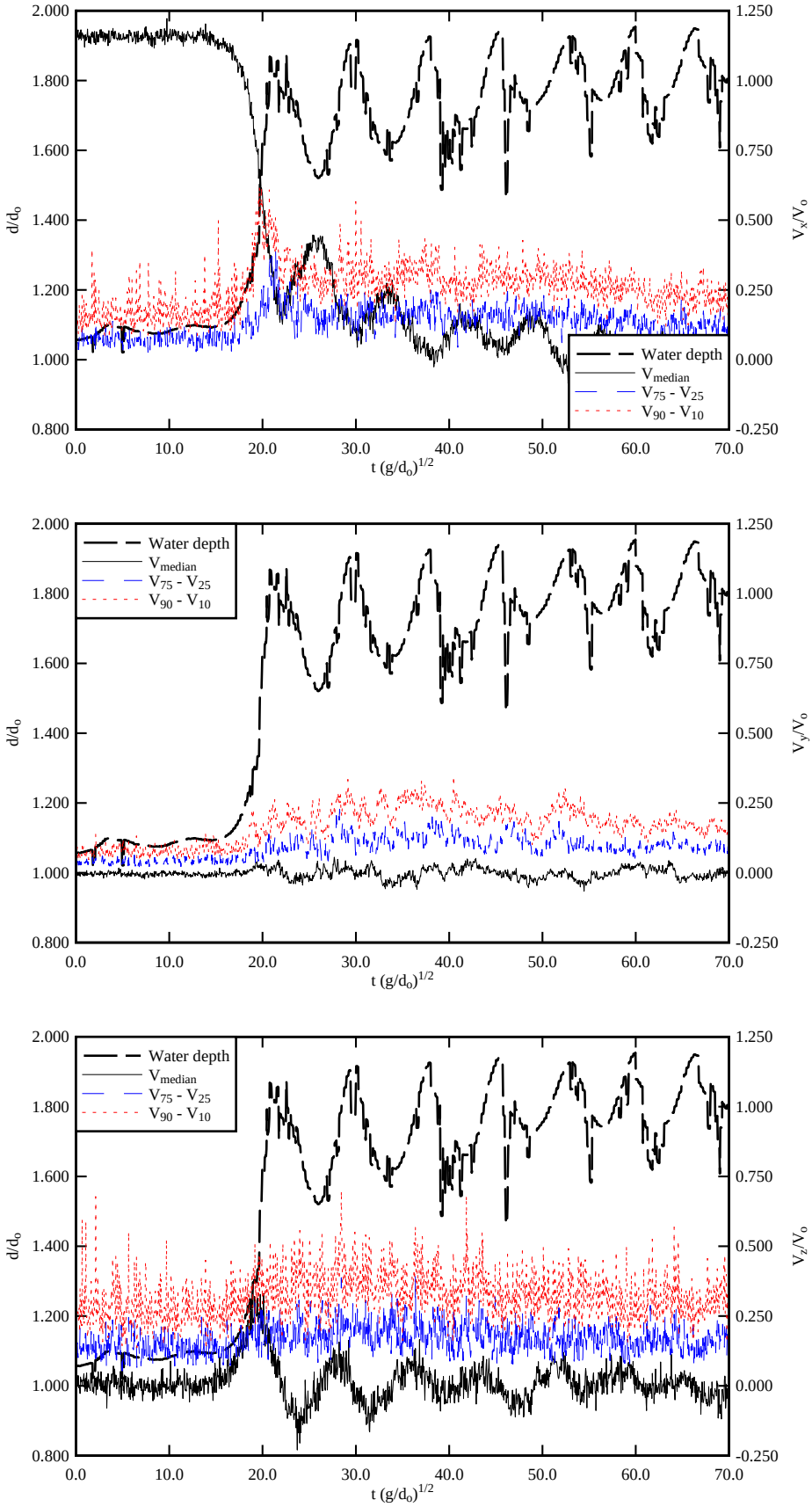

(C) $z/d_o = 0.733$

Fig. C-2 - Ensemble-average median velocity component V_{median}, difference between 3rd and 4th quartiles (V_{75}-V_{25}) and 90% and 10% percentiles (V_{90}-V_{10}), and ensemble-average median water depth d_{median} - Fixed gravel bed - From top to bottom: V_x, V_y, V_z

Appendix D - Unsteady turbulence in a tidal bores: a comparison between ensemble-averaging and variable interval time averaging techniques

D.1 Presentation

In a turbulent flow motion, the velocity is typically divided into a time-average component plus a turbulent fluctuation component:

$$V = \overline{V} + v \quad \text{(D-1)}$$

where V is the instantaneous velocity, $\overline{V}$ is the time-averaged velocity, and v is the instantaneous velocity fluctuation. In Equation (D-1), the minuscule refers to the fluctuating parameter and the overbar refers to the time-averaged quantity. In a steady flow, the time-average of a parameter V at a time t is defined as:

$$\overline{V} = \frac{1}{T} \times \int_{t-T/2}^{t+T/2} V \times dt' \quad \text{(D-2)}$$

where the averaging period T must be large such that the time-average becomes independent of the time t.

When the flow is unsteady, a time average is not meaningful because the long-term trend and the short-term, turbulent fluctuations must be processed separately. The integration limits in Equation (D-3) must be large in comparison with the turbulent time scales but small compared to the time scale of the flow motion (BRADSHAW 1971, LIGGETT 1994). The turbulence in unsteady flows may be analysed by two techniques: ensemble-averaging and variable interval time averaging.

If the unsteady turbulent flow is gradually-varied with some distinct long-term and short-term fluctuation frequencies, $\overline{V}$ is a low-pass filtered component, or variable-interval time average VITA (PIQUET 1999). A cutoff frequency F_{cutoff} is required such that the characteristic time $1/F_{cutoff}$ is greater than the characteristic period of turbulent fluctuations, and small with respect to the characteristic period for the time-evolution of the mean properties (PIQUET 1999, GARCIA and GARCIA 2006, KOCH and CHANSON 2008). The instantaneous fluctuation v becomes the high-pass filtered component of the measured quantity.

In a transient, highly unsteady flow, the quantities of the mean motion are determined by ensemble-averaging (BRADSHAW 1971, SCHLICHTING and GERSTEN 2001). The same experiment is repeated N times and the ensemble average is defined as:

$$\overline{V}(x, y, z, t) = \frac{1}{N} \times \sum_{i=1}^{N} V_i(x, y, z, t) \quad \text{(D-3a)}$$

When the number N of repeats is small, the ensemble-average is best defined in terms of the median value:

$$\overline{V}(x, y, z, t) = \text{Median}\left(V_i(x, y, z, t)\right)_{i=1, N} \quad \text{(D-3b)}$$

The turbulent velocity fluctuation v becomes the deviation of the instantaneous velocity V from the ensemble average $\overline{V}$ (BRADSHAW 1971).

Herein, both the ensemble-average method (EA) and the variable interval time average technique (VITA) were tested in tidal bores with a marked roller. The ensemble-average technique was based upon the repetition of 20 identical experiments (Table D-1) and the ensemble-averaged was calculated using Equation (D-3b). For the VITA method, an upper limit of the filtered signal was the Nyquist frequency (herein 100

Hz) while a lower limit was a period of about 0.9 seconds that corresponded to the period of the residual undulations. The final cut-off frequency was selected based upon a sensitivity analysis that yielded an optimum threshold of F_{cutoff} = 2 Hz, and the filtering was applied to all velocity components. KOCH and CHANSON (2008) selected similarly a cutoff period 1/ F_{cutoff} that was about half the undulation period as in the present study.

Table D-1 - Experimental flow conditions for ensemble-average of turbulent velocity measurements in breaking tidal bores

Q (m^3/s) (1)	S_o (2)	Bed roughness (3)	d_o (m) (4)	V_o (m/s) (5)	Bore type (6)	Fr (7)	U (m/s) (8)	z/d_o (9)
0.050	0.000	Smooth PVC	0.117	0.855	Breaking	1.61	0.869	0.135 0.434 0.733
	0.002	Fixed gravel bed (k_s = 3.4 mm)	0.126	0.794	Undular/Breaking	1.50	0.877	0.135 0.434 0.733

Note: tainter gate opening after closure: h = 0.

Notation

d (a) flow depth (m) measured normal to the invert;
(b) flow depth (m) measured above the fixed gravel bed;

d_o initial flow depth (m) measured normal to the chute invert;

Fr tidal bore Froude number defined as: $Fr = (V_o + U) / \sqrt{g \times d_o}$;

g gravity constant (m/s^2): g = 9.80 m/s^2 in Brisbane, Australia;

Q volume flow rate (m^3/s);

S_o bed slope: $S_o = \sin\theta$;

U tidal bore front celerity (m/s) for an observer standing on the bank, positive upstream;

V_x longitudinal velocity (m/s) positive downstream;

V_y transverse velocity (m/s) positive towards the left sidewall;

V_z vertical velocity (m/s) positive upwards;

V_o initial flow velocity (m/s) positive downstream: $V_o = q/d_o$;

v turbulent velocity fluctuation (m/s): $v = V - \overline{V}$;

x longitudinal distance (m) measured from the channel upstream end, positive downstream;

z distance (m) normal to the bed; it is the vertical distance (m) for a horizontal channel; for the fixed ravel bed, z is measured above the top of the gravel bed;

θ bed slope angle with the horizontal, positive downwards;

Subscript

median	median value;
x	longitudinal component positive downstream;
y	component transverse to the channel centreline;
z	component normal to the invert;
o	initial flow conditions : i.e., upstream of the positive surge front;
10	10% percentile;
25	25% percentile;
75	75% percentile;
90	90% percentile;

Abbreviations

EA	ensemble average;
VITA	variable interval time average.

D.2 Experimental results

Figures D-1 to D-4 illustrates the differences in signal processing techniques. Figures D-1 and D-2 present the median water depth, the median velocity component (median of 20 runs), the median value of the variable interval time average (VITA) velocity component (median value of 20 runs), and all the low-pass filtered velocity components (VITA, Runs 1 to 20).

Figures D-3 and D-4 present the median water depth and the difference between 3rd and 4th quartiles for the water depth (d_{75}-d_{25}). Each graph includes further the median velocity component (median of 20 runs) and the difference between 3rd and 4th quartiles (V_{75}-V_{25}), as well as the median value of the variable interval time average (VITA) velocity component (median value of 20 runs), and the variance of the velocity component v^2.

Herein the median water depth and velocity components were ensemble-averaged over the 20 runs. The low-pass filtered longitudinal velocity or VITA was calculated for each data run. The median VITA value was calculated as the median VITA value for the 20 Runs.

A few points must be discussed. First the VITA value is meaningless at both ends of the record. Second both the median VITA value (for the 20 runs) and the ensemble averaged median value yielded very close results in terms of all the velocity components. While the agreement is expected, the ensemble averaged median value required significantly less post-processing. Third the VITA data based upon a single run highlighted some difference with the EA median results. This is seen in Figures D-1 and D-2 for all velocity components.

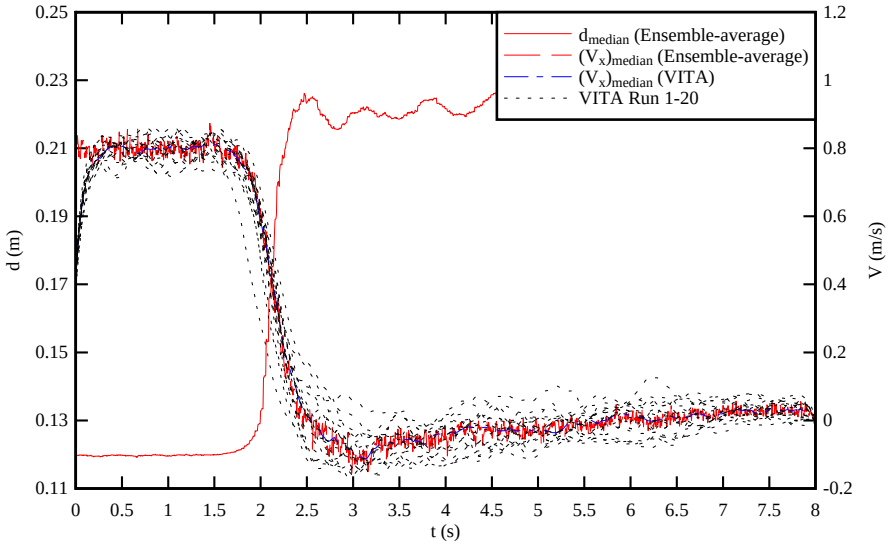
d (m)
V (m/s)
t (s)
d_{median} (Ensemble-average)
$(V_x)_{median}$ (Ensemble-average)
$(V_x)_{median}$ (VITA)
VITA Run 1-20

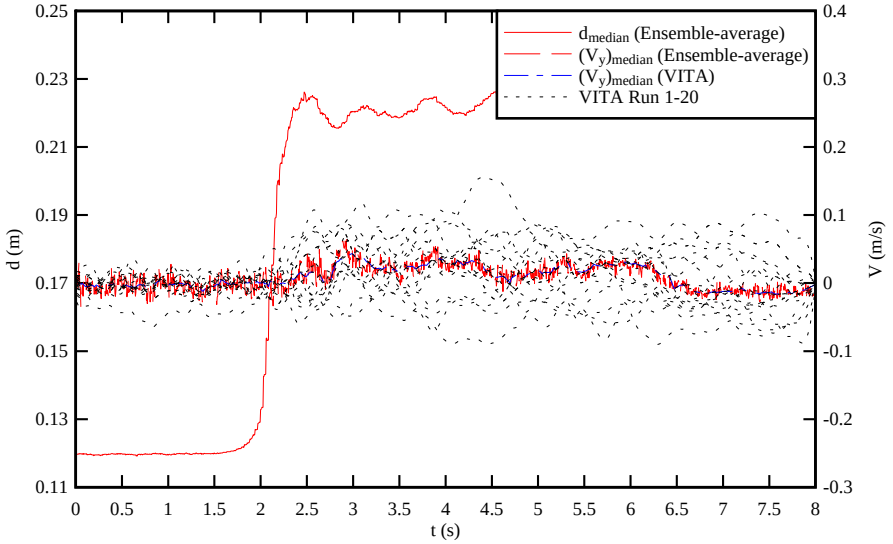
d (m)
V (m/s)
t (s)
d_{median} (Ensemble-average)
$(V_y)_{median}$ (Ensemble-average)
$(V_y)_{median}$ (VITA)
VITA Run 1-20

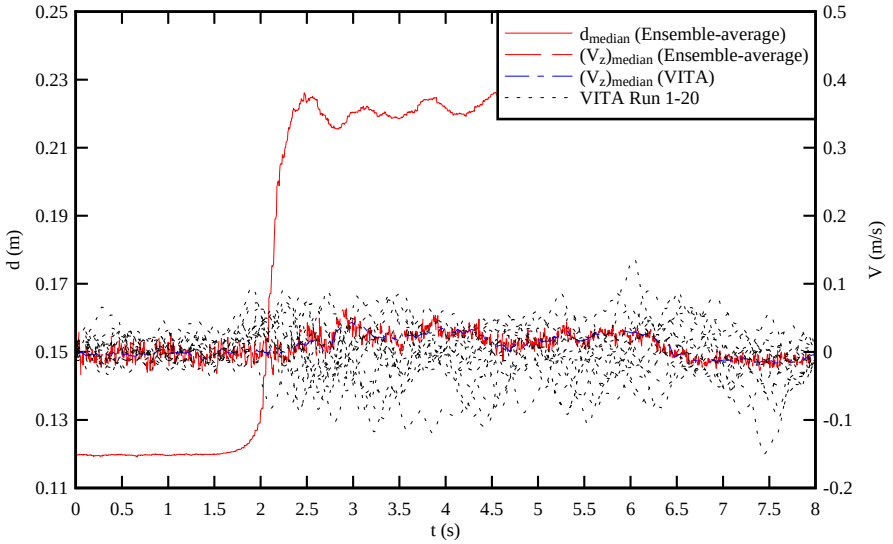
d (m)
V (m/s)
t (s)
d_{median} (Ensemble-average)
$(V_z)_{median}$ (Ensemble-average)
$(V_z)_{median}$ (VITA)
VITA Run 1-20

(A) $z/d_o = 0.135$

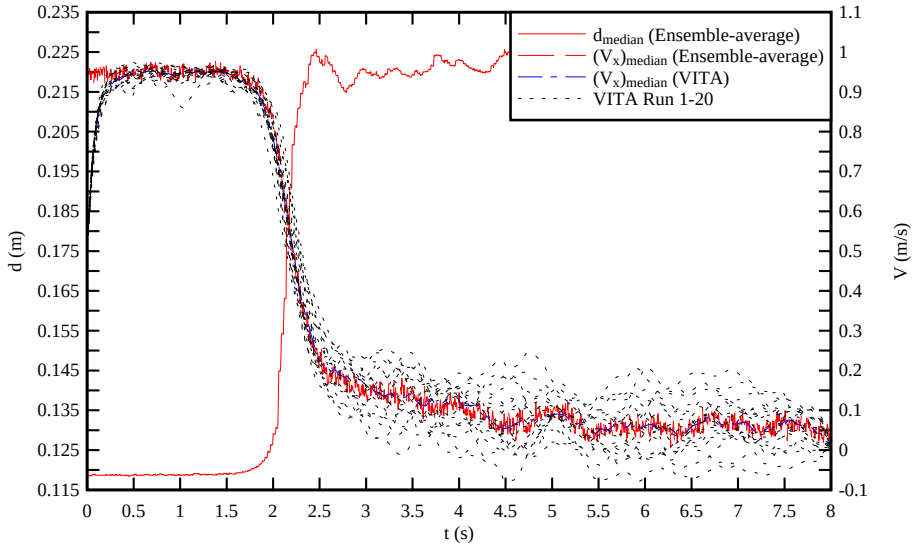
d (m)
V (m/s)
t (s)
d_{median} (Ensemble-average)
$(V_x)_{median}$ (Ensemble-average)
$(V_x)_{median}$ (VITA)
VITA Run 1-20

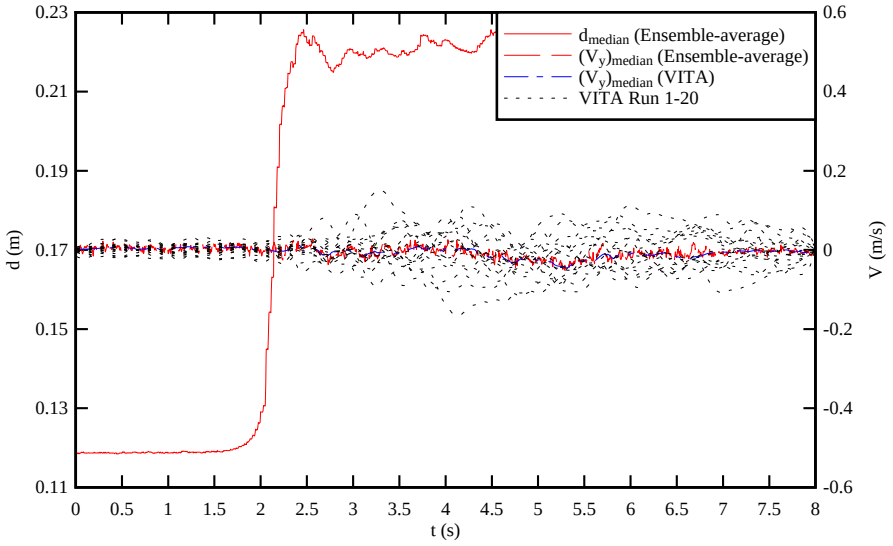
d (m)
V (m/s)
t (s)
d_{median} (Ensemble-average)
$(V_y)_{median}$ (Ensemble-average)
$(V_y)_{median}$ (VITA)
VITA Run 1-20

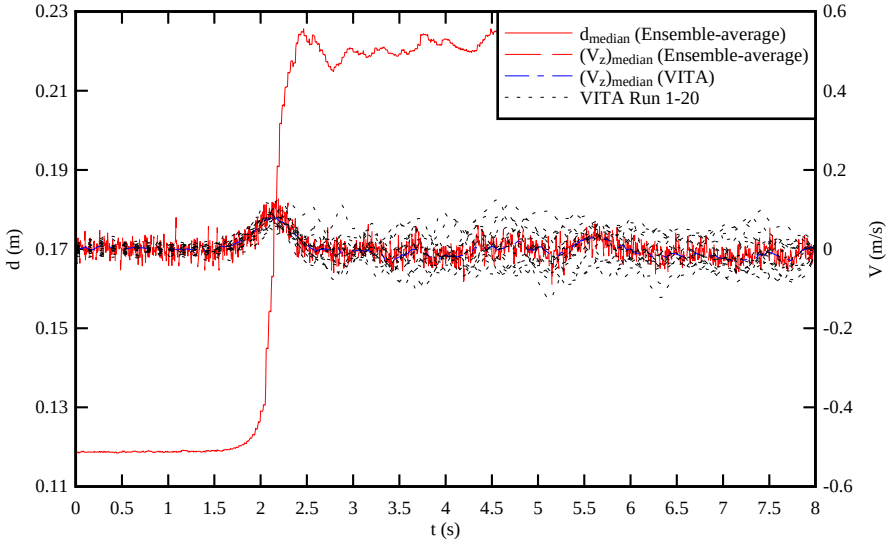
d (m)
V (m/s)
t (s)
d_{median} (Ensemble-average)
$(V_z)_{median}$ (Ensemble-average)
$(V_z)_{median}$ (VITA)
VITA Run 1-20

(B) $z/d_o = 0.434$

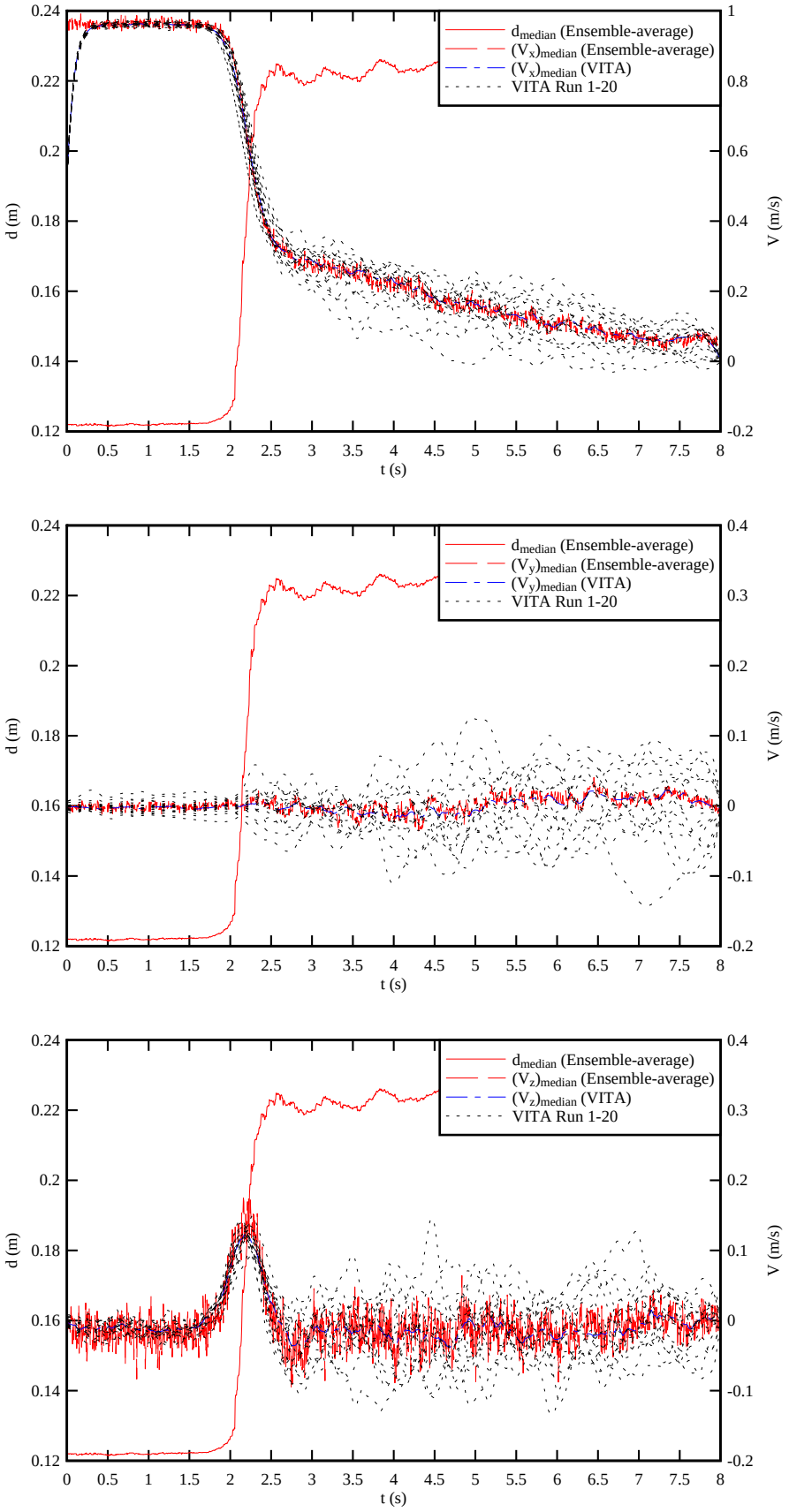

(C) $z/d_o = 0.733$

Fig. D-1 - Ensemble-average median water depth d_{median}, ensemble-average median velocity component V_{median}, median value of the variable interval time average (VITA) velocity component (median value of 20 runs), and low-pass filtered velocity components (VITA Runs 1 to 20) - Smooth PVC bed - From top to

bottom: V_x, V_y, V_z

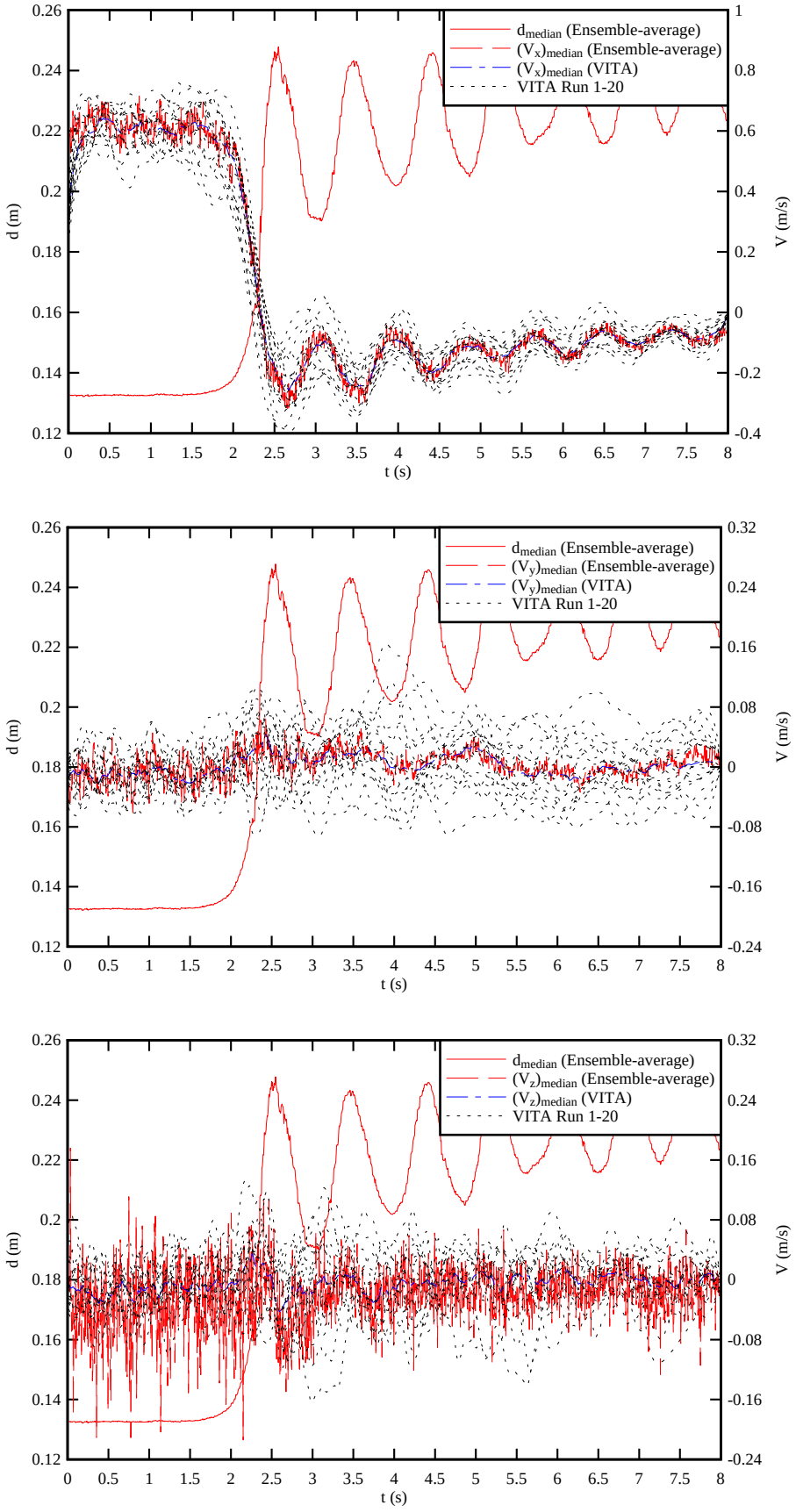

(A) $z/d_o = 0.135$

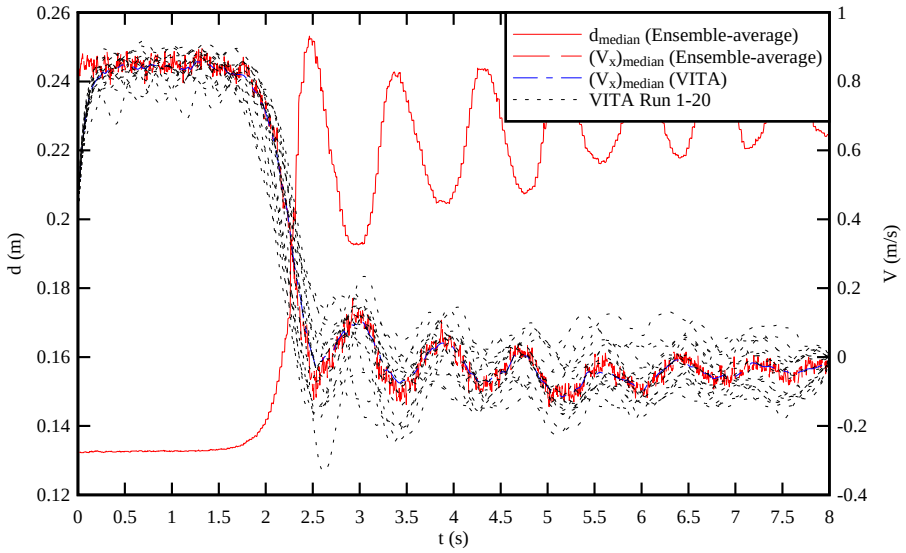
d_{median} (Ensemble-average)
$(V_x)_{median}$ (Ensemble-average)
$(V_x)_{median}$ (VITA)
VITA Run 1-20
d (m)
V (m/s)
t (s)

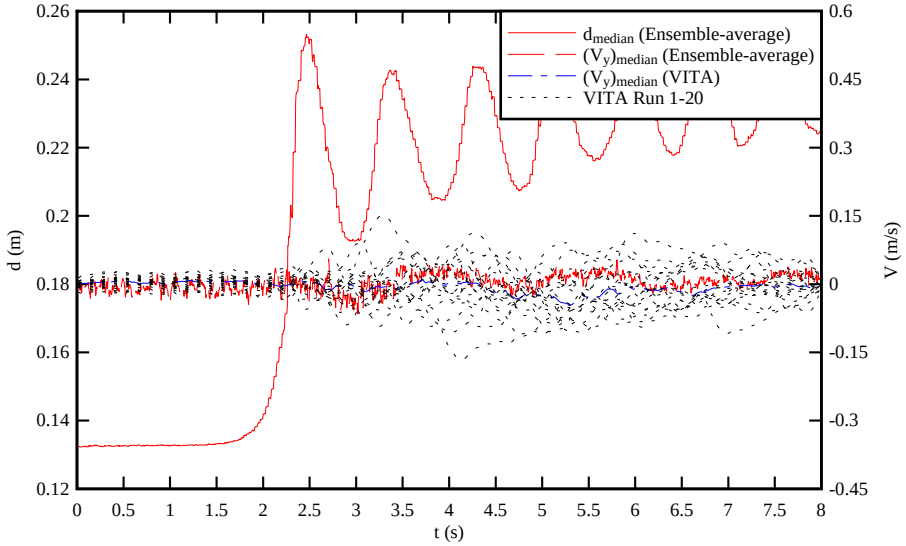
d_{median} (Ensemble-average)
$(V_y)_{median}$ (Ensemble-average)
$(V_y)_{median}$ (VITA)
VITA Run 1-20
d (m)
V (m/s)
t (s)

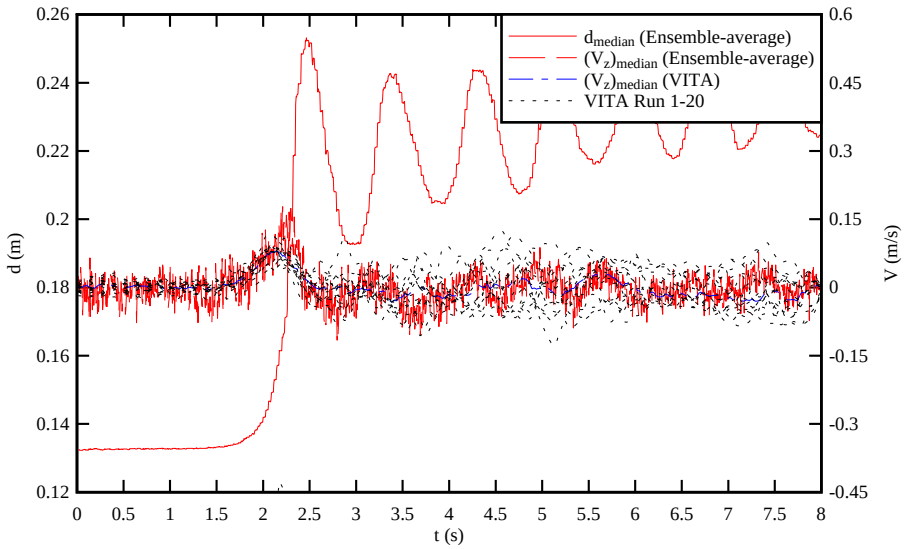
d_{median} (Ensemble-average)
$(V_z)_{median}$ (Ensemble-average)
$(V_z)_{median}$ (VITA)
VITA Run 1-20
d (m)
V (m/s)
t (s)

(B) $z/d_o = 0.434$

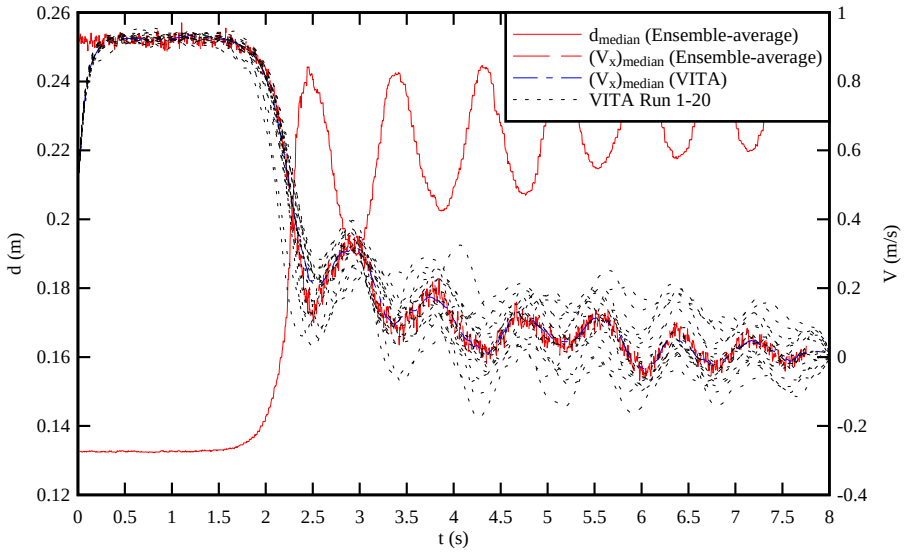

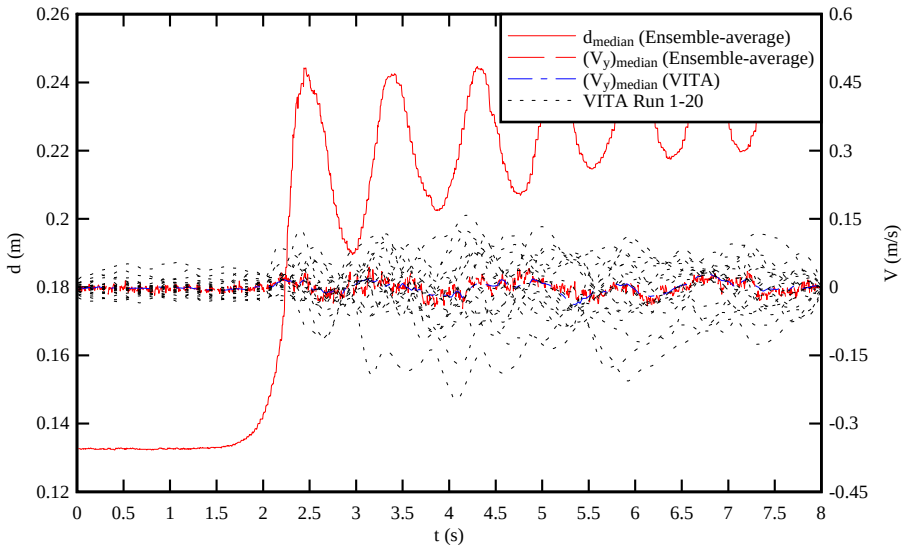

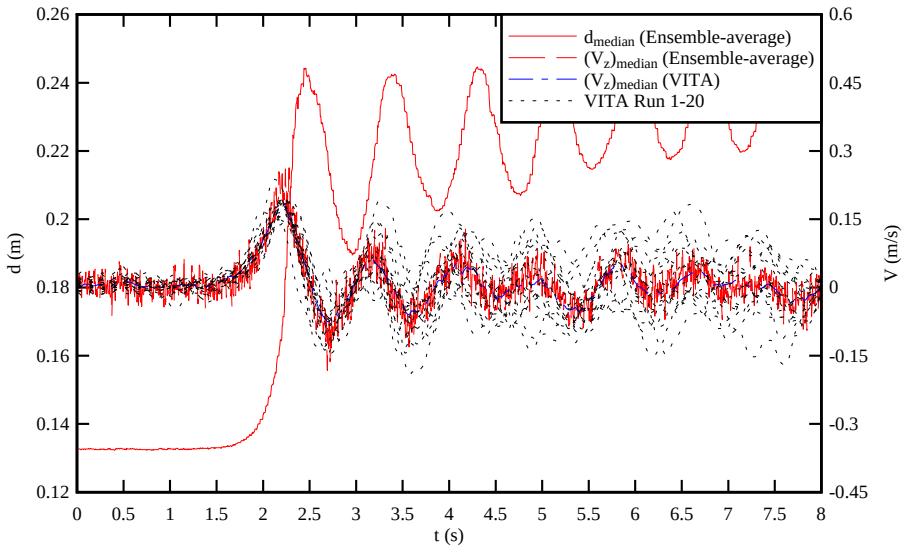

(C) $z/d_o = 0.733$

Fig. D-2 - Ensemble-average median water depth d_{median}, ensemble-average median velocity component V_{median}, median value of the variable interval time average (VITA) velocity component (median value of 20

runs), and low-pass filtered velocity components (VITA Runs 1 to 20) - Fixed gravel bed - From top to bottom: V_x, V_y, V_z

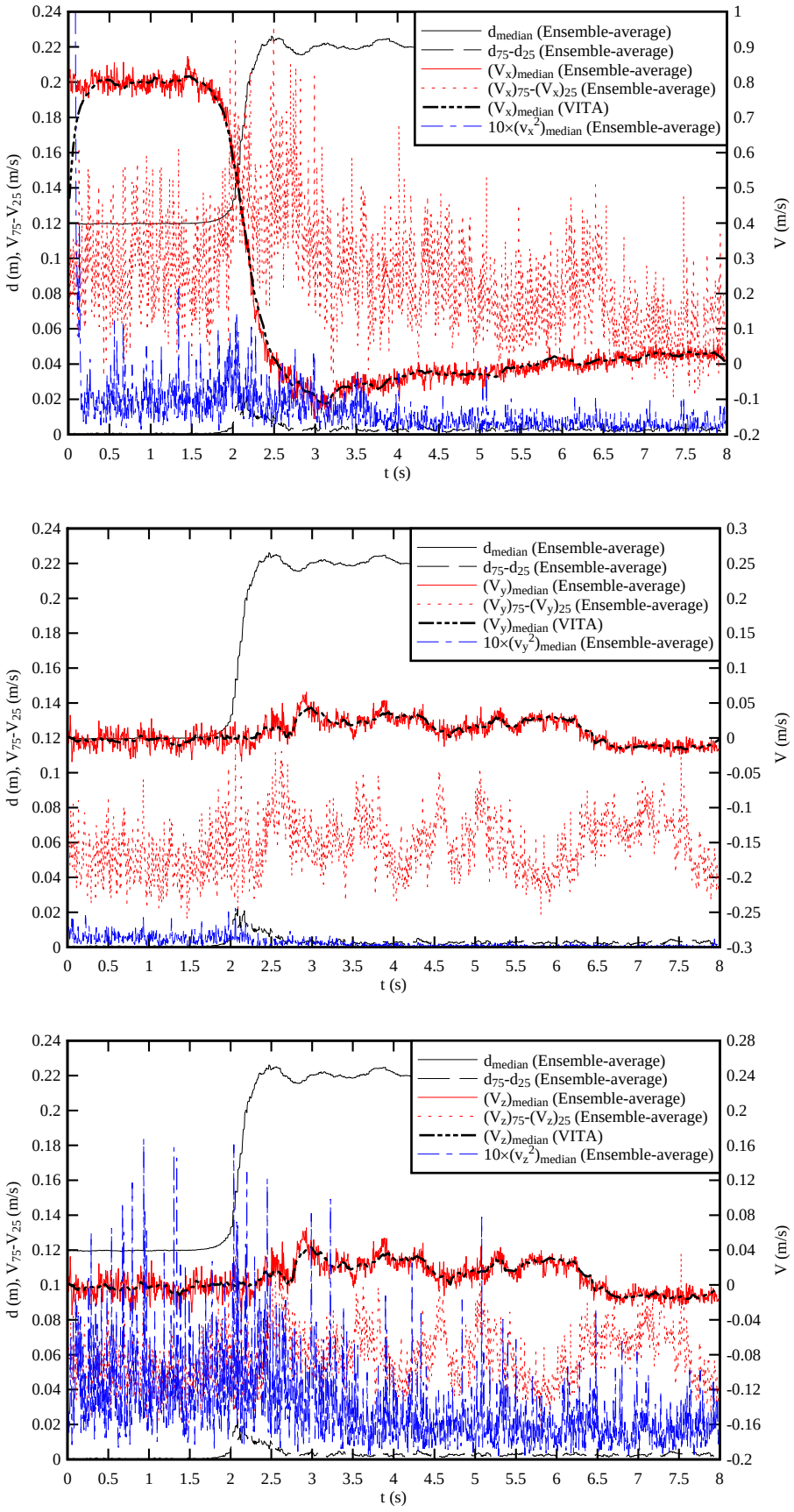

(A) $z/d_o = 0.135$

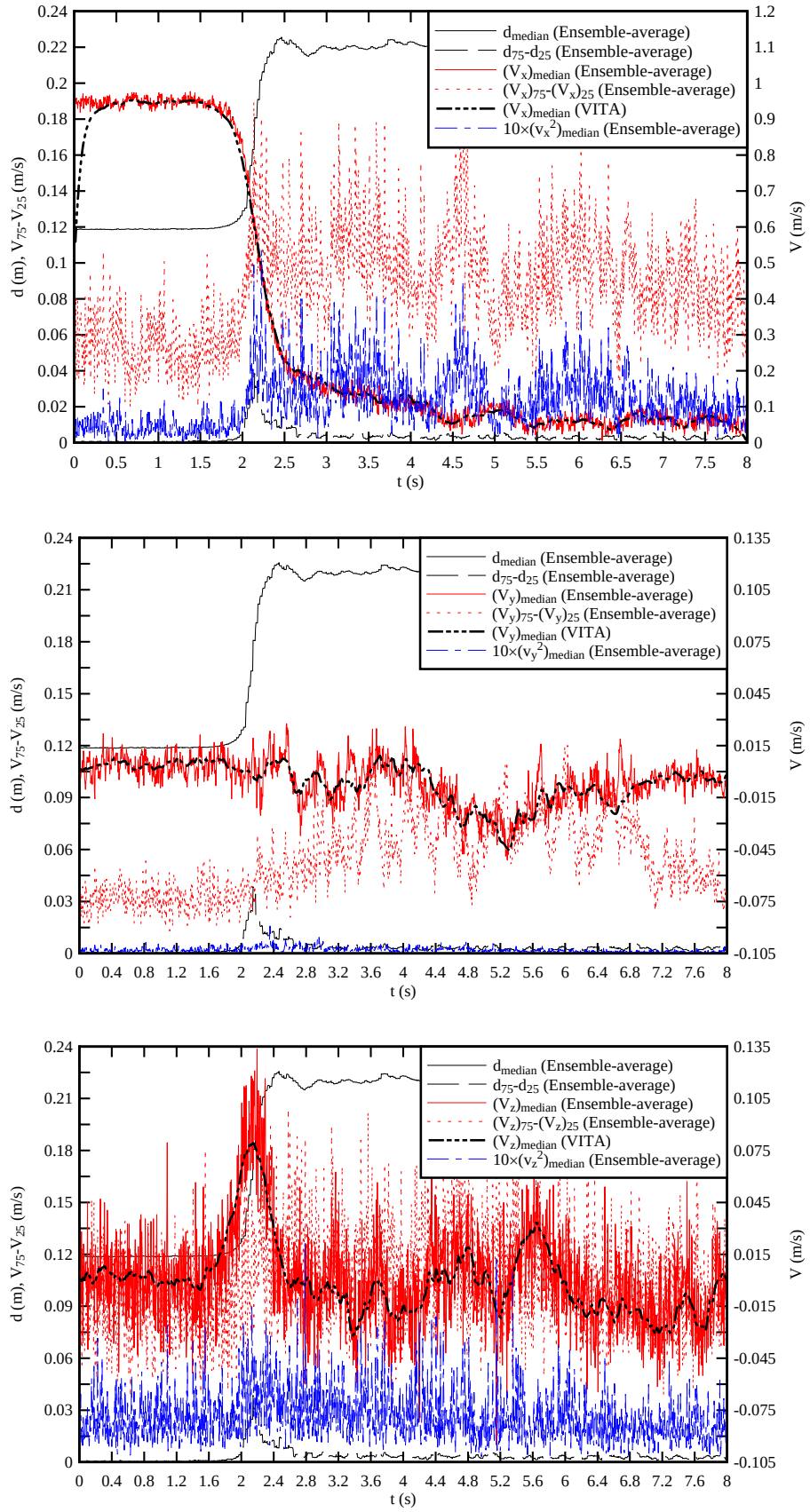
d_median (Ensemble-average)
d75-d25 (Ensemble-average)
(Vx)median (Ensemble-average)
(Vx)75-(Vx)25 (Ensemble-average)
(Vx)median (VITA)
10×(vx2)median (Ensemble-average)
d (m), V75-V25 (m/s)
V (m/s)
t (s)
d_median (Ensemble-average)
d75-d25 (Ensemble-average)
(Vy)median (Ensemble-average)
(Vy)75-(Vy)25 (Ensemble-average)
(Vy)median (VITA)
10×(vy2)median (Ensemble-average)
d (m), V75-V25 (m/s)
V (m/s)
t (s)
d_median (Ensemble-average)
d75-d25 (Ensemble-average)
(Vz)median (Ensemble-average)
(Vz)75-(Vz)25 (Ensemble-average)
(Vz)median (VITA)
10×(vz2)median (Ensemble-average)
d (m), V75-V25 (m/s)
V (m/s)
t (s)

(B) $z/d_o = 0.434$

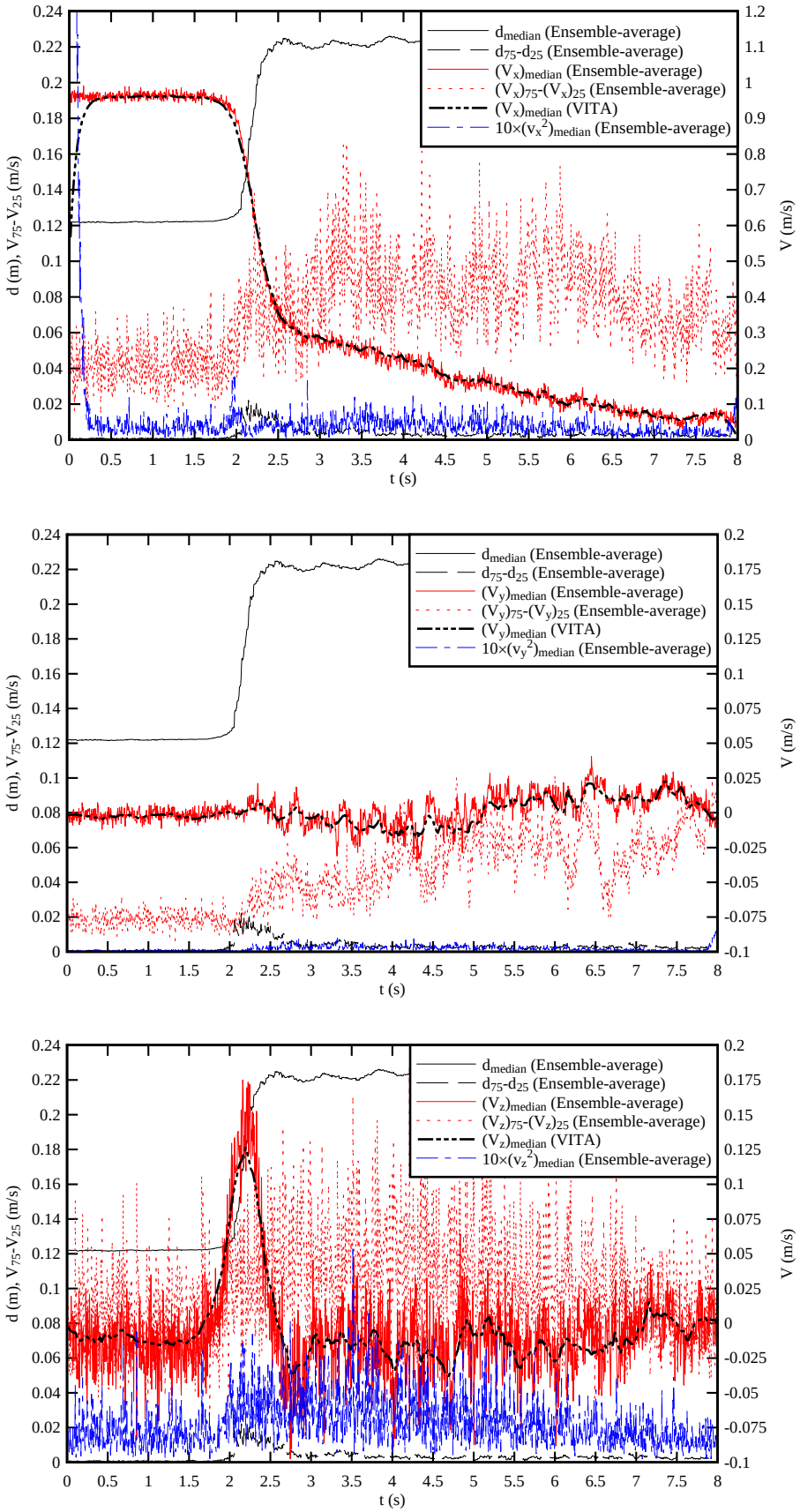

(C) $z/d_o = 0.733$

Fig. D-3 - Ensemble-average median water depth d_{median}, difference between 3rd and 4th quartiles of the water depth (d_{75}-d_{25}), ensemble-average median velocity component V_{median}, difference between 3rd and 4th quartiles of the velocity component (V_{75}-V_{25}), median value of the variable interval time average (VITA)

velocity component (median value of 20 runs), and variance of velocity component v^2 (ensemble-average of 20 runs) - Smooth PVC bed - From top to bottom: V_x, V_y, V_z

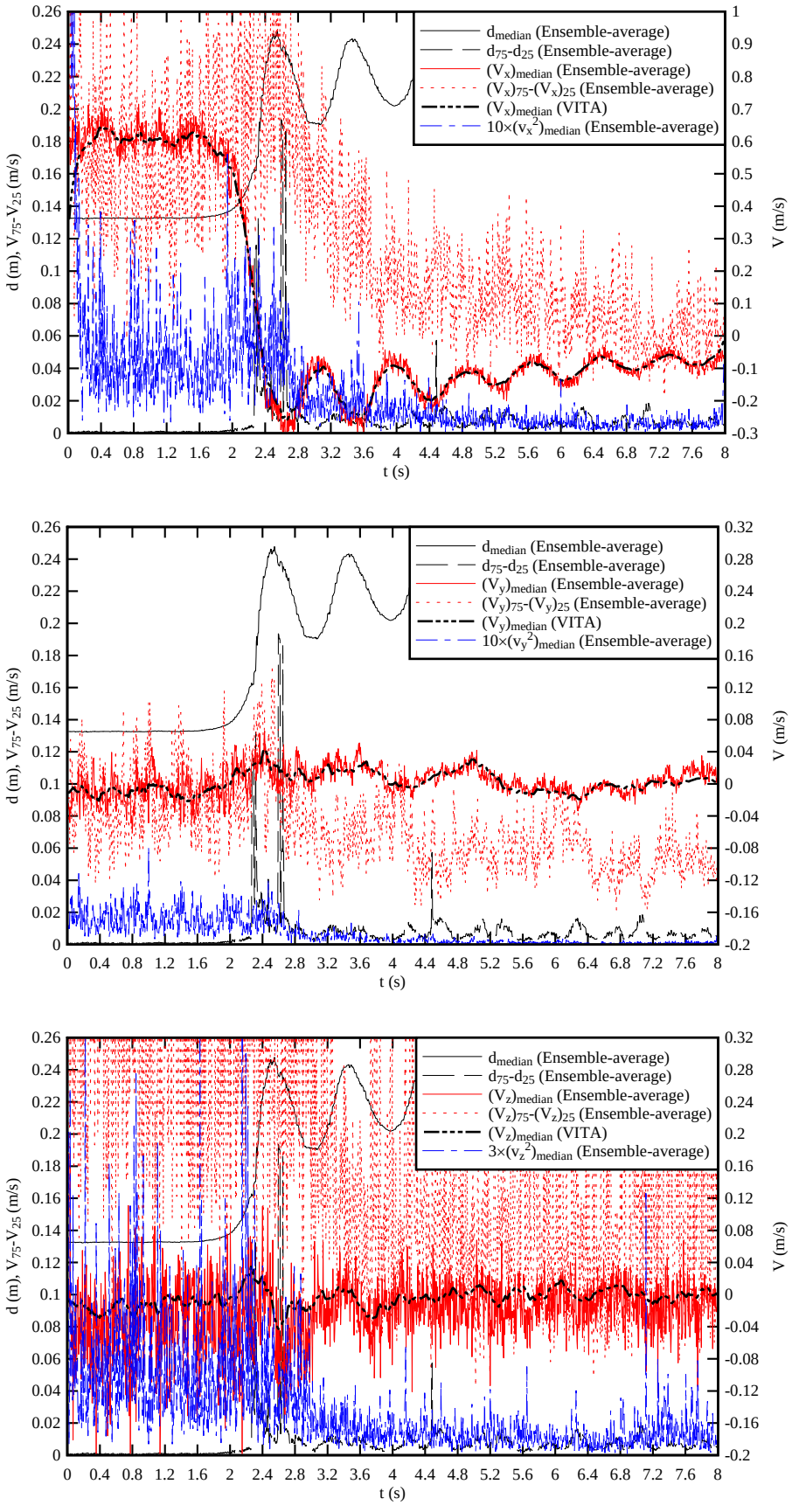

(A) $z/d_o = 0.135$

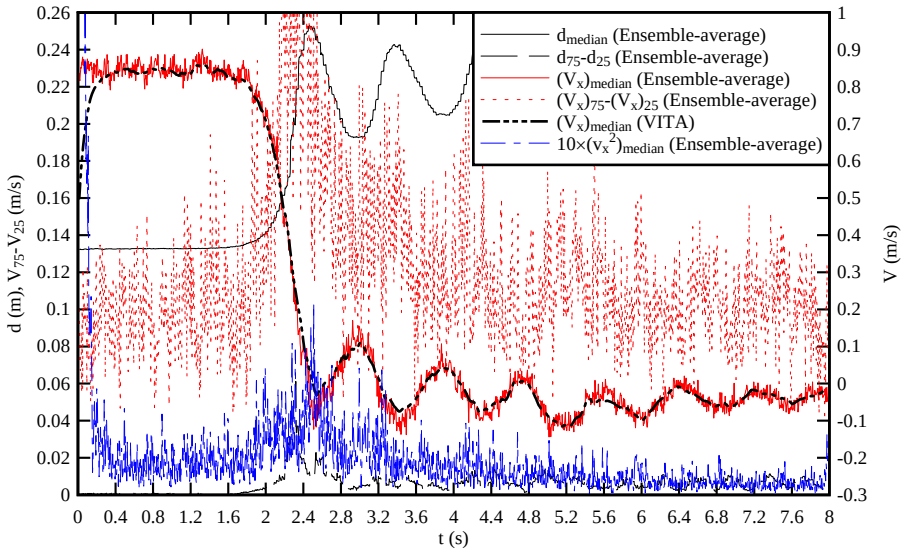
d (m), V75-V25 (m/s)
V (m/s)
t (s)
dmedian (Ensemble-average)
d75-d25 (Ensemble-average)
(Vx)median (Ensemble-average)
(Vx)75-(Vx)25 (Ensemble-average)
(Vx)median (VITA)
10×(vx2)median (Ensemble-average)

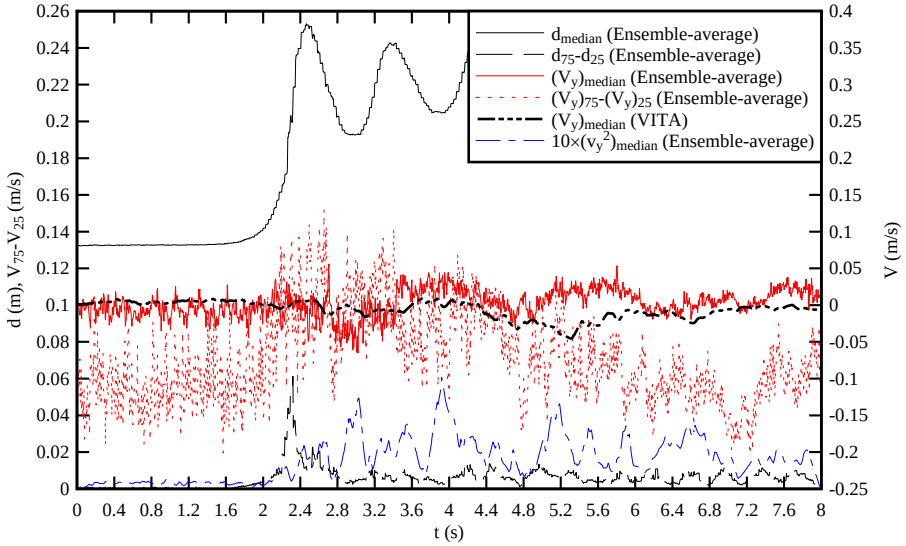
d (m), V75-V25 (m/s)
V (m/s)
t (s)
dmedian (Ensemble-average)
d75-d25 (Ensemble-average)
(Vy)median (Ensemble-average)
(Vy)75-(Vy)25 (Ensemble-average)
(Vy)median (VITA)
10×(vy2)median (Ensemble-average)

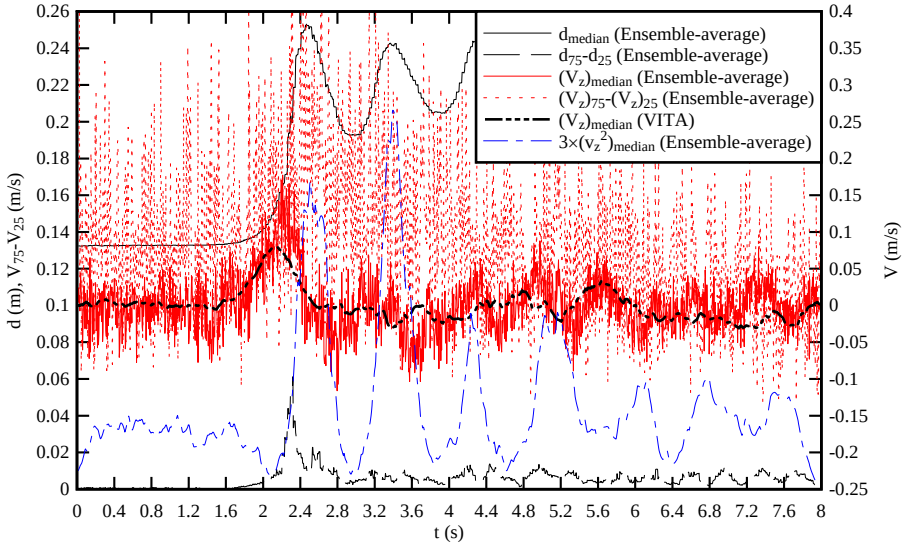
d (m), V75-V25 (m/s)
V (m/s)
t (s)
dmedian (Ensemble-average)
d75-d25 (Ensemble-average)
(Vz)median (Ensemble-average)
(Vz)75-(Vz)25 (Ensemble-average)
(Vz)median (VITA)
3×(vz2)median (Ensemble-average)

(B) $z/d_o = 0.434$

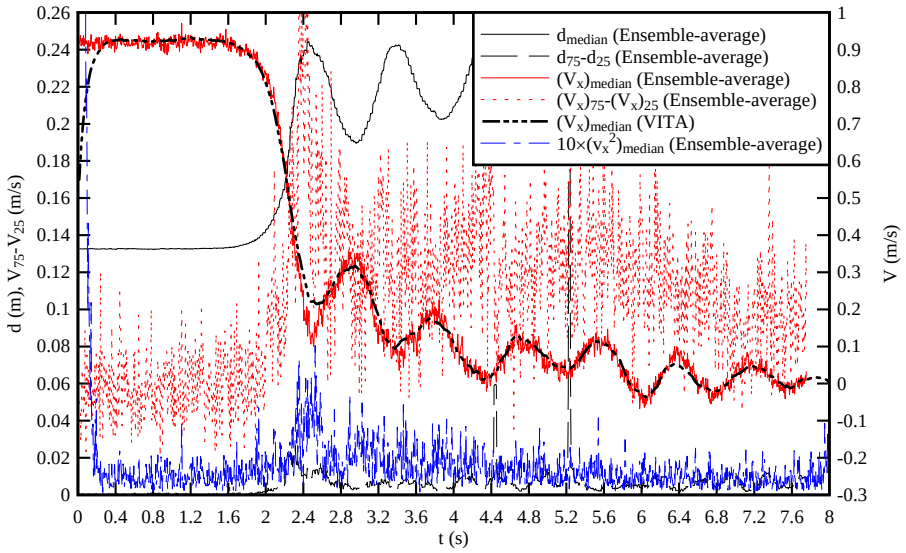

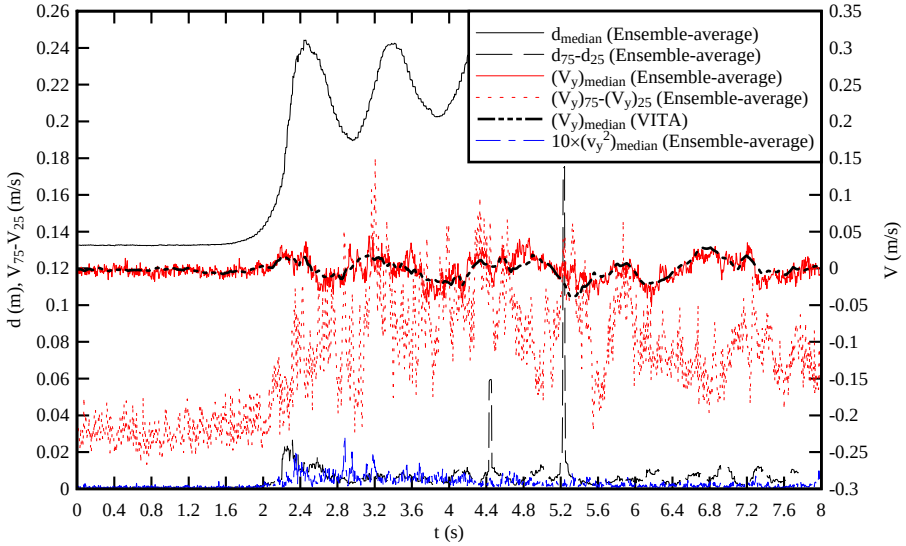

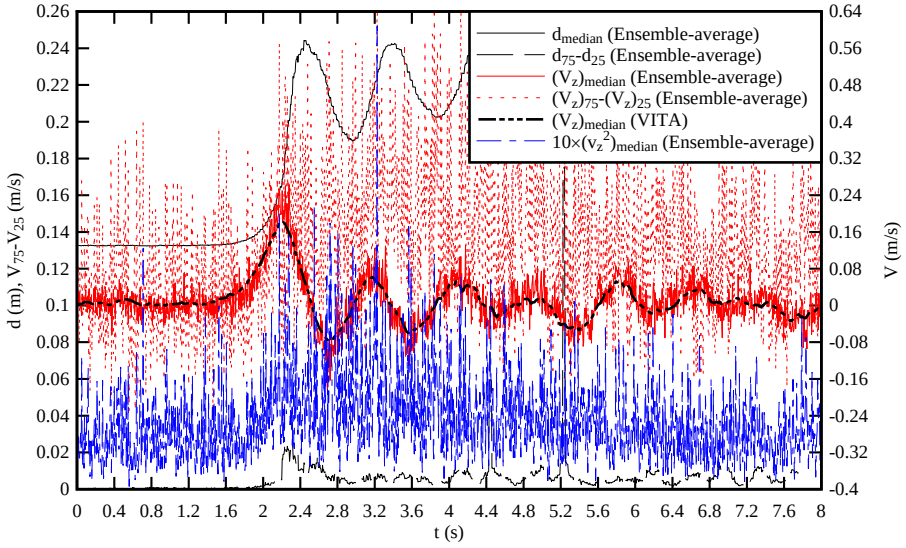

(C) $z/d_o = 0.733$

Fig. D-4 - Ensemble-average median water depth d_{median}, difference between 3rd and 4th quartiles of the water depth (d_{75}-d_{25}), ensemble-average median velocity component V_{median}, difference between 3rd and 4th

quartiles of the velocity component (V_{75}-V_{25}), median value of the variable interval time average (VITA) velocity component (median value of 20 runs), and variance of velocity component v^2 (ensemble-average of 20 runs) - Fixed gravel bed - From top to bottom: V_x, V_y, V_z

Appendix E - Turbulent Reynolds stress tensor in breaking tidal bores

E.1 Presentation

In a turbulent flow, the flux of the x-momentum in the y-direction induces an additional shear stress in the x-direction acting on the surface element normal to the y-direction. This additional stress is called the Reynolds stress or turbulent stress. It is denoted $\rho \times v_x \times v_y$, or more generally $\rho \times v_i \times v_j$ where i, j = x, y, z. The Reynolds stress $\rho \times v_i \times v_j$ characterises the additional shear stress on the faces $dx_i dx_j$ of an elementary control volume (dx, dy, dz), where x_i, x_j = x, y, z. The Reynolds stress tensor is a transport effect resulting from turbulent motion induced by velocity fluctuations with its subsequent increase of momentum exchange and of mixing (PIQUET 1999). This turbulent transport is a property of the flow.

The turbulent stress tensor, or Reynolds stress tensor, includes the normal and tangential stresses, although there is no fundamental difference between normal stress and tangential stress (BRADSHAW 1971). Herein the instantaneous turbulent stresses were calculated using the ensemble-averaging (EA) and variable interval time averaging (VITA) techniques (App. D) for the flow properties summarised in Table E-1.

Table E-1 - Experimental flow conditions for turbulent stress measurements in breaking tidal bores

Q (m^3/s) (1)	S_o (2)	Bed roughness (3)	d_o (m) (4)	V_o (m/s) (5)	Bore type (6)	Fr (7)	U (m/s) (8)	z/d_o (9)
0.050	0.000	Smooth PVC	0.117	0.855	Breaking	1.61	0.869	0.135 0.434 0.733
	0.002	Fixed gravel bed (k_s = 3.4 mm)	0.126	0.794	Undular/Breaking	1.50	0.877	0.135 0.434 0.733

Note: tainter gate opening after closure: h = 0.

Notation

d (a) flow depth (m) measured normal to the invert;
(b) flow depth (m) measured above the fixed gravel bed;

d_o initial flow depth (m) measured normal to the chute invert;

Fr tidal bore Froude number defined as: $Fr = (V_o + U) / \sqrt{g \times d_o}$;

g gravity constant (m/s^2): g = 9.80 m/s^2 in Brisbane, Australia;

Q volume flow rate (m^3/s);

S_o bed slope: $S_o = \sin\theta$;

U tidal bore front celerity (m/s) for an observer standing on the bank, positive upstream;

V_x longitudinal velocity (m/s) positive downstream;

V_y transverse velocity (m/s) positive towards the left sidewall;

V_z vertical velocity (m/s) positive upwards;

V_o initial flow velocity (m/s) positive downstream: $V_o = q/d_o$;

v turbulent velocity fluctuation (m/s): $v = V - \overline{V}$;

x longitudinal distance (m) measured from the channel upstream end, positive downstream;

z distance (m) normal to the bed; it is the vertical distance (m) for a horizontal channel; for the fixed ravel bed, z is measured above the top of the gravel bed;

θ bed slope angle with the horizontal, positive downwards;

Subscript

median median value;

x longitudinal component positive downstream;

y component transverse to the channel centreline;

z component normal to the invert;

o initial flow conditions : i.e., upstream of the positive surge front;

Abbreviations

EA ensemble average;

VITA variable interval time average.

E.2 Experimental results

The basic results are presented herein in terms of the median Reynolds stress tensor components, calculated using either the ensemble-averaging (EA) and variable interval time averaging (VITA) methods (median value of 20 runs). The results are presented in Figures E-1 and E-2 for the smooth PVC and fixed gravel beds respectively.

The experimental results showed a number of basic features. Overall the turbulent stress data suggested that the passage of breaking tidal bores was associated with large turbulent stresses at all vertical elevations. That is, the magnitude of the Reynolds stress tensor components was significantly larger than prior to the bore passage. The finding was consistent with the observations of KOCH and CHANSON (2009), although their study deduced the turbulent stresses from a VITA analysis of a single experiment and they did not present any ensemble-averaged nor VITA median data. Second, in the present study, both the ensemble-averaging and variable interval time averaging techniques yielded comparable results (Fig. E1 & E-2). Third, the data presented a lot of noise close to the bed ($z/d_o = 0.135$). It is believed that this was linked with the ADV signal quality and some acoustic reflections on the bed. This was documented in further details in Appendix B.

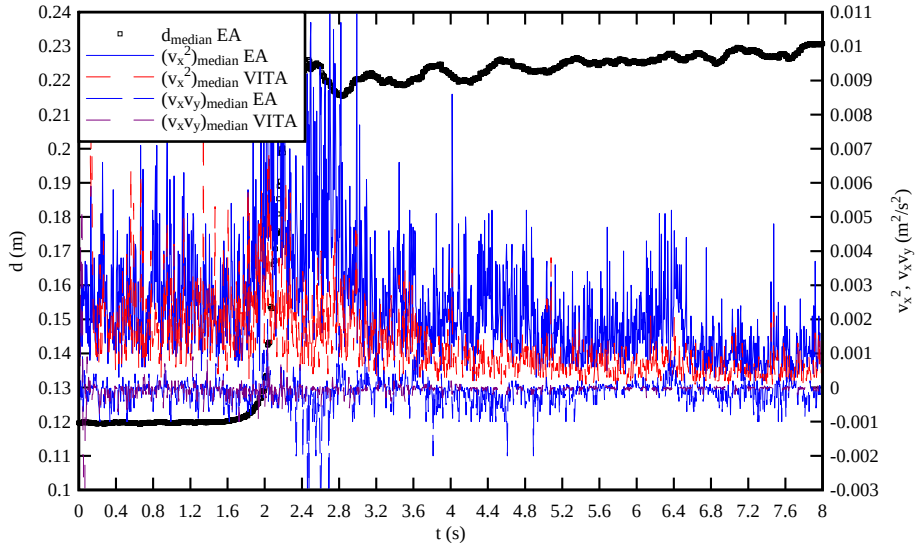
d_median EA
(v_x^2)_median EA
(v_x^2)_median VITA
(v_xv_y)_median EA
(v_xv_y)_median VITA
d (m)
t (s)
v_x^2, v_xv_y (m^2/s^2)

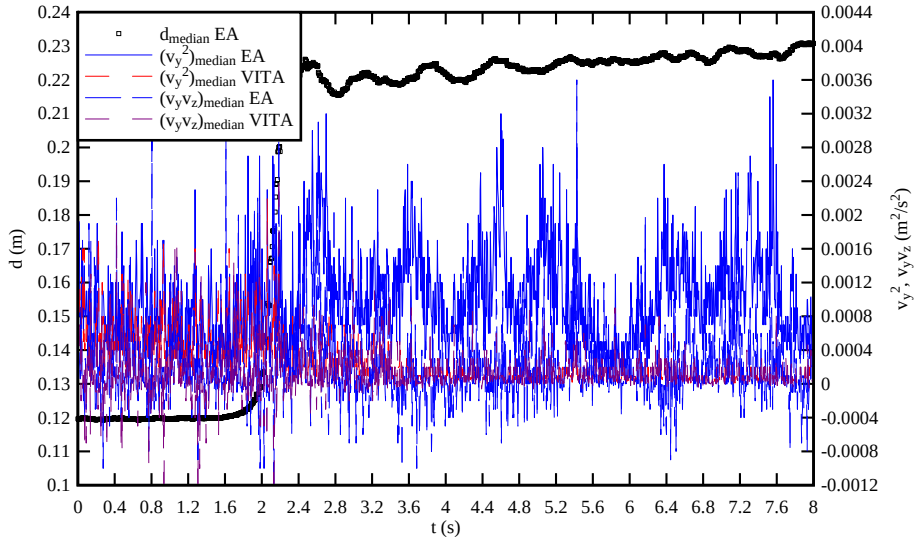
d_median EA
(v_y^2)_median EA
(v_y^2)_median VITA
(v_yv_z)_median EA
(v_yv_z)_median VITA
d (m)
t (s)
v_y^2, v_yv_z (m^2/s^2)

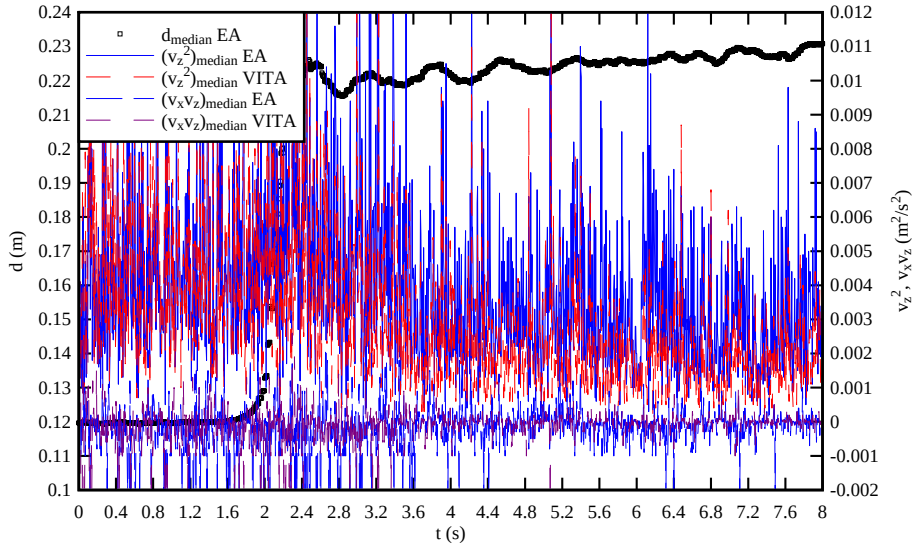
d_median EA
(v_z^2)_median EA
(v_z^2)_median VITA
(v_xv_z)_median EA
(v_xv_z)_median VITA
d (m)
t (s)
v_z^2, v_xv_z (m^2/s^2)

(A) $z/d_o = 0.135$

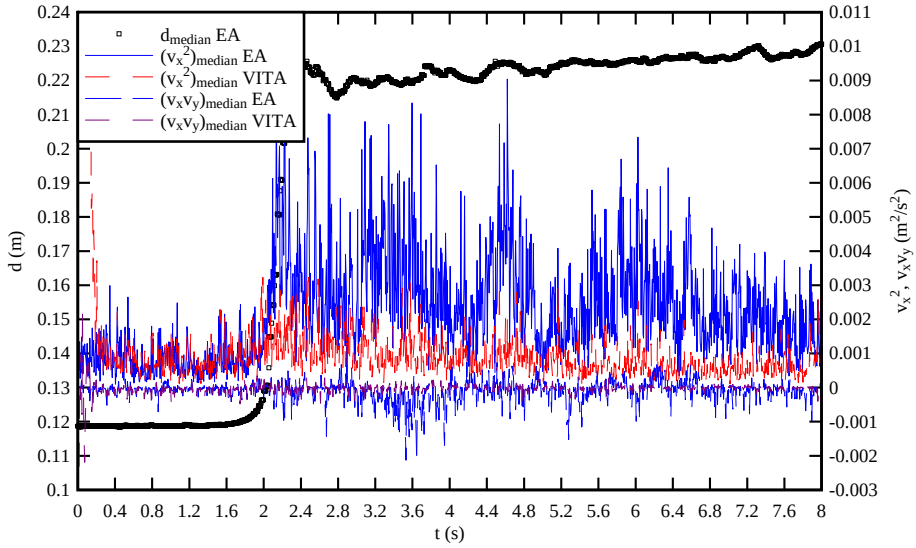
d_median EA
(v_x^2)_median EA
(v_x^2)_median VITA
(v_xv_y)_median EA
(v_xv_y)_median VITA
d (m)
t (s)
v_x^2, v_xv_y (m^2/s^2)

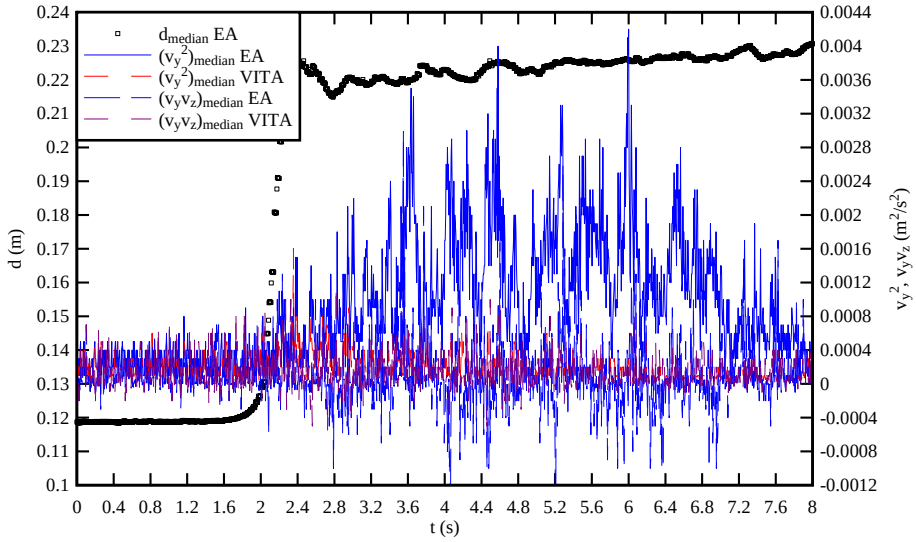
d_median EA
(v_y^2)_median EA
(v_y^2)_median VITA
(v_yv_z)_median EA
(v_yv_z)_median VITA
d (m)
t (s)
v_y^2, v_yv_z (m^2/s^2)

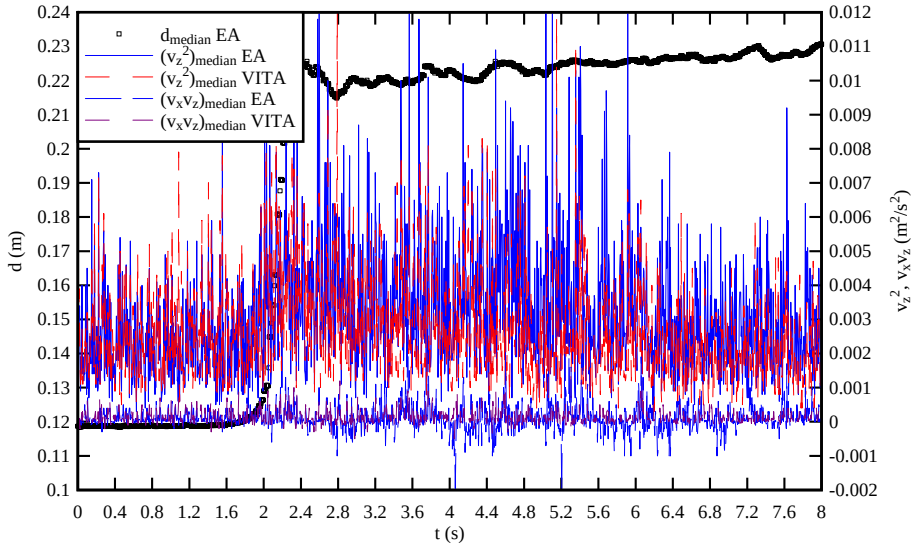
d_median EA
(v_z^2)_median EA
(v_z^2)_median VITA
(v_xv_z)_median EA
(v_xv_z)_median VITA
d (m)
t (s)
v_z^2, v_xv_z (m^2/s^2)

(B) $z/d_o = 0.434$

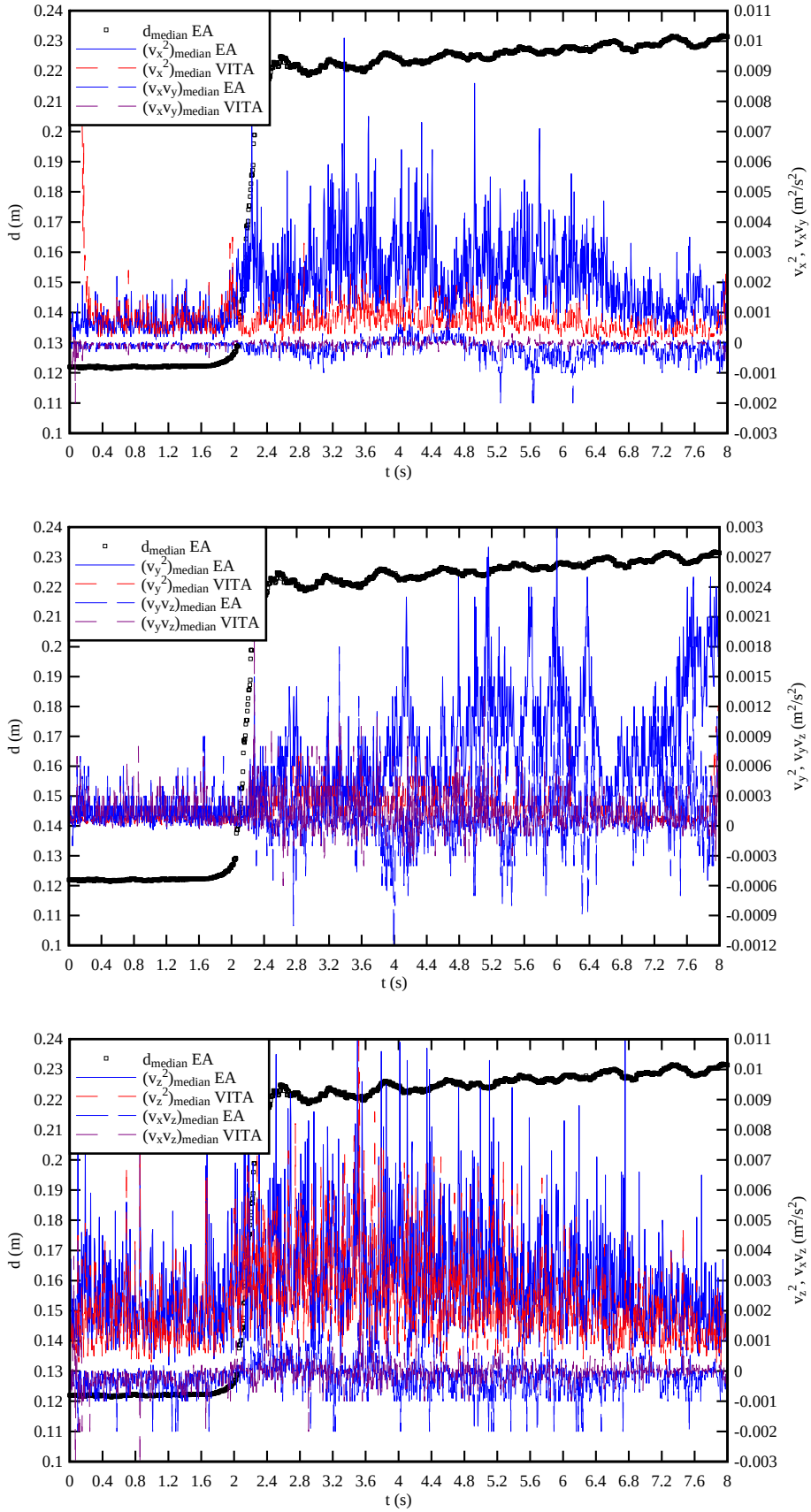

(C) $z/d_o = 0.733$

Fig. E-1 - Ensemble-average median water depth d_{median} and median Reynolds stress tensor components on smooth PVC bed - Comparison between ensemble-averaged median value and median VITA value - From top to bottom: (v_x^2, $v_x \times v_y$), (v_y^2, $v_y \times v_z$), (v_z^2, $v_x \times v_z$)

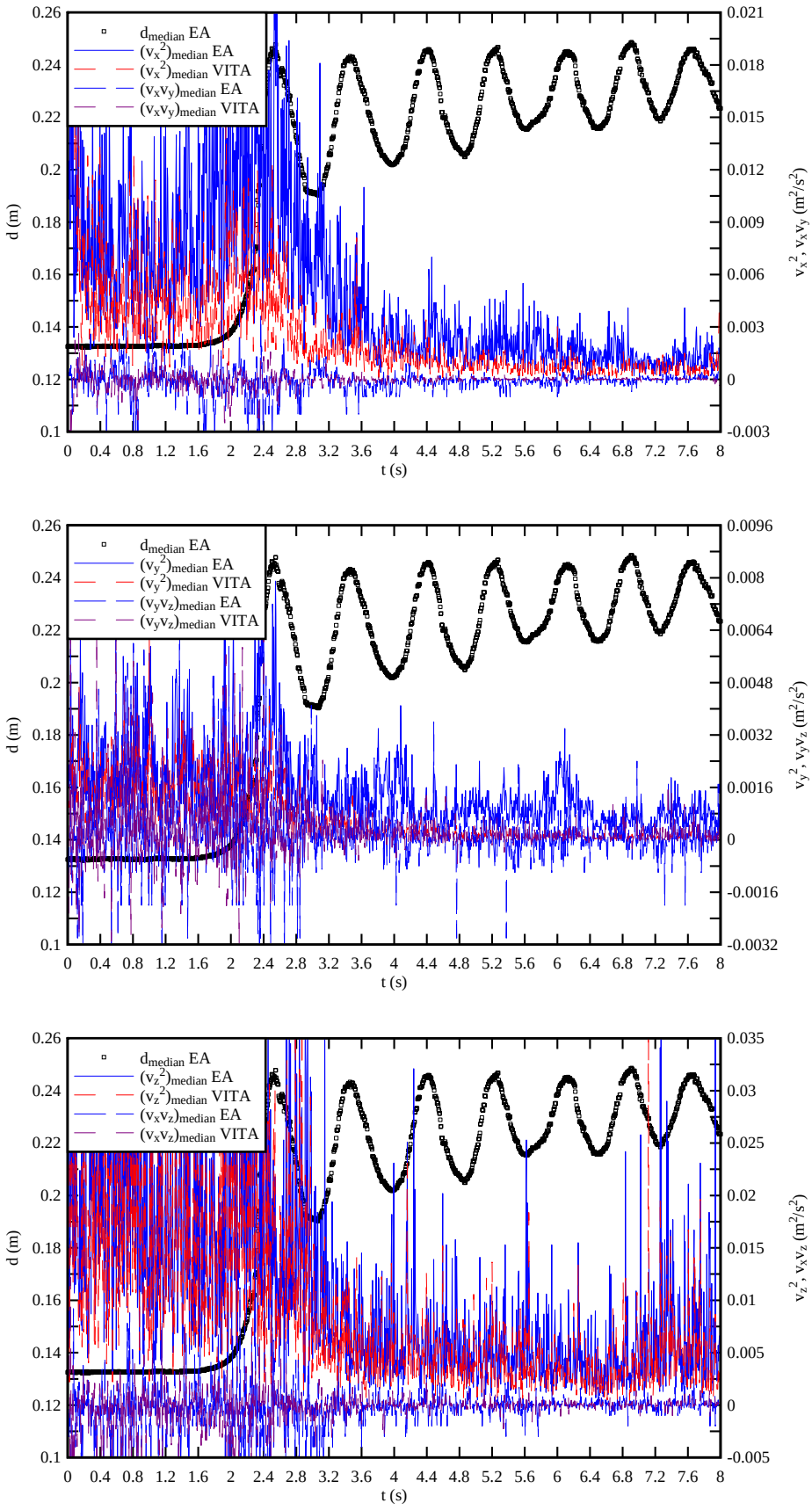
d_median EA
(v_x^2)_median EA
(v_x^2)_median VITA
(v_xv_y)_median EA
(v_xv_y)_median VITA
d (m)
t (s)
v_x^2 , v_xv_y (m^2/s^2)
(v_y^2)_median EA
(v_y^2)_median VITA
(v_yv_z)_median EA
(v_yv_z)_median VITA
v_y^2 , v_yv_z (m^2/s^2)
(v_z^2)_median EA
(v_z^2)_median VITA
(v_xv_z)_median EA
(v_xv_z)_median VITA
v_z^2 , v_xv_z (m^2/s^2)

(A) $z/d_o = 0.135$

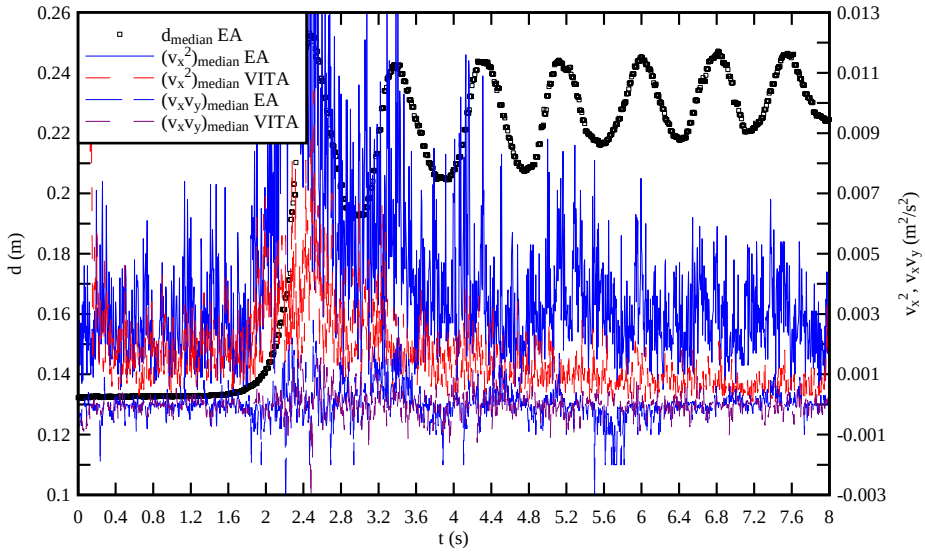
d_median EA
(v_x^2)_median EA
(v_x^2)_median VITA
(v_xv_y)_median EA
(v_xv_y)_median VITA
d (m)
t (s)
v_x^2 , v_xv_y (m^2/s^2)

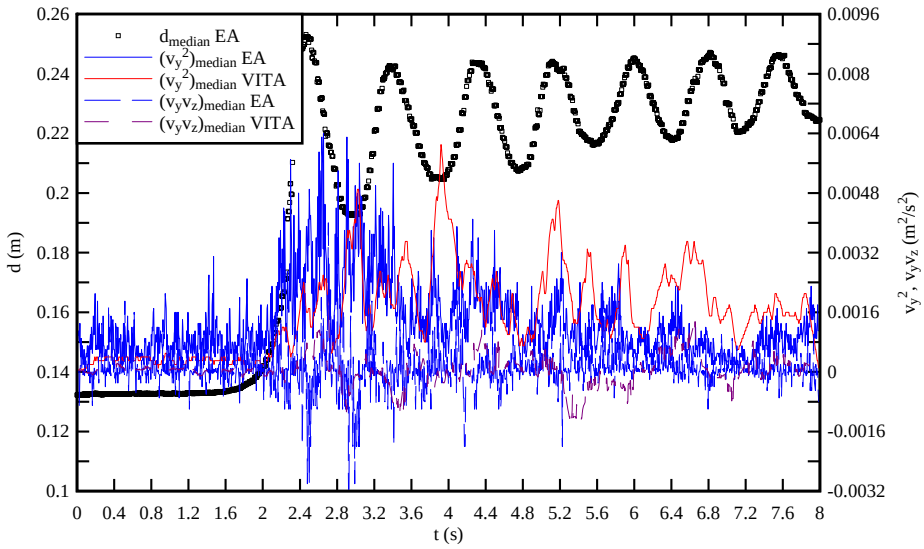
d_median EA
(v_y^2)_median EA
(v_y^2)_median VITA
(v_yv_z)_median EA
(v_yv_z)_median VITA
d (m)
t (s)
v_y^2 , v_yv_z (m^2/s^2)

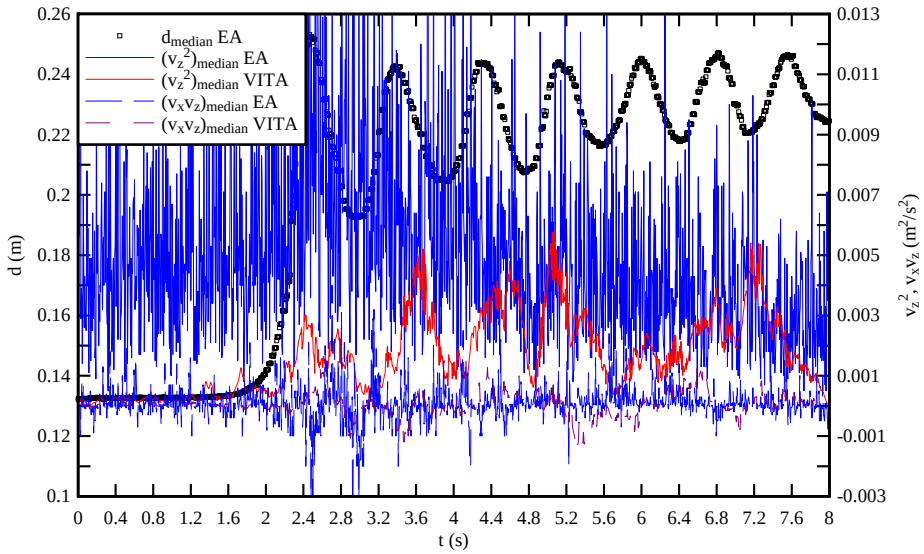
d_median EA
(v_z^2)_median EA
(v_z^2)_median VITA
(v_xv_z)_median EA
(v_xv_z)_median VITA
d (m)
t (s)
v_z^2 , v_xv_z (m^2/s^2)

(B) $z/d_o = 0.434$

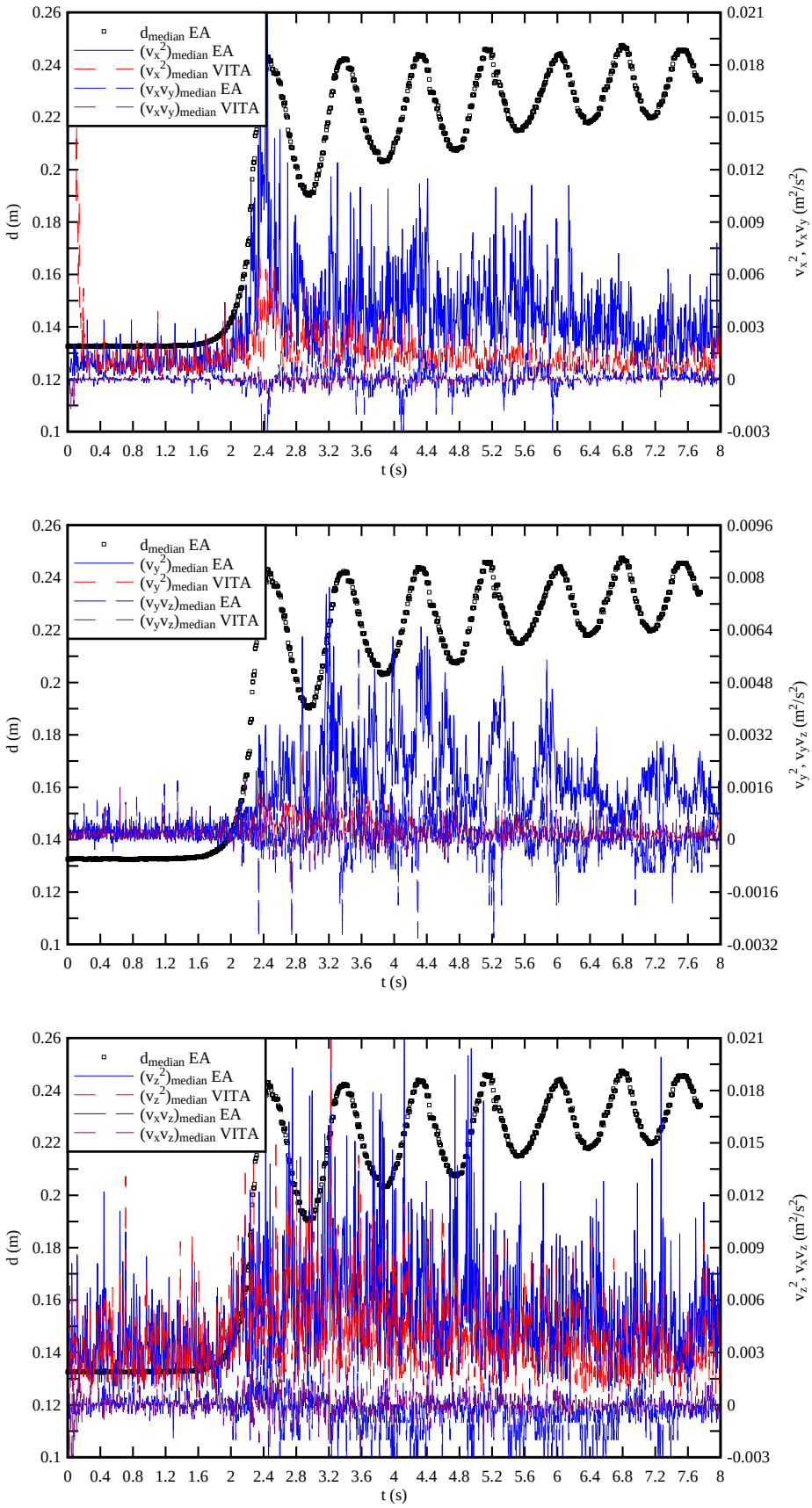

(C) $z/d_o = 0.733$

Fig. E-2 - Ensemble-average median water depth d_{median} and median Reynolds stress tensor components on fixed gravel bed - Comparison between ensemble-averaged median value and median VITA value - From top to bottom: (v_x^2, $v_x \times v_y$), (v_y^2, $v_y \times v_z$), (v_z^2, $v_x \times v_z$)

Appendix F - The underwater noise of breaking tidal bores in laboratory (by H. CHANSON)

F.1 Presentation

In a plunging jet and a hydraulic jump, air bubble entrainment takes place and the entrained bubbles generate some sounds upon formation and deformation that are responsible for most of the noise (MINNAERT 1933, LEIGHTON 1994). In first approximation, the bubble diameter is inversely proportional to the sound frequency: i.e., a small bubble generates a high-frequency sound. The diameter may be crudely approximated by:

$$D_{ab} = \frac{a_o}{F} \quad \text{(F-1)}$$

where D_{ab} is the bubble diameter, F is the acoustic frequency and a_o is the Minnaert factor which is a function the ambient atmospheric pressure (P_{atm}), liquid density (ρ) and depth below the free-surface (d-z):

$$a_o = \frac{1}{2 \times \pi} \times \sqrt{\frac{3 \times \gamma \times (P_{atm} + \rho \times g \times (d - z))}{\rho}} \quad \text{(F-2)}$$

where γ is the specific heat ratio ($\gamma = C_p/C_v = 1.4$ for air), d is the water depth and z is the vertical distance from the bed (MANASSEH et al. 2001).

Herein some underwater acoustic measurements were conducted in a hydraulic laboratory to study the transient underwater noise generated by a breaking tidal bore.

F.2 Laboratory experiments

The new experiments were performed in a relatively large tilting flume at the University of Queensland. The channel was 0.5 m wide 12 m long, and its slope was set horizontal for all experiments. The flume was made of smooth PVC bed and glass walls, and the waters were supplied by a constant head tank. A tainter gate was located at the channel downstream end (x = 11.15 m). The gate was fast-closing (closure time less than 0.2 s) and used to generate the tidal bore.

The water discharge was measured with two orifice meters that were designed based upon the British Standards (British Standard 1943). The percentage of error was expected to be less than 2%. In steady flows, the water depths were measured using rail mounted pointer gauges. The surge propagation was studied with a digital video camera Sony DSR-PD100AP equipped with a 3CCD sensor ([1]). The camera was equipped with a stereo electret condenser microphone and could be connected to an external audio input. The audio signal pulse-code modulation (PCM) was: 16 bit, 48 kHz/2 channels.

The underwater acoustic properties were measured with a hydrophone Dolphin Ear™ connected to a charge amplifier. The hydrophone and amplifier were previously used by CHANSON (2002,2007) in a large size dropshaft. The amplifier had a high-pass filter cut-off set at 400 Hz. (That is, it reached 100% at 400 Hz, admitting all frequencies above 400 Hz unchanged, and rolling off below 400 Hz. Hence acoustic data below 400 Hz can be disregarded.). The hydrophone was located just beneath the initially steady free-surface on the

[1] 25 frames per second.

channel centreline. It was attached to a hard-plastic support. The relative flexibility of the support ensured that its resonance frequency did not disturb the sound recordings. The acoustic recordings were conducted for 30 seconds. The signal was digitised either by the digital video camera at 32 kHz, or by a Yamaha AC-XG WDM Audio card at 48.0 kHz implying an alias frequency of about 24 kHz. The range of tidal bore conditions caused a difference in acoustic signal power of up to 20 dB corresponding to a factor of 10 in sound amplitude during the record.

In addition, some data were recorded and processed with a bubble acoustic software StreamTone™ (MANASSEH et al. 2001). In that case, the acoustic data were analysed following principles detailed in MANASSEH et al. (2001). A discrete, pulse-wise analysis was used. The technique can give good accuracy on the true bubble frequencies, but the conversion to bubble size spectra relies upon a questionable assumption that bubbles of different sizes are perturbed to the same proportional extent. It also assumes that the bubbles do not interact acoustically (CHANSON and MANASSEH 2003). The Streamtone™ software was set with a sound sampling rate of 11,025 Hz, a data length of 1000 samples, a trigger level of 0.1 Volt and a SuperWindow factor of 7.0.

F.3 Basic results

F.3.1 Presentation

The experiments were conducted in tidal bores with Froude numbers Fr between 1.4 and 1.7 and initial flow depths d_o between 0.09 and 0.13 m. For tidal bore Froude numbers between 1.4 and 1.5, the bore had a breaking front followed by an undular profile with relatively flat secondary waves. For Froude numbers larger than 1.5, the breaking bore advanced rapidly and no secondary free-surface undulation was observed. The breaking bore was characterised by a marked roller, some strong turbulence and some air bubbles were entrained at the roller toe into the developing mixing layer. This is illustrated in Figure F-1.

(A) Fr = 1.36, U = 0.95 m/s, d_o = 0.138 m, Run 091110b - Looking downstream at the incoming bore front

(B) Fr = 1.41, U = 0.96 m/s, d_o = 0.144 m, Run 091116 - Looking downstream at the incoming bore front

(C) Fr = 1.41, U = 0.96 m/s, d_o = 0.144 m, Run 091116 - Side view, looking beneath the bore roller

Fig. F-1 - Photographs of breaking tidal bores

F.3.2 Experimental results

The acoustic spectra were measured for several tidal bore flow conditions corresponding to a breaking tidal bore with Froude numbers between 1.4 and 1.7. Figure F-2 shows some data for a number of experiments. The data include the instantaneous signal (left) and the power spectrum density function of the signal (right). In the latter, note that the horizontal axis has a logarithmic scale.

First the raw data showed the rapid arrival of the tidal bore, the large underwater noise associated with passage of the bore roller and the decaying underwater noise as the bore roller travelled upstream beyond the hydrophone (Fig. F-2 Left).

Second the acoustic data highlighted the high pitch of the sound, in sharp contrast with the rumble noise of tidal bore heard from far away (CHANSON 2009). The passage of the bore corresponded to a rapid succession of high frequency sounds that were characteristics of the sounds produced by the formation and deformation of air bubbles.

Third the filter-amplifier had a high-pass cut-off at 400 Hz. No inference can be made on acoustic data at frequencies below 400 Hz; but any distinctive feature at, for example 800 or 1,200 Hz, are genuine properties of the raw acoustic data. The aliasing frequency of the equipment was 16 or 24 kHz. Since the peaks fall off well before 3 kHz (Fig. F-2 Right), it is believed that they are genuine acoustic properties, subject only to the uncertainties of the assumptions in the analysis.

For all flow conditions, the underwater acoustic signatures of the tidal bore characterised clearly the passage

of the bore and the air entrapment of bubbles in the roller mixing layer (Fig. F-1), even with the crudest record. The result suggests that an acoustic technique, calibrated through detailed laboratory measurements, may provide useful insights in the tidal bore properties where the robust sensor can be used in hostile field conditions. Indeed, most underwater acoustic sensors are made from robust piezoelectric crystals and a key advantage is their robustness for use in the field and in hostile environments.

The acoustic signature characterises the noise created by the entrained air bubbles in the tidal bore at the roller toe. Therefore the location and orientation of the hydrophone was important. MANASSEH and CHANSON (2001) and CHANSON and MANASSEH (2003) discussed this issue for a vertical plunging jet. In the present study, the hydrophone was placed just beneath the free-surface of the initially steady flow: it was fully-submerged for the entire duration of the experiment. The hydrophone and its support induced some drag and perturbed the flow, and it is acknowledged that the setup had some limitations.

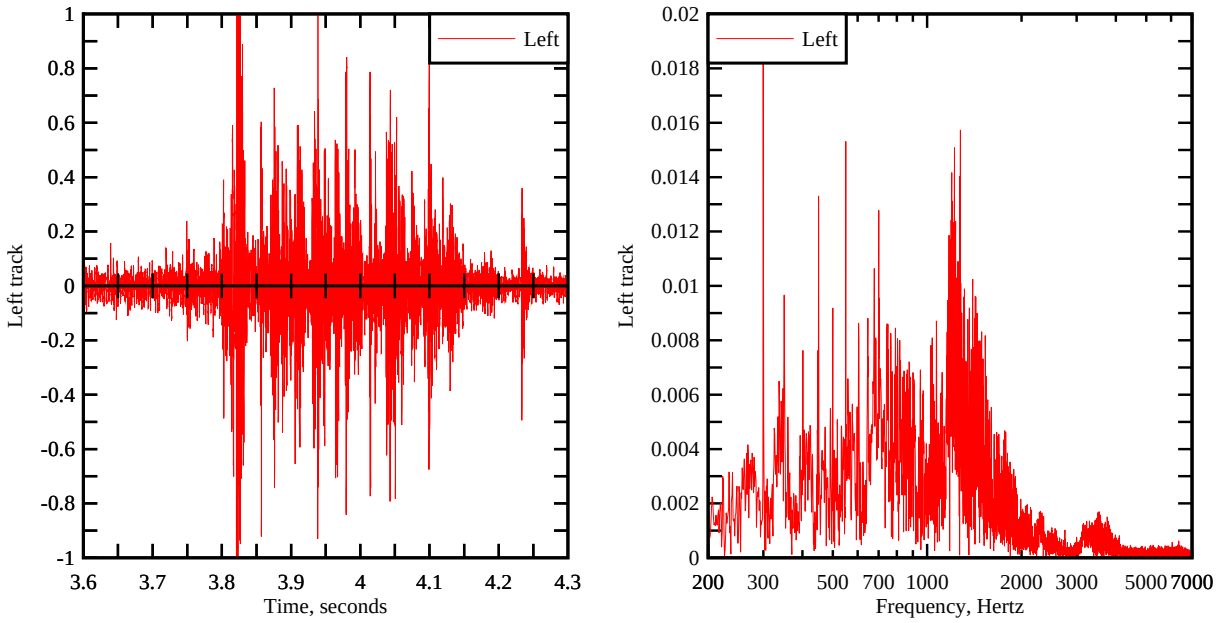

(A) Fr = 1.36, U = 0.82 m/s, d_o = 0.100 m, Run 091103 (recording with digital video camera Sony DSR-PD100AP)

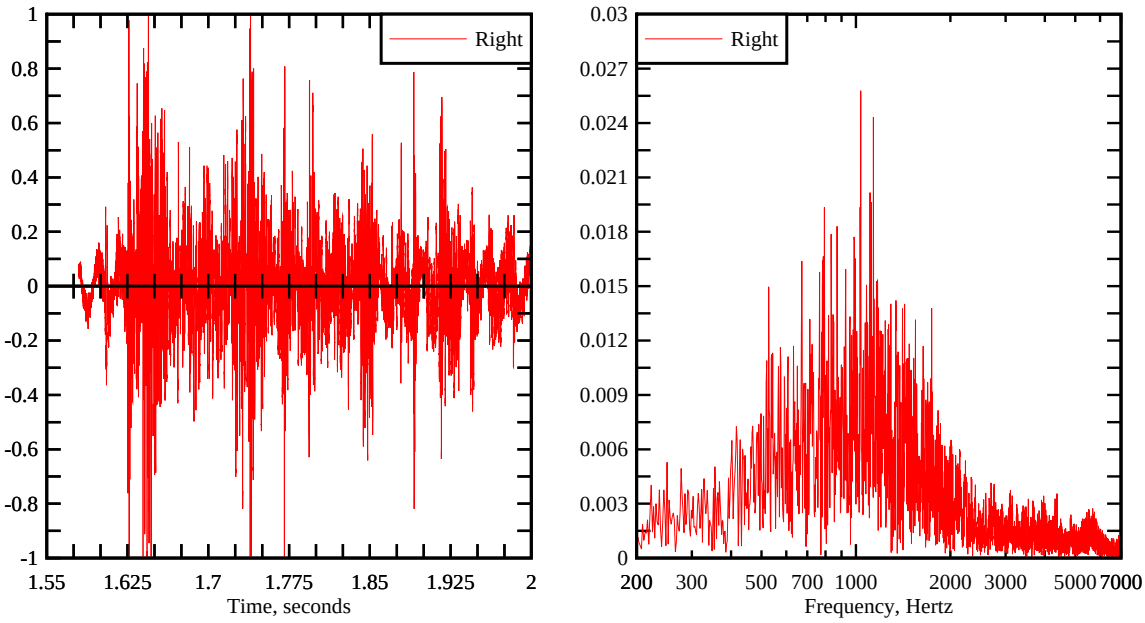

(B) Fr = 1.36, U = 0.95 m/s, d_o = 0.138 m, Run 091110b (recording with digital video camera Sony DSR-PD100AP)

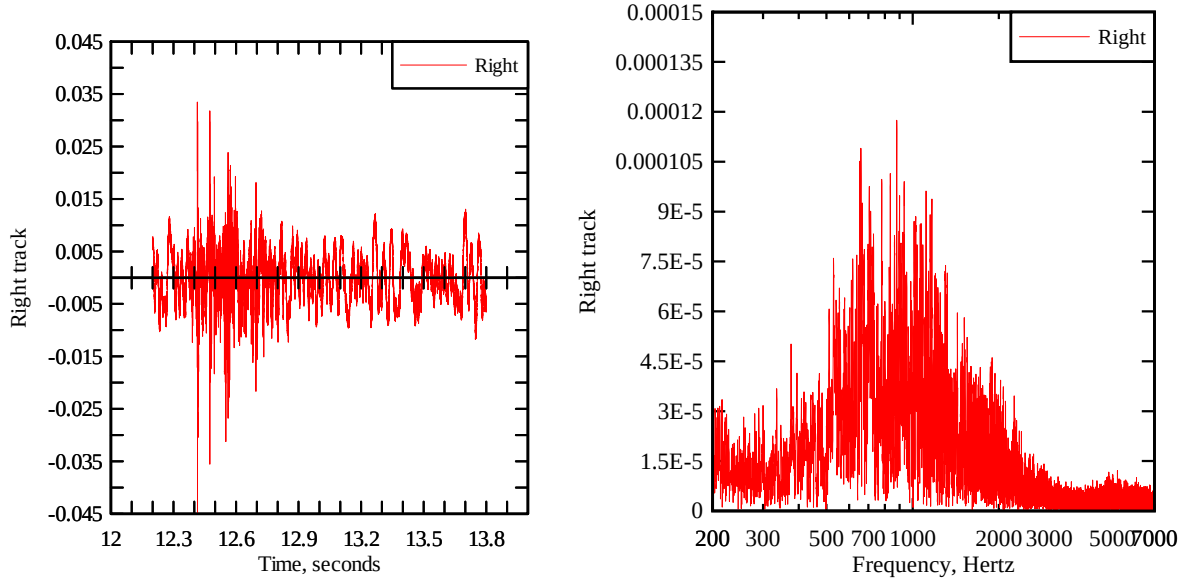

(C) Fr = 1.68, U = 0.83 m/s, d_o = 0.116 m, Run 091125 (recording with MS Sound Recorder software)

Fig. F-2 - Underwater acoustic signatures of the bubbly flow in the roller of breaking tidal bores

F.4 Discussion

Some acoustic data were analysed using a discrete, pulse-wise analysis following the 'first-period' method of MANASSEH et al. (2001). In a steady flow, the pulse-wise analysis gives good accuracy on the true bubble acoustic frequencies, and offers the benefit of bubble count-rates, although the low bubble count rates with the acoustic method was caused by sound sampling limitations of the sound card and PC-computer. However, in correcting the pulse-wise distributions to account for the greater amplitude of large bubbles, the conversion to bubble-size spectra relies on a questionable assumption: i.e., that bubbles of different sizes are perturbed to the same proportional extent (CHANSON and MANASSEH 2003). The technique also assumes

the bubbles do not interact acoustically. Basically, the "acoustic" bubble size distributions must not be expected to reproduce the bubble size distribution measured by an independent method. In the software Streamtone, a bubble was selected as the first pulse that had a trigger level above the threshold as soon as the hardware (sound card & PC) and software had finished buffering and processing the previous pulse (MANASSEH 2002, *Person. Comm.*). Thus the process was not a "selection" as much as a severe sub-sampling of the data. If the data is statistically stationary, this sub-sampling would not in itself introduce a bias. In any case, past experiences suggested that the Streamtone™ software was not properly calibrated and tested for the tidal bore flows. Further aspects of the techniques relevant to the present study are detailed in MANASSEH et al. (2001).

Table F-1 presents a typical data set. It illustrates the small number of bubbles detected and processed by the software within about 1 second after the tidal bore passage. Beyond that time, the underwater acoustic signature did not detect any entrapped bubble. Further the data (Table F-1) yielded bubble sizes that were significantly larger than the visual observations. The latters suggested entrained bubbles of 2-5 mm in diameters: i.e., with typical radii between 1.25 to 2.5 mm.

Table F-1 - Bubble radii detected by the Streamtone™ software - Flow conditions: Fr = 1.68, U = 0.83 m/s, d_o = 0.116 m, Run 091125

t s (1)	Radius (mm) (2)
13.540	3.582
13.810	3.582
14.081	2.388
14.351	4.179

Notes: tidal bore arrival at t = 13.4 to 13.5 s; sound trigger level = 0.1 V.

F.5 Acknowledgments

Hubert CHANSON thanks Dr Richard MANASSEH (formerly CSIRO Melbourne) for his valuable advice on acoustic measurements, and for providing the hydrophone and the Streamtone™ software. He acknowledges the technical assistance of Graham ILLIDGE and Clive BOOTH (The University of Queensland).

References

ANDERSEN, V.M. (1978). "Undular Hydraulic Jump." *Jl of Hyd. Div.*, ASCE, Vol. 104, No. HY8, pp. 1185-1188. Discussion : Vol. 105, No. HY9, pp. 1208-1211.

BARRÉ de SAINT-VENANT, A.J.C. (1871). "Théorie et Equations Générales du Mouvement Non Permanent des Eaux Courantes." *Comptes Rendus des séances de l'Académie des Sciences*, Paris, France, Séance 17 July 1871, Vol. 73, pp. 147-154 (in French).

BAZIN, H. (1865). "Recherches Expérimentales sur la Propagation des Ondes." ('Experimental Research on Wave Propagation.') *Mémoires présentés par divers savants à l'Académie des Sciences*, Paris, France, Vol. 19, pp. 495-644 (in French).

BENET, F., and CUNGE, J.A. (1971). "Analysis of Experiments on Secondary Undulations caused by Surge Waves in Trapezoidal Channels." *Jl of Hyd. Res.*, IAHR, Vol. 9, No. 1, pp. 11-33.

BENJAMIN, T.B., and LIGHTHILL, M.J. (1954). "On Cnoidal Waves and Bores." *Proc. Royal Soc. of London, Series A, Math. & Phys. Sc.*, Vol. 224, No. 1159, pp. 448-460.

BLANCKAERT, K.,and LEMMIN, U. (2006). "Means of Noise reduction in Acoustic Turbulence Measurements." *Jl of Hyd. Res.*, IAHR, Vol. 44, No. 1, pp. 3-17.

BOUSSINESQ, J.V. (1871). "Théorie de l'Intumescence appelée Onde Solitaire ou de Translation se Propageant dans un Canal Rectangulaire." ('Theory of the Solitary Wave propagating in an Rectangular Channel.') *Comptes-Rendus de l'Académie des Sciences*, Paris, France, Vol. 72, pp. 755-759.

BOUSSINESQ, J.V. (1877). "Essai sur la Théorie des Eaux Courantes." ('Essay on the Theory of Water Flow.') *Mémoires présentés par divers savants à l'Académie des Sciences*, Paris, France, Vol. 23, Série 3, No. 1, supplément 24, pp. 1-680 (in French).

BRADSHAW, P. (1971). "An Introduction to Turbulence and its Measurement." *Pergamon Press*, Oxford, UK, The Commonwealth and International Library of Science and technology Engineering and Liberal Studies, Thermodynamics and Fluid Mechanics Division, 218 pages.

British Standard (1943). "Flow Measurement." *British Standard Code BS 1042:1943*, British Standard Institution, London.

CHANSON, H,. (2002). "An Experimental Study of Roman Dropshaft Operation : Hydraulics, Two-Phase Flow, Acoustics." *Report CH50/02*, Dept of Civil Eng., Univ. of Queensland, Brisbane, Australia, 99 pages.

CHANSON, H. (2004). "The Hydraulics of Open Channel Flow: An Introduction." *Butterworth-Heinemann*, 2nd edition, Oxford, UK, 630 pages.

CHANSON, H. (2005). "Physical Modelling of the Flow Field in an Undular Tidal Bore." *Jl of Hyd. Res.*, IAHR, Vol. 43, No. 3, pp. 234-244.

CHANSON, H. (2007). "Air Entrainment Processes in Rectangular Dropshafts at Large Flows." *Journal of Hydraulic Research*, IAHR, Vol. 45, No. 1, pp. 42-53.

CHANSON, H. (2008a). "Turbulence in Positive Surges and Tidal Bores. Effects of Bed Roughness and Adverse Bed Slopes." *Hydraulic Model Report No. CH68/08*, Div. of Civil Engineering, The University of Queensland, Brisbane, Australia, 121 pages & 5 movie files.

CHANSON, H. (2008b). "Acoustic Doppler Velocimetry (ADV) in the Field and in Laboratory: Practical Experiences." *Proceedings of the International Meeting on Measurements and Hydraulics of Sewers IMMHS'08*, Summer School GEMCEA/LCPC, 19-21 Aug. 2008, Bouguenais, Frédérique LARRARTE and Hubert CHANSON Eds., Hydraulic Model Report No. CH70/08, Div. of Civil Engineering, The University of Queensland, Brisbane, Australia, Dec., pp. 49-66.

CHANSON, H. (2009). "The Rumble Sound Generated by a Tidal Bore Event in the Baie du Mont Saint Michel." *Journal of Acoustical Society of America*, Vol. 125, No. 6, pp. 3561-3568 (DOI: 10.1121/1.3124781).

CHANSON, H. (2010a). "Current Knowledge in Tidal bores and their Environmental, Ecological and Cultural Impacts." *Environmental Fluid Mechanics*, Vol. 10, No. 4 (DOI: 10.1007/s10652-009-9160-5). (**In print**)

CHANSON, H. (2010b). "Unsteady Turbulence in Tidal Bores: the Effects of Bed Roughness." *Journal of Waterway, Port, Coastal, and Ocean Engineering*, ASCE, Vol. 136 (ISSN 0733-950X). (**In print**)

CHANSON, H. (2010b). "Tidal Bores, Aegir and Pororoca: the Geophysical Wonders." *Proc. of 17th Congress of IAHR Asia and Pacific Division*, IAHR-APD, Auckland, New Zealand, 21-24 Feb., B. MELVILLE, G. DE COSTA, and T. SWANN Eds., Invited keynote lecture, 18 pages.

CHANSON, H., AOKI, S., and MARUYAMA, M. (2002). "Unsteady Two-Dimensional Orifice Flow: a Large-Size Experimental Investigation." *Journal of Hydraulic Research*, IAHR, Vol. 40, No. 1, pp. 63-71.

CHANSON, H., and MANASSEH, R. (2003). "Air Entrainment Processes in a Circular Plunging Jet. Void Fraction and Acoustic Measurements." *Journal of Fluids Engineering*, Trans. ASME, Vol. 125, No. 5, Sept., pp. 910-921.

CHANSON, H., TREVETHAN, M., and AOKI, S. (2008a). "Acoustic Doppler Velocimetry (ADV) in Small Estuary : Field Experience and Signal Post-Processing." *Flow Measurement and Instrumentation*, Vol. 19, No. 5, pp. 307-313 (DOI: 10.1016/j.flowmeasinst.2008.03.003).

CHANSON, H., TAKEUCHI, M., and TREVETHAN, M. (2008b). "Using Turbidity and Acoustic Backscatter Intensity as Surrogate Measures of Suspended Sediment Concentration in a Small Sub-Tropical Estuary." *Journal of Environmental Management*, Vol. 88, No. 4, Sept., pp. 1406-1416 (DOI: 10.1016/j.jenvman.2007.07.009).

DOROUDIAN, B., HURTHER, D., and LEMMIN, U. (2007). "Turbulence Measurements with Acoustic Doppler Velocimeters. Discussion." *Journal of Hydraulic Engineering*, ASCE, Vol. 133, No. 11, pp. 1286-1289.

FAVRE, H. (1935). "Etude Théorique et Expérimentale des Ondes de Translation dans les Canaux Découverts." ('Theoretical and Experimental Study of Travelling Surges in Open Channels.') *Dunod*, Paris, France (in French).

GARCIA, C.M., and GARCIA, M.H. (2006). "Characterization of Flow Turbulence in Large-Scale Bubble-Plume Experiments." *Experiments in Fluids*, Vol. 41, No. 1, pp. 91-101..

GORING, D.G., and NIKORA, V.I. (2002). "Despiking Acoustic Doppler Velocimeter Data." *Jl of Hyd. Engrg.*, ASCE, Vol. 128, No. 1, pp. 117-126. Discussion: Vol. 129, No. 6, pp. 484-489.

HENDERSON, F.M. (1966). "Open Channel Flow." *MacMillan Company*, New York, USA.

HINZE, J.O. (1975). "Turbulence." *McGraw-Hill Publ.*, 2nd Edition, New York, USA.

HORNUNG, H.G., WILLERT, C., and TURNER, S. (1995). "The Flow Field Downsteam of a Hydraulic Jump." *Jl of Fluid Mech.*, Vol. 287, pp. 299-316.

KOCH, C., and CHANSON, H. (2005). "An Experimental Study of Tidal Bores and Positive Surges: Hydrodynamics and Turbulence of the Bore Front." *Report No. CH56/05*, Dept. of Civil Engineering, The University of Queensland, Brisbane, Australia, July, 170 pages.

KOCH, C., and CHANSON, H. (2008). "Turbulent Mixing beneath an Undular Bore Front." *Journal of Coastal Research*, Vol. 24, No. 4, pp. 999-1007 (DOI: 10.2112/06-0688.1).

KOCH, C., and CHANSON, H. (2009). "Turbulence Measurements in Positive Surges and Bores." *Journal of Hydraulic Research*, IAHR, Vol. 47, No. 1, pp. 29-40 (DOI: 10.3826/jhr.2009.2954).

LEIGHTON, T. G. (1994). "The Acoustic Bubble." *Academic Press*, London.

LEMMIN, U., and LHERMITTE, R. (1999). "ADV Measurements of Turbulence: can we Improve their Interpretation ? Discussion" *Jl of Hyd. Engrg.*, ASCE, Vol. 125, No. 6, pp. 987-988.

LEMOINE, R. (1948). "Sur les Ondes Positives de Translation dans les Canaux et sur le Ressaut Ondulé de Faible Amplitude." ('On the Positive Surges in Channels and on the Undular Jumps of Low Wave Height.') *Jl La Houille Blanche*, Mar-Apr., pp. 183-185 (in French).

LEWIS, A.W. (1972). "Field Studies of a Tidal Bore in the River Dee." *M.Sc. thesis*, Marine Science Laboratories, University College of North Wales, Bangor, UK.

LIGGETT, J.A. (1994). "Fluid Mechanics." *McGraw-Hill*, New York, USA.

LIU, M., ZHU, D., and RAJARATNAM, N. (2002). "Evaluation of ADV Measurements in Bubbly Two-Phase Flows." *Proc. Conf. on Hydraulic Measurements and Experimental Methods*, ASCE-EWRI & IAHR, Estes Park, USA, 10 pages (CD-ROM).

LUBIN, P., CHANSON, H., and GLOCKNER, S. (2010). "Large Eddy Simulation of Turbulence Generated by a Weak Breaking Tidal Bore." *Environmental Fluid Mechanics*, Vol. 10 (DOI: 10.1007/s10652-009-9165-0) (**In Print**).

MANASSEH, R., LAFONTAINE, R.F., DAVY, J., SHEPHERD, I.C., and ZHU, Y. (2001). "Passive Acoustic Bubble Sizing in Sparged Systems" *Exp. Fluids*, Vol. 30, No. 6, pp. 672-682.

McLELLAND, S.J., and NICHOLAS, A.P. (2000). "A New Method for Evaluating Errors in High-Frequency ADV Measurements." *Hydrological Processes*, Vol. 14, pp. 351-366.

MINNAERT, M. (1933). "On Musical Air Bubbles and the Sound of Running Water." *Philos. Mag.*, Vol. 16, pp. 235-248.

MONTES, J.S. (1998). "Hydraulics of Open Channel Flow." *ASCE Press*, New-York, USA, 697 pages.

MOUAZE, D., MURZYN, F., and CHAPLIN, J.R. (2005). "Free Surface Length Scale Estimation in Hydraulic Jumps." *Jl of Fluids Eng.*, Trans. ASME, Vol. 127, pp. 1191-1193.

MURZYN, F., and CHANSON, H. (2009). "Free-Surface Fluctuations in Hydraulic Jumps: Experimental Observations." *Experimental Thermal and Fluid Science*, Vol. 33, No. 7, pp. 1055-1064 (DOI: 10.1016/j.expthermflusci.2009.06.003).

NAVARRE, P. (1995). "Aspects Physiques du Caracteres Ondulatoire du Macaret en Dordogne." ('Physical Features of the Undulations of the Dordogne River Tidal Bore.') *D.E.A. thesis*, Univ. of Bordeaux, France, 72 pages (in French).

NIKORA, V.I., and GORING, D.G. (1998). "ADV Measurements of Turbulence: can we Improve their Interpretation ?" *Jl of Hyd. Engrg.*, ASCE, Vol. 124, No. 6, pp. 630-634. Discussion: Vol. 125, No. 9, pp. 987-988.

PEREGRINE, D.H. (1966). "Calculations of the Development of an Undular Bore." *Jl. Fluid Mech.*, Vol 25, pp.321-330.

PIQUET, J. (1999). "Turbulent Flows. Models and Physics." *Springer*, Berlin, Germany, 761 pages.

RAYLEIGH, Lord (1908). "Note on Tidal Bores." *Proc. Royal Soc. of London, Series A containing Papers of a Mathematical and Physical Character*, Vol. 81, No. 541, pp. 448-449.

SERRE, F. (1953). "Contribution à l'Etude des Ecoulements Permanents et Variables dans les Canaux." ('Contribution to the Study of Permanent and Non-Permanent Flows in Channels.') *Jl La Houille Blanche*, Dec., pp. 830-872 (in French).

TRESKE, A. (1994). "Undular Bores (Favre-Waves) in Open Channels - Experimental Studies." *Jl of Hyd. Res.*, IAHR, Vol. 32, No. 3, pp. 355-370. Discussion : Vol. 33, No. 3, pp. 274-278.

VOULGARIS, G., and TROWBRIDGE, J.H. (1998). "Evaluation of the Acoustic Doppler Velocimeter (ADV) for Turbulence Measurements." *Jl Atmosph. and Oceanic Tech.*, Vol. 15, pp. 272-289.

WAHL, T.L. (2003). "Despiking Acoustic Doppler Velocimeter Data. Discussion." *Jl of Hyd. Engrg.*, ASCE, Vol. 129, No. 6, pp. 484-487.

WOLANSKI, E., WILLIAMS, D., SPAGNOL, S., and CHANSON, H. (2004). "Undular Tidal Bore Dynamics in the Daly Estuary, Northern Australia." *Estuarine, Coastal and Shelf Science*, Vol. 60, No. 4, pp. 629-636 (DOI: 10.1016/j.ecss.2004.03.001).

Bibliographic reference of the Report CH76/10

The Hydraulic Model research report series CH is a refereed publication published by the School of Civil Engineering at the University of Queensland, Brisbane, Australia.

The bibliographic reference of the present report is :

DOCHERTY, N.J., and CHANSON, H. (2010). "Characterisation of Unsteady Turbulence in Breaking Tidal Bores including the Effects of Bed Roughness." *Hydraulic Model Report No. CH76/10*, School of Civil Engineering, The University of Queensland, Brisbane, Australia, 112 pages (ISBN 9781864999884).

The Report CH76/10 is available, in the present form, as a PDF file on the Internet at UQeSpace:

http://espace.library.uq.edu.au/

It is listed at:

http://espace.library.uq.edu.au/list/author_id/193/

Hydraulic model research report CH

The Hydraulic Model Report CH series is published by the School of Civil Engineering at the University of Queensland. Orders of any reprint(s) of the Hydraulic Model Reports should be addressed to the School Secretary.

School Secretary, School of Civil Engineering, The University of Queensland
Brisbane 4072, Australia - Tel.: (61 7) 3365 3619 - Fax : (61 7) 3365 4599
Url: http://www.eng.uq.edu.au/civil/ Email: hodciveng@uq.edu.au

Report CH	**Unit price**	Quantity	**Total price**
DOCHERTY, N.J., and CHANSON, H. (2010). "Characterisation of Unsteady Turbulence in Breaking Tidal Bores including the Effects of Bed Roughness." *Hydraulic Model Report No. CH76/10*, School of Civil Engineering, The University of Queensland, Brisbane, Australia, 112 pages (ISBN 9781864999884).	AUD$60.00		
CHANSON, H. (2009). "Advective Diffusion of Air Bubbles in Hydraulic Jumps with Large Froude Numbers: an Experimental Study." *Hydraulic Model Report No. CH75/09*, School of Civil Engineering, The University of Queensland, Brisbane, Australia, 89 pages & 3 videos (ISBN 9781864999730).	AUD$60.00		
CHANSON, H. (2009). "An Experimental Study of Tidal Bore Propagation: the Impact of Bridge Piers and Channel Constriction." *Hydraulic Model Report No. CH74/09*, School of Civil Engineering, The University of Queensland, Brisbane, Australia, 110 pages and 5 movies (ISBN 9781864999600).	AUD$60.00		
CHANSON, H. (2008). "Jean-Baptiste Charles Joseph BÉLANGER (1790-1874), the Backwater Equation and the Bélanger Equation." *Hydraulic Model Report No. CH69/08*, Div. of Civil Engineering, The University of Queensland, Brisbane, Australia, 40 pages (ISBN 9781864999211).	AUD$60.00		
GOURLAY, M.R., and HACKER, J. (2008). "Reef-Top Currents in Vicinity of Heron Island Boat Harbour, Great Barrier Reef, Australia: 2. Specific Influences of Tides Meteorological Events and Waves." *Hydraulic Model Report No. CH73/08*, Div. of Civil Engineering, The University of Queensland, Brisbane, Australia, 331 pages (ISBN 9781864999365).	AUD$60.00		
GOURLAY, M.R., and HACKER, J. (2008). "Reef Top Currents in Vicinity of Heron Island Boat Harbour Great Barrier Reef, Australia: 1. Overall influence of Tides, Winds, and Waves." *Hydraulic Model Report CH72/08*, Div. of Civil Engineering, The University of Queensland, Brisbane, Australia, 201 pages (ISBN 9781864999358).	AUD$60.00		
LARRARTE, F., and CHANSON, H. (2008). "Experiences and Challenges in Sewers: Measurements and Hydrodynamics." *Proceedings of the International Meeting on Measurements and Hydraulics of Sewers*, Summer School GEMCEA/LCPC, 19-21 Aug. 2008, Bouguenais, Hydraulic Model Report No. CH70/08, Div. of Civil Engineering, The University of Queensland, Brisbane, Australia (ISBN 9781864999280).	AUD$60.00		
CHANSON, H. (2008). "Photographic Observations of Tidal Bores (Mascarets) in France." *Hydraulic Model Report No. CH71/08*, Div. of Civil Engineering, The University of Queensland, Brisbane, Australia, 104 pages, 1 movie and 2 audio files (ISBN 9781864999303).	AUD$60.00		

CHANSON, H. (2008). "Turbulence in Positive Surges and Tidal Bores. Effects of Bed Roughness and Adverse Bed Slopes." *Hydraulic Model Report No. CH68/08*, Div. of Civil Engineering, The University of Queensland, Brisbane, Australia, 121 pages & 5 movie files (ISBN 9781864999198)	AUD$70.00		
FURUYAMA, S., and CHANSON, H. (2008). "A Numerical Study of Open Channel Flow Hydrodynamics and Turbulence of the Tidal Bore and Dam-Break Flows." *Report No. CH66/08*, Div. of Civil Engineering, The University of Queensland, Brisbane, Australia, May, 88 pages (ISBN 9781864999068).	AUD$60.00		
GUARD, P., MACPHERSON, K., and MOHOUPT, J. (2008). "A Field Investigation into the Groundwater Dynamics of Raine Island." *Report No. CH67/08*, Div. of Civil Engineering, The University of Queensland, Brisbane, Australia, February, 21 pages (ISBN 9781864999075).	AUD$40.00		
FELDER, S., and CHANSON, H. (2008). "Turbulence and Turbulent Length and Time Scales in Skimming Flows on a Stepped Spillway. Dynamic Similarity, Physical Modelling and Scale Effects." *Report No. CH64/07*, Div. of Civil Engineering, The University of Queensland, Brisbane, Australia, March, 217 pages (ISBN 9781864998870).	AUD$60.00		
TREVETHAN, M., CHANSON, H., and BROWN, R.J. (2007). "Turbulence and Turbulent Flux Events in a Small Subtropical Estuary." Report No. CH65/07, Div. of Civil Engineering, The University of Queensland, Brisbane, Australia, November, 67 pages (ISBN 9781864998993)	AUD$60.00		
MURZYN, F., and CHANSON, H. (2007). "Free Surface, Bubbly flow and Turbulence Measurements in Hydraulic Jumps." *Report CH63/07*, Div. of Civil Engineering, The University of Queensland, Brisbane, Australia, August, 116 pages (ISBN 9781864998917).	AUD$60.00		
KUCUKALI, S., and CHANSON, H. (2007). "Turbulence in Hydraulic Jumps: Experimental Measurements." *Report No. CH62/07*, Div. of Civil Engineering, The University of Queensland, Brisbane, Australia, July, 96 pages (ISBN 9781864998825).	AUD$60.00		
CHANSON, H., TAKEUCHI, M, and TREVETHAN, M. (2006). "Using Turbidity and Acoustic Backscatter Intensity as Surrogate Measures of Suspended Sediment Concentration. Application to a Sub-Tropical Estuary (Eprapah Creek)." *Report No. CH60/06*, Div. of Civil Engineering, The University of Queensland, Brisbane, Australia, July, 142 pages (ISBN 1864998628).	AUD$60.00		
CAROSI, G., and CHANSON, H. (2006). "Air-Water Time and Length Scales in Skimming Flows on a Stepped Spillway. Application to the Spray Characterisation." *Report No. CH59/06*, Div. of Civil Engineering, The University of Queensland, Brisbane, Australia, July (ISBN 1864998601).	AUD$60.00		
TREVETHAN, M., CHANSON, H., and BROWN, R. (2006). "Two Series of Detailed Turbulence Measurements in a Small Sub-Tropical Estuarine System." *Report No. CH58/06*, Div. of Civil Engineering, The University of Queensland, Brisbane, Australia, Mar. (ISBN 1864998520).	AUD$60.00		
KOCH, C., and CHANSON, H. (2005). "An Experimental Study of Tidal Bores and Positive Surges: Hydrodynamics and Turbulence of the Bore Front." *Report No. CH56/05*, Dept. of Civil Engineering, The University of Queensland, Brisbane, Australia, July (ISBN 1864998245).	AUD$60.00		
CHANSON, H. (2005). "Applications of the Saint-Venant Equations and Method of Characteristics to the Dam Break Wave Problem." *Report No. CH55/05*, Dept. of Civil Engineering, The University of Queensland, Brisbane, Australia, May (ISBN 1864997966).	AUD$60.00		
CHANSON, H., COUSSOT, P., JARNY, S., and TOQUER, L. (2004). "A Study of Dam Break Wave of Thixotropic Fluid: Bentonite Surges down an Inclined plane." *Report No. CH54/04*, Dept. of Civil Engineering, The University of Queensland, Brisbane, Australia, June, 90 pages (ISBN 1864997710).	AUD$60.00		

CHANSON, H. (2003). "A Hydraulic, Environmental and Ecological Assessment of a Sub-tropical Stream in Eastern Australia: Eprapah Creek, Victoria Point QLD on 4 April 2003." *Report No. CH52/03*, Dept. of Civil Engineering, The University of Queensland, Brisbane, Australia, June, 189 pages (ISBN 1864997044).	AUD$90.00		
CHANSON, H. (2003). "Sudden Flood Release down a Stepped Cascade. Unsteady Air-Water Flow Measurements. Applications to Wave Run-up, Flash Flood and Dam Break Wave." *Report CH51/03*, Dept of Civil Eng., Univ. of Queensland, Brisbane, Australia, 142 pages (ISBN 1864996552).	AUD$60.00		
CHANSON, H,. (2002). "An Experimental Study of Roman Dropshaft Operation : Hydraulics, Two-Phase Flow, Acoustics." *Report CH50/02*, Dept of Civil Eng., Univ. of Queensland, Brisbane, Australia, 99 pages (ISBN 1864996544).	AUD$60.00		
CHANSON, H., and BRATTBERG, T. (1997). "Experimental Investigations of Air Bubble Entrainment in Developing Shear Layers." *Report CH48/97*, Dept. of Civil Engineering, University of Queensland, Australia, Oct., 309 pages (ISBN 0 86776 748 0).	AUD$90.00		
CHANSON, H. (1996). "Some Hydraulic Aspects during Overflow above Inflatable Flexible Membrane Dam." *Report CH47/96*, Dept. of Civil Engineering, University of Queensland, Australia, May, 60 pages (ISBN 0 86776 644 1).	AUD$60.00		
CHANSON, H. (1995). "Flow Characteristics of Undular Hydraulic Jumps. Comparison with Near-Critical Flows." *Report CH45/95*, Dept. of Civil Engineering, University of Queensland, Australia, June, 202 pages (ISBN 0 86776 612 3).	AUD$60.00		
CHANSON, H. (1995). "Air Bubble Entrainment in Free-surface Turbulent Flows. Experimental Investigations." *Report CH46/95*, Dept. of Civil Engineering, University of Queensland, Australia, June, 368 pages (ISBN 0 86776 611 5).	AUD$80.00		
CHANSON, H. (1994). "Hydraulic Design of Stepped Channels and Spillways." *Report CH43/94*, Dept. of Civil Engineering, University of Queensland, Australia, Feb., 169 pages (ISBN 0 86776 560 7).	AUD$60.00		
POSTAGE & HANDLING (per report)	AUD$10.00		
GRAND TOTAL			

Other hydraulic research reports

Reports/Theses	Unit price	Quantity	Total price
TREVETHAN, M. (2008). "A Fundamental Study of Turbulence and Turbulent Mixing in a Small Subtropical Estuary." Ph.D. thesis, Div. of Civil Engineering, The University of Queensland, 342 pages.	AUD$100.00		
GONZALEZ, C.A. (2005). "An Experimental Study of Free-Surface Aeration on Embankment Stepped Chutes." *Ph.D. thesis*, Dept of Civil Engineering, The University of Queensland, Brisbane, Australia, 240 pages.	AUD$80.00		
TOOMBES, L. (2002). "Experimental Study of Air-Water Flow Properties on Low-Gradient Stepped Cascades." *Ph.D. thesis*, Dept of Civil Engineering, The University of Queensland, Brisbane, Australia.	AUD$100.00		
CHANSON, H. (1988). "A Study of Air Entrainment and Aeration Devices on a Spillway Model." *Ph.D. thesis*, University of Canterbury, New Zealand.	AUD$60.00		
POSTAGE & HANDLING (per report)	AUD$10.00		
GRAND TOTAL			

Civil Engineering research report CE

The Civil Engineering Research Report CE series is published by the School of Civil Engineering at the University of Queensland. Orders of any of the Civil Engineering Research Report CE should be addressed to the School Secretary.

School Secretary, School of Civil Engineering, The University of Queensland
Brisbane 4072, Australia
Tel.: (61 7) 3365 3619 Fax : (61 7) 3365 4599
Url: http://www.eng.uq.edu.au/civil/ Email: hodciveng@uq.edu.au

Recent Research Report CE	Unit price	Quantity	Total price
CALLAGHAN, D.P., NIELSEN, P., and CARTWRIGHT, N. (2006). "Data and Analysis Report: Manihiki and Rakahanga, Northern Cook Islands - For February and October/November 2004 Research Trips." *Research Report CE161*, Division of Civil Engineering, The University of Queensland (ISBN No. 1864998318).	AUD$10.00		
GONZALEZ, C.A., TAKAHASHI, M., and CHANSON, H. (2005). "Effects of Step Roughness in Skimming Flows: an Experimental Study." *Research Report No. CE160*, Dept. of Civil Engineering, The University of Queensland, Brisbane, Australia, July (ISBN 1864998105).	AUD$10.00		
CHANSON, H., and TOOMBES, L. (2001). "Experimental Investigations of Air Entrainment in Transition and Skimming Flows down a Stepped Chute. Application to Embankment Overflow Stepped Spillways." *Research Report No. CE158*, Dept. of Civil Engineering, The University of Queensland, Brisbane, Australia, July, 74 pages (ISBN 1 864995297).	AUD$10.00		
HANDLING (per order)	AUD$10.00		
GRAND TOTAL			

Note: Prices include postages and processing.

PAYMENT INFORMATION

1- VISA Card

Name on the card :	

Visa card number :	
Expiry date :	
Amount :	AUD$ .....

2- Cheque/remittance payable to: THE UNIVERSITY OF QUEENSLAND and crossed "Not Negotiable".

N.B. For overseas buyers, cheque payable in Australian Dollars drawn on an office in Australia of a bank operating in Australia, payable to: THE UNIVERSITY OF QUEENSLAND and crossed "Not Negotiable".

Orders of any Research Report should be addressed to the School Secretary.

School Secretary, School of Civil Engineering, The University of Queensland
Brisbane 4072, Australia - Tel.: (61 7) 3365 3619 - Fax : (61 7) 3365 4599
Url: http://www.eng.uq.edu.au/civil/ Email: hodciveng@uq.edu.au